STUDY TO EVALUATE THE INTEGRATION
OF A MASS SPECTROMETER
WITH A WET CHEMISTRY INSTRUMENT

REPORT NO. 24012-6001-RU-00

31 MARCH 1974

FINAL REPORT

Prepared under
CONTRACT NO. NAS2-7685

for

AMES RESEARCH CENTER
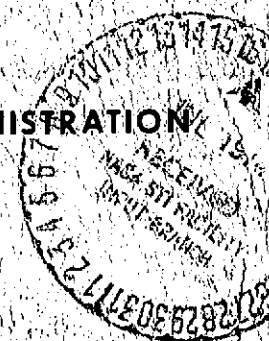NATIONAL AERONAUTICS AND SPACE ADMINISTRATION

TRW
SYSTEMS GROUP

ONE SPACE PARK · REDONDO BEACH · CALIFORNIA

PREFACE

The Study to Evaluate the Integration of a Mass Spectrometer with a Wet Chemistry Instrument described in this document was undertaken for the National Aeronautics and Space Administration, Ames Research Center, under Contract No. NAS2-7685. The study was under the direction of Mr. G. Thorley, Technical Monitor, NASA/Ames Research Center.

The program at TRW Systems Group was performed by the Instrument Systems Department under the direction of Dr. H. S. Suer. Mr. S. L. Korn acted as Study Manager; Mr. A. Cole and Dr. R. F. Day were responsible for the experimental investigations and mass spectrometer evaluation. Perkin-Elmer, Aerospace Division, supported the evaluation of the mass spectrometer under subcontract to TRW Systems.

CONTENTS

CONTENTS (Continued)

1. INTRODUCTION

This document is the final report for a Study to Evaluate the Integration of a Mass Spectrometer with a Wet Chemistry Instrument. The program was carried out by TRW Systems for the National Aeronautics and Space Administration, Ames Research Center (NASA/ARC) under Contract No. NAS2-7685.

Experiments capable of analyzing amino acids in planetary soils and of determining whether the amino acids are optically active are important to establish whether life as we know it does currently exist or has existed in the past on other planets.

TRW, under Contracts No. NAS2-6218 and No. NAS2-7198, has developed a wet chemistry instrument design and carried out a breadboard program which yielded generally unambiguous identification of amino acids with earth soils (TRW Report No. 23197-6001-RU-00). Work with meteorites at NASA/ARC revealed, however, the presence of amino acids which required different gas chromatographic columns than those selected for the wet chemistry instrument. From these results it appears that, in the analysis of extraterrestrial material, there is always some risk that there can be unexpected amino acids. It is possible that, since the system is not optimized to detect all possibilities of amino acids, some ambiguities could occur in portions of the amino acid spectrum.

The purpose of this program was to study the integration of a mass spectrometer with the wet chemistry instrument to provide mass number identification of the amino acid fragments, and thus positive identification of the amino acid fragments, separated by the wet chemistry instrument. The mass spectrometer from the Viking '75 Gas Chromatograph/Mass Spectrometer Instrument (GCMS) was the only flight type instrument identified whose capability approaches the sensitivity and mass number range requirements for the amino acid analysis. A major portion of this study was, therefore, directed to determining whether this mass spectrometer, which was developed by Perkin-Elmer, could be adapted to the wet chemistry instrument design with minimum modifications. A major subcontract was issued to Perkin-Elmer, Aerospace Division, to aid in the analysis of the GCMS mass spectrometer.

This report is divided into seven major subsections. Section 2, Summary, summarizes the analysis and instrument concept, and the major accomplishments and recommendations of this study.

Section 3, Wet Chemistry Instrument, describes the operation of the Wet Chemistry Instrument and the amino acid analysis sequence. The GCMS operation and performance capabilities are presented in Section 4. The components necessary to interface the mass spectrometer with the wet chemistry instrument are described in Section 5, Supporting Components.

Section 6, Wet Chemistry/Mass Spectrometer Instrument System Design, first discusses the MS instrument parameters and then describes the conceptual instrument system design. This is followed by a comparison of the experiment requirements and instrument performance capabilities. Recommended mass spectrometer upgrading is discussed at the end of the section.

Laboratory measurements of gas chromatograph column bleed and hydrogen separator test are described in Section 7, Laboratory Investigation.

2. SUMMARY

The chemical approach of life detection carried out with the Wet Chemistry/Mass Spectrometer instrument consists of searching for optically active amino acids in planetary soils. It is expected that the amino acids present are at least partially in the form of biopolymers (peptides and proteins).

The first steps in the separation and identification process are carried out in the wet chemistry part of the instrument. They consist of a water extraction of the amino acids (in their biopolymer form) from the soil, which is followed by an acid hydrolysis to break the polymers down into the individual amino acids. Any interfering materials are separated from the amino acids in a desalting process using an ion exchange column. The purified amino acids are then derivatized with optically active reagents. The resultant diasterioisomers are separated with a self-heated, capillary type gas chromatographic column and detected with a flame ionization detector. Preliminary identification is achieved by the characteristic retention time of the different amino acids in the GC column.

In order to achieve unambiguous identification of the amino acids the effluent coming out of the GC column is analyzed in the mass spectrometer to provide mass number identification of the diasterioisomer fragments. The flow rate into the mass spectrometer is controlled by effluent dividers, and the GC carrier gas is removed by a hydrogen separator. The mass spectrometer is a double focusing Nier-Johnson instrument. The amino acid derivatives are ionized by an electron beam in the ion source and then extracted into the velocity focusing 90-degree electrostatic sector, from where they enter the mass focusing 90-degree magnetic sector. The ion current is measured with an electron multiplier behind the magnetic sector exit slit.

The main effort of this study was directed to the evaluation of the Viking '75 GCMS mass spectrometer and to determine what the requirements for the integration into the wet chemistry instrument are.

Major accomplishments of this study can be summarized as follows:

The characteristics and performance capability of the current Viking '75 GCMS Mass Spectrometer have been reviewed and are documented.

Requirements determined by the wet chemistry instrument for operation with a mass spectrometer have been analyzed and compared with the MS performance capabilities. This comparison has established that the mass spectrometer is basically able to meet the additional requirements for amino acid analysis.

The Wet Chemistry/Mass Spectrometer interface requirements were established and a preliminary interface design is presented. A simulated flight investigation of the interface components (effluent divider, hydrogen separator) was carried out.

Some remaining mass spectrometer problems, e.g., high mass discrimination and vacuum requirements, have been identified and possible solutions are discussed. Suggestions for future investigations, tradeoff studies and design modifications are presented.

Gas chromatograph column bleed measurements were carried out, and the effect of a palladium hydrogen separator on GC effluent characteristics was investigated.

A preliminary design of an integrated Wet Chemistry/Mass Spectrometer instrument is presented, including an estimate of the additional weight, volume and power requirements.

3. WET CHEMISTRY INSTRUMENT

3.1 INSTRUMENT DESIGN AND ANALYSIS SEQUENCE

The Automated Wet Chemistry Instrument is designed to analyze at least three soil samples for optically active amino acids under the conditions specified in NASA/ARC Specification A-16231, Revision 3, Automated Wet Chemistry Instrument for Landed Planetary Missions. A list of mandatory and desirable amino acids the instrument shall be capable of analyzing as well as the basic sequence for accomplishing the analysis, including types and amounts of reagents, order of addition, and processing times and temperatures are also defined in Specification A-16231. Performance requirements such as resolution and separation of and sensitivity to amino acids, and internal calibration requirements are also specified in the document. Portions of the specification are included in Table 3-1 for reference.

The processing sequence contains the following basic operations: internal calibration, soil handling, amino acid extraction, hydrolysis, purification, derivitization and gas chromatographic analysis. The components necessary to perform these operations are:

- Soil distributor for soil handling

- Extractor cell for amino acid extraction

- Hydrolyzer/Evaporator cell for hydrolysis and then HCl evaporation

- Ion exchange column for desalting

- Derivatizer cell for derivitization of the amino acids

- Gas Chromatographic Column and detector for gas chromatographic analysis.

Additional components necessary to implement the functions in an automated system are:

- Reagent storage containers and injection systems

- Gas supply subsystems

- Interconnecting plumbing and valves

- Electronic subsystem.

Table 3-1. Analysis Requirements (From Specification
A-16231, Rev. 3)

Analysis Sequence:

Step 1. Place a 1-cubic-centimeter soil sample in a chamber.

Step 2. Add 10 milliliters of water.

Step 3. Heat to 165 5°C for 1 hour.

Step 4. Allow to cool and filter off the insoluble soil residue.

Step 5. Add 10 milliliters of 6N HCl to the filtrate from Step 4.

Step 6. Heat solution to 110°C for 5 hours.

Step 7. Evaporate to dryness.

NOTE: The following step is performed on the ion exchange column prior to proceeding to Step 9. The reagent volumes for Step 8 are given for a 5-milliliter Dowex 50H+ column.

Step 8. Place 10 milliliters of 4N NaOH on ion exchange column. Follow this with 20 milliliters of water directly onto the ion exchange column. Follow this with 15 milliliters of 6N HCl directly onto the ion exchange column. Follow this with 20 milliliters of water directly onto the ion exchange column.

Step 9. After evaporating to dryness (Step 7), dissolve the amino acids and residual salts in 5 milliliters of water. (It may be necessary to heat a short time to assure solution.)

Step 10. Place solution (Step 9) on strong cation exchange column for amino acid exchange, cation and neutral organic removal. Follow the amino acid solution immediately with 15 milliliters of water directly onto the ion exchange collum. Follow this with 10 milliliters of 4N NH_4OH and start collecting the amino acids when the ammonia begins to break through the ion exchange column. Collect only the first 1 to 2 milliliters.

Step 11. Evaporate the amino acid solution to dryness at 100°C.

Step 12. To the dried sample add 0.5 milliliter of (+) 2-butanol containing sufficient anhydrous HCl to make it 4N.

Step 13. Heat solution to 100°C in a closed chamber for 2 hours.

Step 14. Evaporate to dryness. Cool to below 35°C.

Step 15.   To the dried sample add 0.1 milliliter of trifluoracetic
anhydride and 0.4 milliliter of methylene chloride. Heat
in a closed chamber for 1 hour at 35° to $40^{\circ}C$.

Step 16.   Evaporate the solvents at a temperature below $10^{\circ}C$.

Step 17.   The resultant sample is analyzed for composition by gas
chromatography.

Sample Size - The size of the soil sample shall be between 1 and
10 cubic centimeters.

Gas Chromatography - The analysis shall be performed meeting the
following conditions:

Carrier Gas - TBD

Columns - The column(s) shall be capable of separating the amino
acids listed below. All of the amino acids on both the mandatory
and goal lists must be identifiable by retention time. The instru-
ment is required to work only for the mandatory list. The goal list
is both a goal and to identify the most probable compounds that might
also be present and require some identification.

Mandatory Detectable Amino Acids	Design Goal Detectable Amino Acids
1. Alanine	1. Ornithine
2. Valine	2. ϵ - Amino Caproic Acid*
3. Isoleucine	3. δ - Amino Valeric Acid*
4. Leucine	4. γ - Amino Butyric Acid*
5. Glycine*	5. α - Amino Adipic Acid
6. Proline	6. Alloisoleucine
7. Aspartic Acid	7. β - Amino- -Butyric
8. Methionine	8. β - Amino - Isobutyric
9. Phenylalanine	9. N - Methyl-alanine
10. Glutamic Acid	10. Isovaline
11. Beta alanine*	
12. Norvaline	
13. Norleucine	

*Denotes that the amino acid is not optically active.

14. α - Amino -η-Butyric

15.   Lysine

16.   Pipecolic acid

17. α - Amino isobutyric*

GC Peak Resolution and Separation.   Definitions: Resolution is used
to denote the separation of the diastereomeric peaks of a single racemic
amino acid and is to be determined according to R. Kaiser, Gas Chroma-
tography Vol. 1, p. 39 (1963) Butterworth, Washington. Separation is
used to denote the separation of a diastereomeric pair of one amino acid
from the diastereomeric pair of another amino acid.

The resolution of the peaks of a single racemic amino acid shall be
90 percent or better for all optically active amino acids on the mandatory
and goal lists except for aspartic acid (40 percent) lysine and ornithine
(65 percent), β -amino-isobutyric (TBD), Isovaline, N-methyl-alanine,
and β -amino-η-butyric (0 percent). This resolution is to be obtained for
amino acid concentrations up to 50 nanomoles per amino acid. For con-
centrations above 50 nanomoles, the resolution may be degraded.

The separation of a mixture of the racemic mandatory amino acids
shall be such that of these acids all will be separated with resolution
being no less than 50 percent in any conflict. Such conflicts shall not in-
volve more than three of the amino acids on the mandatory list. The goal
shall be 100 percent separation of all acids on the mandatory list.

Column Temperature. The temperature programming and readout
accuracy shall be $\pm0.5^{\circ}C$.

Column Retention Time. The retention time precision for each
amino acid shall be within $0.5^{\circ}C$ of its retention time.

Detector. The overall sensitivity (total scheme, sensitivity at
detector output after data processing) shall be such that 0.1 nanomole and
less than 50 nanomoles of each of the amino acids on the mandatory list

---

*Denotes that the amino acid is not optically active.

in Table 3-1 can be detected in the soil sample. It is a design goal that 0. 01 nanomole or less of each of the amino acids in a soil sample be detected.

Detector Dynamic Range. The detector dynamic range shall be six decades. The peak area accuracy for each decade of peak height (concentration) shall be 1 percent.

Internal Calibration. A mixture of two (TBS) racemic amino acids or peptides shall be carried in the instrument for calibration of the experiment system for each of the processed soil samples. The (TBS) racemic amino acids or peptides shall be placed in each hydrolysis chamber with the soil sample prior to the addition of HCl.

A system block diagram of the basic system components, including summaries of the process operations performed with each component, is presented in Figure 3-1. A complete instrument system schematic is shown in Figure 3-2. A short description of the system is presented in the following paragraphs.

The soil metering and distribution subsystem which is based on the VLBI soil distributor receives soil from the Lander soil processor via the soil feed tube, meters out a fixed volume of the soil sample and deposits the sample in the extractor after removal of the top cover of the extractor. Leftover soil is deposited in a dump cell.

A set of processing cells which can be used repeatedly is provided for preparing the sample for gas chromatographic analysis. The set consists of the extractor, hydrolyzer/evaporator, ion exchange column and derivatizer, and the associated plumbing and valves. Each component is equipped with heaters to maintain the required temperature environment. The derivatizer, in addition, is connected via a heatpipe to a thermoelectric cooler to maintain the cell temperature below $10^{o}C$ during evaporation

SOIL FEED TUBE

SOIL DISTRIBUTION ASSEMBLY

SOIL VALVE

EXTRACTOR

VALVE

H_2O, $6\underline{N}$ HCl
He/H_2
$4\underline{N}$ NH_4OH

VALVE

VENT

HYDROLYZER/ EVAPORATOR

VALVE

H_2O, $6\underline{N}$ HCl, $4\underline{N}$ NH_4OH,

LIQUID SENSOR
$2\underline{N}$ NaOH

ION EXCHANGE COLUMN

VENT
VALVE He/H_2, 2 BUTANOL/HCl, TFAA/MC

VALVE
VENT

DERIVATIZER

VALVE

He/H_2 O_2

GAS CHROMATOGRAPH COLUMN

FLAME IONIZATION DETECTOR

VENT

SOIL HANDLING
RECEIVE SOIL FROM LANDER
METER 1 CC SAMPLE
OPEN SOIL VALVE AT CELL SOIL INLET PORT
TRANSFER 1 CC SAMPLE TO EXTRACTOR CELL
DEPOSIT EXCESS SOIL IN DUMP RECEPTACLE
CLOSE SOIL VALVE

EXTRACTION
INJECT 10 ML OF H_2O AND CALIBRATION AMINO ACIDS
HEAT TO 165+5°C FOR ONE HOUR
ALLOW TO COOL AND FILTER INTO HYDROLYZER

HYDROLYSIS
RECEIVE FILTRATE
ADD 10 ML OF $6\underline{N}$ HCL
HEAT AT 110±5°C FOR FIVE HOURS
EVAPORATE TO DRYNESS
DISSOLVE THE RESIDUE IN 5 ML OF H_2O

ION EXCHANGE
FILTER THE SOLUTION AND PASS THE FILTRATE
    THROUGH THE ION EXCHANGE COLUMN AND VENT
WASH THE ION EXCHANGE COLUMN DIRECTLY WITH
    15 ML OF H_2O AND VENT
FOLLOW DIRECTLY WITH 10 ML OF $4\underline{N}$ NH_4OH THROUGH
    THE COLUMN

DERIVATIZATION
COLLECT THE FIRST 1 TO 2 ML OF COLUMN EFFLUENT
    CONTAINING AMINO ACIDS
EVAPORATE THE ION EXCHANGE COLUMN EFFLUENT TO DRYNESS
INJECT 0.5 ML OF 2-BUTANOL/HCL (4N)
HEAT TO 100°C FOR 2 HOURS
EVAPORATE THE SOLUTION TO DRYNESS
COOL TO BELOW 35°C
INJECT 0.2 ML OF TRIFLUOROACETIC ANHYDRIDE AND
    o.4 ML OF METHYLENE CHLORIDE
HEAT TO 35-40°C FOR ONE HOUR
0.4 EVAPORATE THE SOLVENTS AT A TEMPERATURE BELOW
    10°C (THROUGH THE VENT)

GAS CHROMATOGRAPHIC ANALYSIS
HEAT THE SAMPLE TO 150°C AND INJECT INTO THE GAS
    CHROMATOGRAPHIC COLUMN
TEMPERATURE PROGRAM THE GAS CHROMATOGRAPHIC COLUMN
    FROM 25°C TO 200°C
DETECT AMINO ACIDS

Figure 3-1. Wet Chemistry System Block Diagram
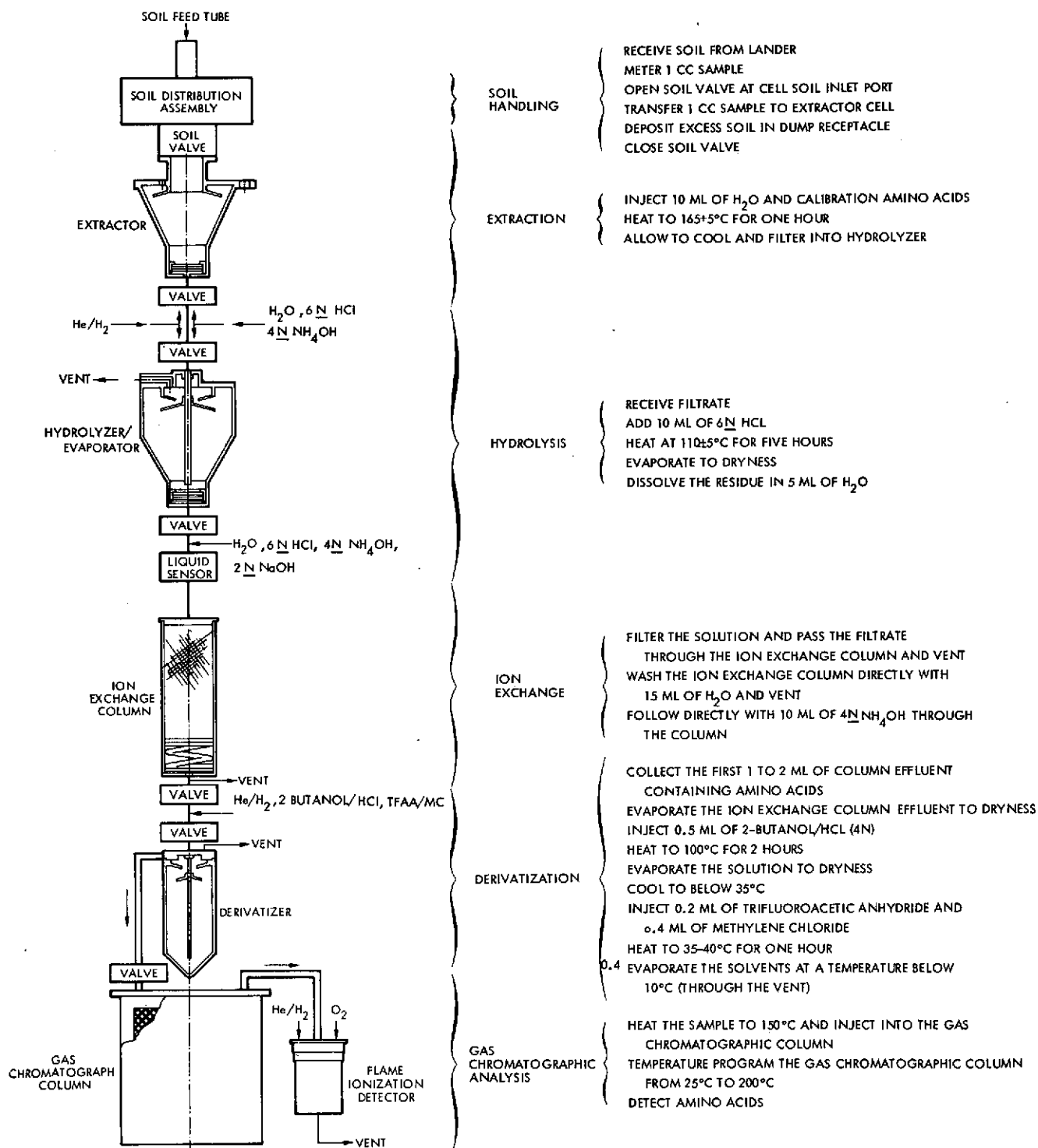
Figure 3-2. Instrument System Schematic

of solvents after amino acid derivitization. The ion exchange column has gas actuated isolation valves at inlet and outlet to preclude drying of the resin during interplanetary cruise.

The instrument contains a single capillary tube self-heated gas chromatographic column which is used, in the baseline configuration, in conjunction with a flame ionization detector. The stainless steel column is used as a resistance element heater and is designed to provide uniform column temperatures during steady-state and programmed temperature control. Active temperature control is maintained by sensing the change in column electrical resistance as the column is heated. The column inlet and outlet are close coupled to the derivatizer outlet and detector, respectively. The amino acids are injected directly into the column from the derivatizer. Cold trapping of amino acid derivatives is provided by the column liquid phase.

The baseline instrument contains a single flame ionizaation detector. The detector has inlets for the He/H_2 carrier gas from the gas chromatographic column, makeup He/H_2 gas, and O_2 gas. A single outlet is provided with a gas actuated valve and flow restrictor. The detector has a separate heater and temperature sensor to maintain the detector temperature at a constant value, slightly above the maximum programmed gas chromatographic column temperature.

Two gas supplies are used in the instrument. One provides oxygen for the flame ionization detector. For long term storage, the oxygen supply is isolated by a thermally actuated isolation valve which is actuated at the start of the experiment. A control valve is used to turn the gaseous oxygen on and off as required.

A second gas supply contains a mixture of helium and hydrogen (approximately 44 percent H_2 by volume). This system has three branches. The first branch is connected downstream of the first pressure regulator (approximately 165 psia) and is used to pressurize the gas actuated isolation valves on all reagent containers and on the ion exchange column. It will also be used for all gas actuated tantalum diaphragm valves (control valves) in the instrument, and for the gas actuated extractor cover. The

other two branches are connected downstream of the second stage regulator (18 psia); one branch supplies carrier gas through the gas chromatographic column and then through the flame ionization detector. Gas from each of these branches is controlled by a separate valve. Low pressure gas is also used for pressurization of the various cells, for purging and gas drying, and for fluid routing and reagent injection. The gas supply is sealed with a thermally actuated isolation valve for long term storage.

Identical reagent storage containers and injectors are used in the current design. The reagents are stored in compatible metallic containers and a gas actuated isolation valve is used to seal the container for long term storage. After actuation the flow of the reagent is maintained by the low pressure He/H_2 gas, and the amount of reagent delivered to the cell is determined by the open time of the control valve of the outlet.

Because of shelf life limitations, the 2-butanol and anhydrous HCl are stored separately. The anhydrous Hcl is stored in a small pressure vessel at approximately 900 psi. Ten percent of this volume contains helium gas. The 2-butanol is stored in a separate container under its own vapor pressure. The two vessels are isolated from each other and from the rest of the system by gas actuated isolation valves. Upon actuation of the valve between the two vessels, the HCl gas and 2-butanol in the adjacent reservoir are allowed to react. The inert helium is used as the driving pressure (blowdown mode) for reagent injection. Injection is accomplished by first opening the gas actuated isolation valve downstream of the 2-butanol reservoir and then opening the control valve for a predetermined time to meter the mixture to the derivatizer.

The instrument contains two vent systems internal to the package (as compared to three previously). These are connected to a single outlet vent for interfacing with the Lander. A common vent manifold is used for the extractor, hydrolyzer/evaporator, derivatizer, and ion exchange column. Valves at the outlets of these cells prevent backflow and cross contamination between cells. The second vent system is used on the outlet of the gas chromatographic column and flame ionization detector and for the two gas supply systems.

Control and routing of reagents, gases and samples are accomplished with a fluid system consisting of small diameter tubing and gas actuated control and isolation valves. The plumbing system is designed to contain a minimum number of valves and to prevent cross contamination between various cells. Two- and three-way solenoid valves, most thermally actuated isolation valves and (passive) check valves incorporated in the previous design have been eliminated and/or replaced.

The electronic subsystem provides the regulated power, instrument control functions and data processing. This subsystem receives, decodes and distributes commands from the Lander.

4. MASS SPECTROMETER

4.1 MASS SPECTROMETER OPERATION

The Viking '75 mass spectrometer analyzer is a 90-degree electrostatic, 90-degree magnetic sector, Nier Johnson configuration instrument. The design parameters for the instrument are summarized in Table 4-1, and an outline drawing of the instrument is shown in Figure 4-1. The instrument has a magnetic ion source (electron beam magnetically constrained). It is equipped with an ion pump which is integral at the magnetic sector.
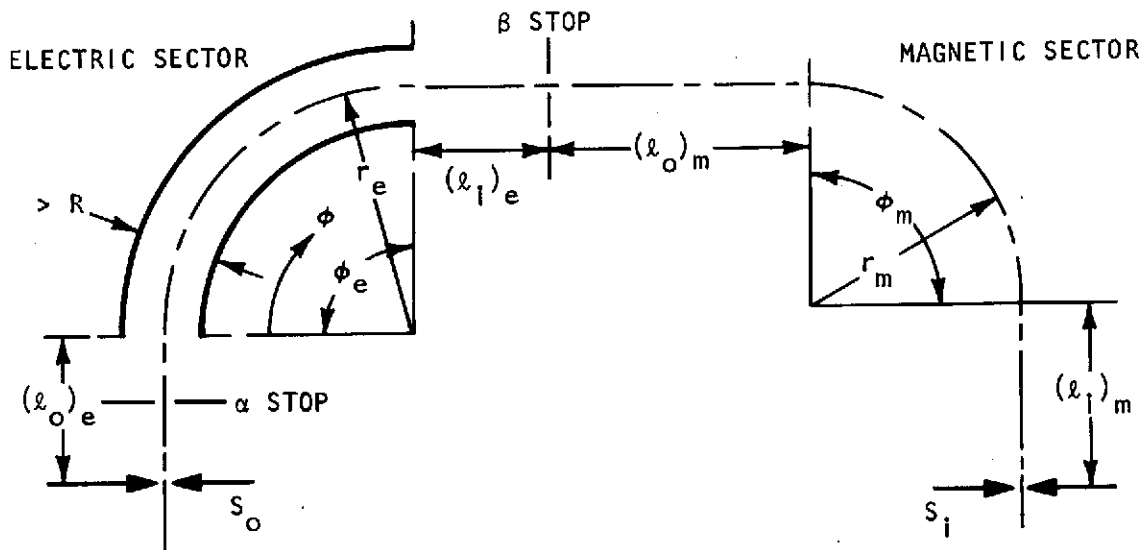
A single magnet assembly provides the field for the analyzer and the ion pump. The resolved ion current is detected by an electron multiplier tube. Electrical interfaces for the analyzer are shown schematically in Figure 4-2.

4.1.1 Ion Source

The ion source is shown in detail in Figures 4-3 and 4-4. This dual filament source is designed to interface with the analyzer, providing minimum energy spread in the ion beam. The source has two filaments to provide redundancy for space applications. The filaments (tungsten - 3 percent rhenium) are positioned slightly off axis to the electron beam entrance cone, and an electron focus lens system is used to direct the beam into the ionization region. A cylindrical magnet contained within the source mounting block constrains the angular spread of the beam through the ionization region. The end of the magnet extends around the filament region, and forms part of the electron focusing system. The electron beam walks in the extraction field (between the repeller and the saddle lens) at an angle of approximately 2 degrees with the optic axis of the analyzer. The source is tilted to align the beam with the optic axis. Most of the electron beam strikes the repeller; only a small fraction originally entered the low conductance aperture to the anode. This aperture has been eliminated and an anode placed behind the exit slit from the repeller. Emission is regulated on total electron beam current, which is measured on all surfaces in the source.

Gas enters the instrument through a tube in the mounting block, flows around the mounting block, and enters the source through the ion

Table 4-1. Double Focusing Mass Spectrometer Configuration

β STOP

ELECTRIC SECTOR

MAGNETIC SECTOR

> R

r_e

$(\ell_i)_e$

$(\ell_o)_m$

ϕ

ϕ_e

ϕ_m

r_m

$(\ell_o)_e$ ── α STOP

$(\ell_i)_m$

S_o

S_i

$(\ell_o)e$ = object distance, electric sector = 0.652 in.

$(\ell_i)e$ = image distance, electric sector = 0.652 in.

$(\ell_o)m$ = object distance, magnetic sector = 2.217 in.

$(\ell_i)m$ = image distance, magnetic sector = 1.115 in.

ϕ_e = electric sector angle = 90 degrees

ϕ_m = magnetic sector angle = 90 degrees

r_e = radius "optical axis", electric sector = 1.86 in.

r_m = radius "optical axis", magnetic sector = 1.5 in.

s_o = object slit width = 2.00×10^{-3} in.

S_i = image slit width = 2.00×10^{-3} in.

α_o = angle spread in beam at S_o = ± 2 degrees

$\Delta V/V$ = energy spread in beam at S_o = ± 0.01 max (normalized)

β_o = velocity spread in beam at S_o = $\Delta v_o/v$ = ± 0.005 max (normalized)

M_m = magnification in magnetic sector = -0.68

ΔR = electric sector gap width = 0.125 in.
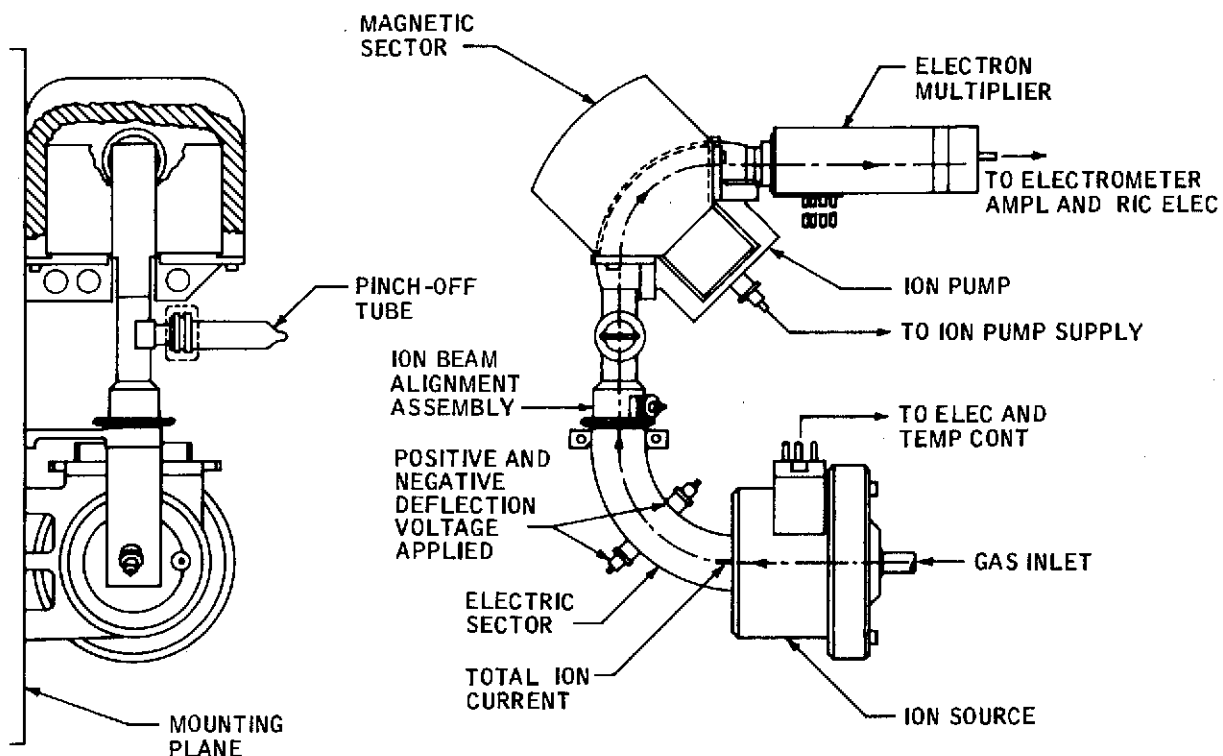
g = magnet gap width = 0.100 in.

Figure 4-1. Viking MS Outline Drawing

exit aperture in the cylindrical magnet. The conductance of the modified source is approximately 32 cc/sec at 210°C.

Ions formed by electron bombardment are extracted from the source by the field between the repeller and the source magnet (which is at the mounting block potential). Since the ions are not formed right at repeller, there is a constant offset potential applied on the repeller, relative to the scan voltage, to overcome this offset and to allow tracking of the electric sector. A saddle lens is also placed between the mounting block and the split lens to neutralize the offset from the extraction potential and also to block the leakage field from the split lens into the ionizing region. This further improves tracking of the electric sector.

The ions are accelerated through the split lens (J_1 and J_2) to the object slit. A voltage differential is applied to the split lens to correct for any misalignment with the object slit. An angle limiting baffle (the alpha stop) is located between the object slit and the electrostatic sector to limit the beam angular deviations to 1.5 degrees.
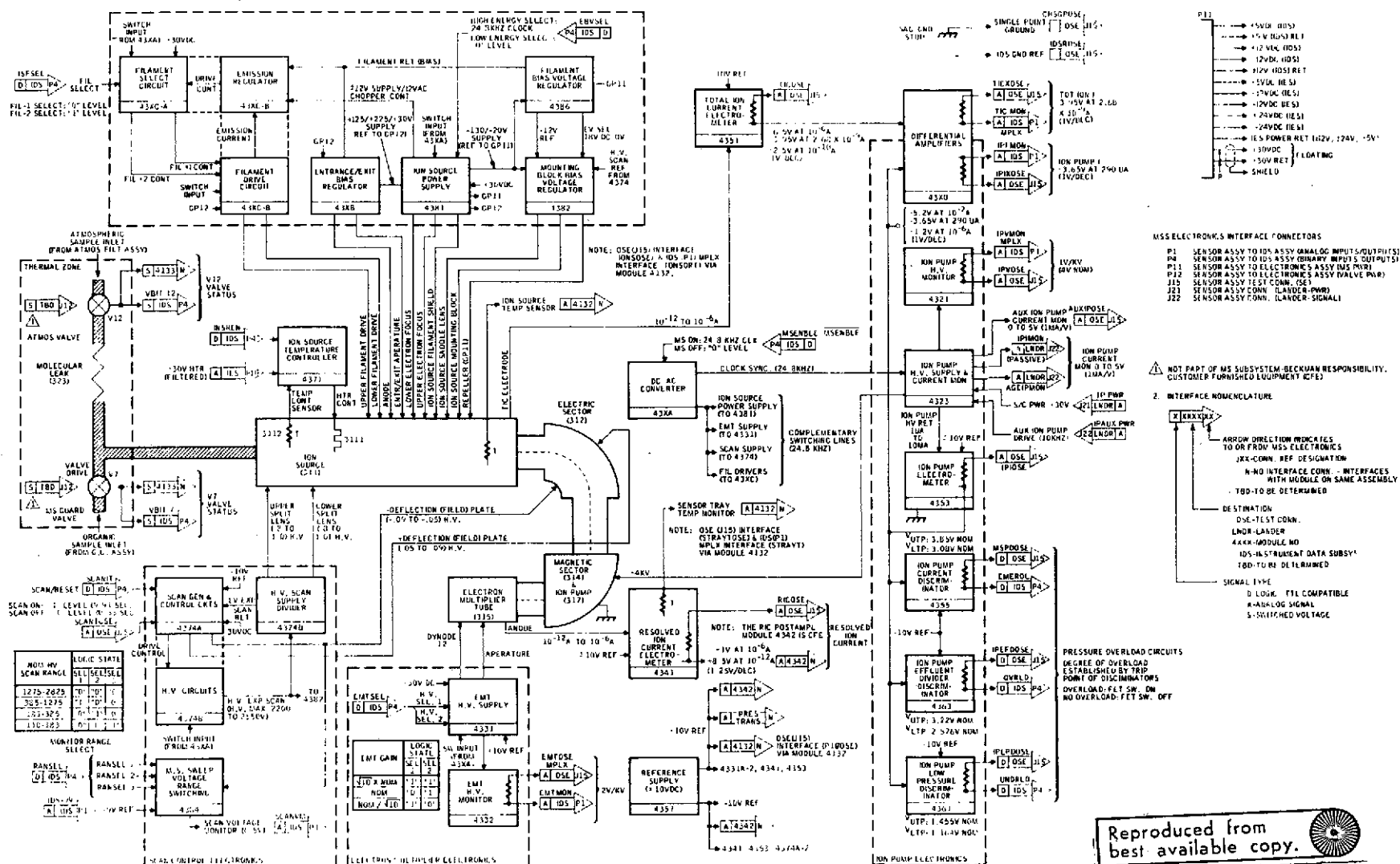
Figure 4-2. Viking Lander GCMS Subsystem Block Diagram

4-4

FILAMENT SPRINGS

OUTER FILAMENT SHIELD

INNER FILAMENT SHIELD

UPPER FILAMENT

OUTER ELECTRON FOCUS

LOWER FILAMENT

ENTRANCE CONE

INNER ELECTRON FOCUS

LOW CONDUCTANCE ENTRANCE APERTURE

MAGNET

REPELLER

LOW CONDUCTANCE EXIT APERTURE

ANODE

Figure 4-3.   Dual Filament Block Assembly

SADDLE LENS

LOWER HEATER

UPPER LENS (J1)

LOWER LENS (J2)

DUAL FILAMENT ELECTRON GUN ASSEMBLY

HEATER

OBJECT SLIT

ION BEAM EXIT

SAMPLE INLET

TOTAL ION CURRENT MONITOR

ACCELERATOR BLOCK

MAGNET

ANODE ASSEMBLY

CERAMIC SPACER

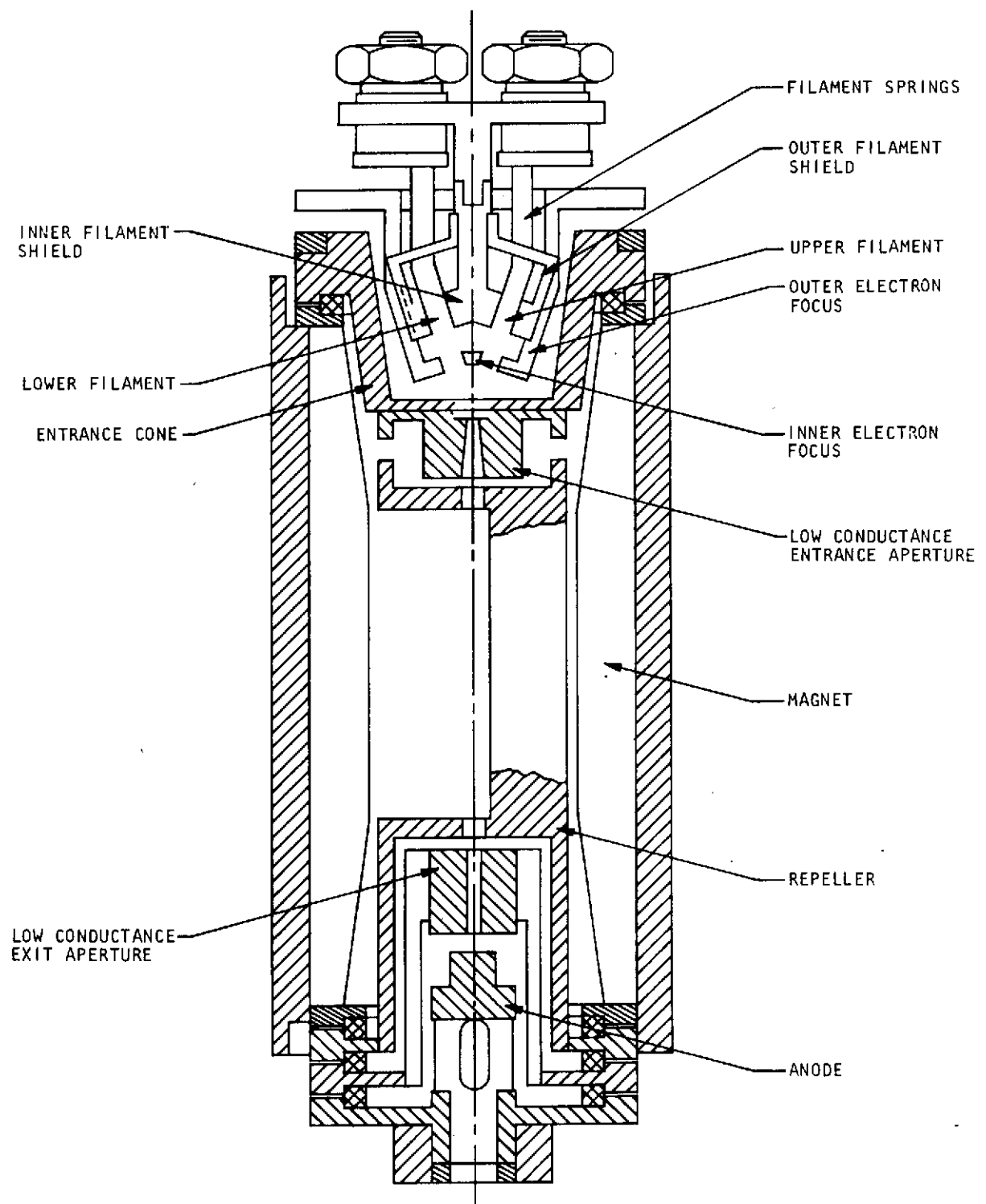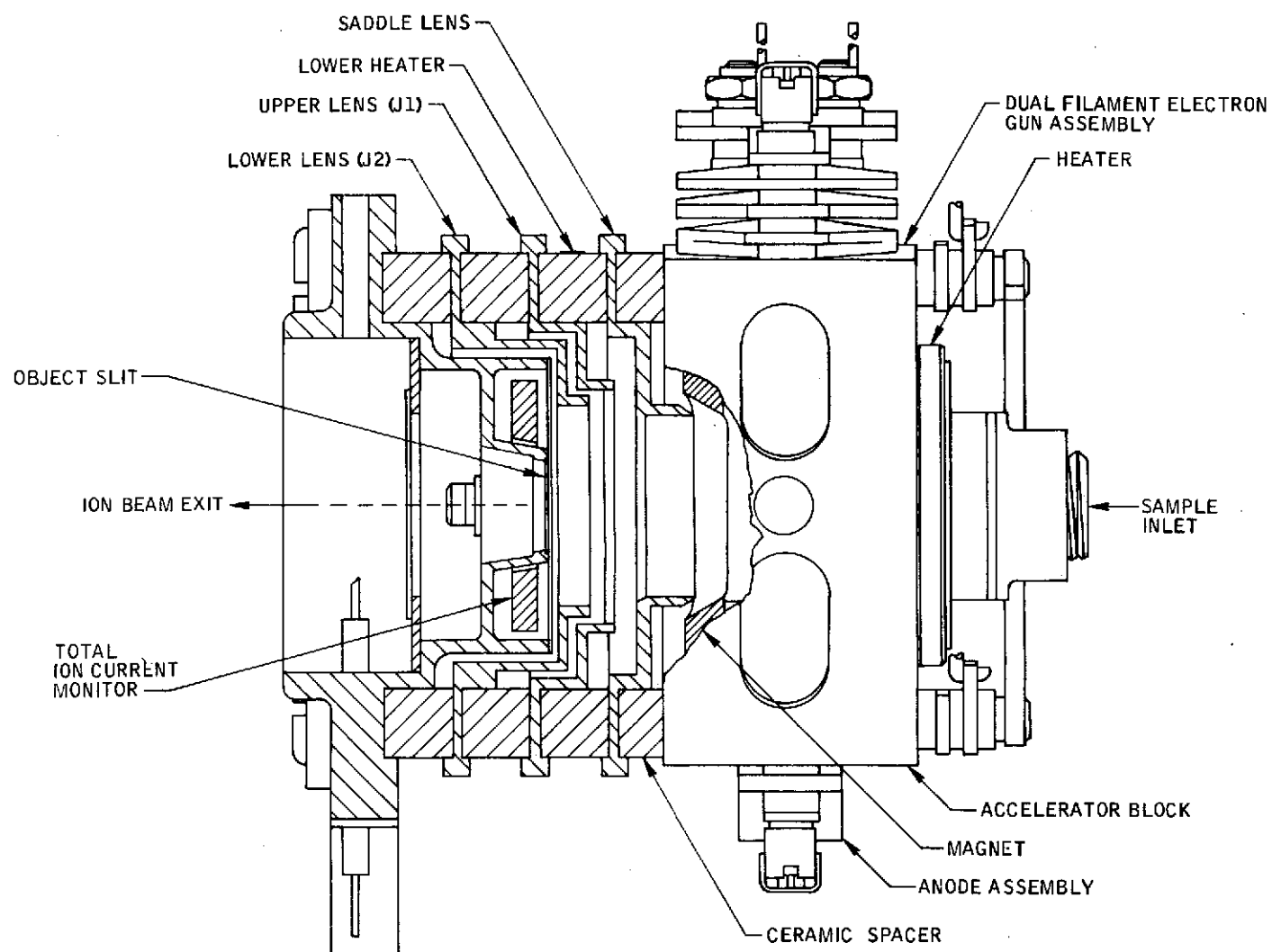Figure 4-4. Ion Source Assembly (Side View)

4.1.2 The Analyzer

The analyzer is a tandem electrostatic magnetic sector design.
Mass dispersion is achieved by a 90-degree, 1.5-inch radius magnetic
sector. Velocity aberrations are compensated in the 1.803-inch radius,
90-degree electric sector. The electric sector has an aspect ratio of 3
which is the ratio of the height of the electric sector to the gap between
them. There are Rose shims on the ends of the sector plates to provide
field uniformity. A Herzog shunt is used to minimize edge effects at the
end of the sector. A beam alignment slit in the drift tube facilitates adjust-
ment of the repeller potential and sector voltages to obtain an energy focus.

4.1.3 Magnetic Analyzer

Mass dispersion occurs in the magnetic sector. As the beam energy
is scanned, ions of different mass-to-charge ratio are focused at the image
slit plane. The image is corrected to first order in angular and velocity
aberrations and to second order in angular aberrations. The 90-degree
sector has a 1.5-inch radius and a height of 0.100 inch. Pole pieces are
welded in the vacuum envelope. An Alnico V-7 magnet provides a field
strength of approximately 6300 gauss.

4.1.4 Ion Pump

An ion pump with a nominal speed of 0.5 liter per second is located
on the inside radius of the magnetic sector. The pole pieces for the mag-
netic sector extend over the pump to provide the field required for the
pump. The 1-inch square titanium cathodes are slotted to provide surface
area for noble gas pumping. The anode is stainless steel and consists of
an array of 16 equal spaced holes, 0.232-inch diameter, drilled through
the 1-inch by 0.12-inch plate. The flux density required for operation is
2030 gauss.

4.1.5 Ion Detection

The ions exiting from the magnetic sector are focused at the image
slit. The position of this exit aperture is located in test. An electron
multiplier tube (ITT) is located behind the image slit. This multiplier is
a 10 dynode device; some of the characteristics are summarized in Table
4-2.

Table 4-2.   Data For ITT Multiplier After Power Aging

Temperature	$23^{\circ}C$
Dynode one current	1×10^{-11} amps
Voltage for 3×10^2 gain	664 volts
Voltage for 1×10^4 gain	1110 volts

Source Voltage	Anode Current (amps)	Gain	Dark Current
1800	6.8×10^{-6}	6.8×10^5	6.5×10^{-13}
1600	2.5×10^{-6}	2.5×10^5	3.5×10^{-13}
1400	8.5×10^{-7}	8.5×10^4	
1200	2.1×10^{-7}	2.1×10^4	
1000	3.8×10^{-8}	3.8×10^3	
800	7.6×10^{-9}	7.6×10^2	
600	1.65×10^{-9}	1.65×10^2	
500	4.7×10^{-10}	4.7×10^1	

Time to decay from

1.0×10^{-6} to 1.0×10^{-9} amp	0.4 ms
1.0×10^{-6} to 5.0×10^{-12} amp	100 ms

4.1.6 Electronics Interface

The mass spectrometer electronics are contained on the instrument subsystem tray. These include the ion pump electronics, source and bias voltage control electronics, scan control and electron multiplier electronics. The MS electronics receive and transmit both analog and digital signals to the Instrument Data System (IDS) Digital inputs control:

1) Electron beam voltage select
2) Ion source filament select
3) Ion source heater enable
4) EMT high voltage select

5)   MS operation

6)   Scan initiate

7)   Scan monitor select (4 segments in scan voltage change).

The electronics interface with the mass spectrometer is shown in Figure 4-2.

4.2   SYSTEM PERFORMANCE CAPABILITY

The projected performance capability of the existing Viking '75 mass spectrometer analyzer is summarized in Table 4-3 and discussed briefly in this section.

4.2.1 Mass Range

The mass scan range of the instrument is from m/e 11.5 to m/e 223.   The low mass limit is determined by the analyzer magnetic sector; the high mass end is determined by the voltage scanning to assure that mass 200 is included in the scan range.

4.2.2 Scan Time

The scan time for the Viking '75 analyzer is 10.3 seconds for m/e 12 to m/e 200. Scan rates are selected primarily on the basis of the time width of a gas chromatograph peak.   It is desirable to have at least two mass scans on every GC peak.   However, selection of high scan rates has an impact on the electronics design, and on the minimum detectable signal since increasing the scan rate requires faster response times for the electronics with correspondingly higher noise levels.   The voltage is scanned exponentially, and the maximum response time is derived from the time interval between the last two peaks in the mass range.   While the scan range from m/e 50 to 300 is effectively smaller than the scan range from m/e 12 to 200, a more rapid response would be required to resolve mass 240 and 241 with the existing instrument operating parameters.

4.2.3 Sensitivity

The sensitivity measured for instruments in test ranges from 6 to 1×10^{-6} amp per torr nitrogen in the source for filament No. 1.   It is usually a factor of two to four less than this for filament No. 2.   The source is tuned for optimum performance with filament No. 1, but some effort is made to obtain reasonably acceptable values for filament No. 2

4-9

Table 4-3. Performance Summary for Viking '75 Mass
Spectrometer Analyzer

Mass Range	m/e 11.5 to 223
Scan Time	10.3 seconds
Sensitivity	
Filament No. 1	3×10^{-6} Ion amps/torr Source, N_2
Filament No. 2	8×10^{-7} amps
Resolution	
Nitrogen (m/e 28)	200
m/e 181.5 (% Valley)	15
m/e 200 (% Valley)	20
Mass Discrimination[1]	5
Pumping Speed	500 cc/sec (N_2 at p = 10^{-5} torr)
Noise Level[2]	2×10^{-12} amps
Minimum Detectable Signal (S/N = 3)	6×10^{-12} amps
Dynamic Range (Analyzer)	
(Source Linearity)	20,000
Source Conductance	
(at 210°C)	32 cc/s
(at room ambient)	25 cc/s
System Weight	18.958 lb
System Volume	500 cu in.
System Power	
Operational	27.5 watts

[1]Measured ratio of m/e 31 to m/e 181 for perfluorobutene-2.

[2]Referred to the output of EMT, gain = 1000.

at the same time. The source voltages are not selectable for each filament, and accordingly, optimum performance cannot be obtained for both fila-ments simultaneously.

The sensitivity values are for ion amps into the electron multiplier; the output signal is larger by the gain of the multiplier which may be set to three different values determined during test. The first gain value, G, is set to give an output of 1×10^{-6} amps for a 4.2×10^{-3} torr - cc/sec

flow of CO_2. The second gain value G_2 is obtained by setting the multiplier voltage to the maximum available on the power supply. The third gain G_3 is the harmonic mean of G_1 and G_2; $G_3 = \sqrt{G_1 G_2}$.

The source conductance is 32 cc/sec at a source temperature of $210^\circ C$. Therefore, a source sensitivity of 3×10^{-6} amps/torr corresponds to a flow sensitivity of about 1×10^{-7} amps/torr cc/sec. The output sensitivity would then be $1 \times 10^{-7} G_1$ amps/torr cc/sec.

A summary of typical data for sensitivity, resolution and mass discrimination is presented in Table 4-4.

Linearity of the source for nitrogen, m/e 28 peak, as a function of pressure is shown in Figure 4-5. Figure 4-6 shows similar data for the principal masses in the PFB-2 spectra. It is noted that the source is linear for nitrogen for source pressures of up to 1×10^{-4} torr. However, the source becomes nonlinear for the principal peaks in PFB-2, particularly for the heavier mass peaks, at source pressures above 1×10^{-5} torr. Nonlinearity in the source is caused mainly by space charge effects which are dependent on sample pressure and ionization probability. Thus, because of the higher ionization in PFB-2, the m/e 31 peak is not as linear with pressure as the m/e 28 peak. In addition, the high mass ions are more sensitive to space charge effects because they are focused at lower accelerating voltages. Thus the m/e 200 peak (which comes in at 140 volts on the accelerator) is more nonlinear than the m/e 31 peak (which comes in at 900 volts on the accelerator).

4.2.4 Resolution

The resolution requirement for the Viking '75 instrument is 5 percent valley for $M/\Delta M = 140$ and 20 percent valley for $M/\Delta M = 200$. The resolution is measured at m/e 181.5, conveniently, because there are two appreciable peaks on either side of that mass number in perfluorobutene-2. The values measured at 181.5 (15 percent valley) are consistent with the resolution requirement.

In some of the instruments deterioration in the resolution has been observed. In certain cases the deterioration has been gradual while in others it has been abrupt, especially following long exposure of the instrument to PFB-2 sample. In most cases, the loss in the resolution was

Table 4-4. ABMS Analyzer

	DTU
Sensitivity (amps per torr source, N_2)	
Filament No. 1	5.2×10^{-6}
Filament No. 2	1.2×10^{-6}
Resolution	
Filament No. 1 (N_2 at 5% Valley)	237
m/e 181.5 (% Valley)	10.7
Filament No. 2 (N_2 at 5% Valley)	225
m/e 181.5 (% Valley)	17.4
Mass Discrimination	
(Ratio of m/e 31 to 181 for Perfluorobutene-2)	
Filament No. 1	18 32, 22[2]
Filament No. 2	19

[1]Flight electronics

[2]32 and 5 torr inlet system pressure, 22 at 0.58 torr inlet system pressure. These values are for output from multiplier.

Table 4-4. ABMS Analyzer (Continued)

PTC

Sensitivity (amps/torr source, N_2)		(1)	(2)	(3)	(4)
Filament No. 1	2.63×10^{-6}	3.0×10^{-6}	1.9×10^{-6}		
Filament No. 2	1.31×10^{-6}	8.7×10^{-7}	1.85×10^{-6}		

Resolution

		(1)	(2)	(3)	(4)
Filament No. 1 (N_2 at 5% Valley)	294, 288, 275	194	250		
m/e 181.5 (% Valley)	13.8 8.9 14.8	38.5	5.7	12.6	18.1
Filament No. 2 (N_2 at 5% Valley)	292 257 264	200	286		
m/e 181.5 (% Valley)	14.5 7.3 18.1	22	7.6	10.0	14.9

Mass Discrimination*

(Ratio of m/e 31 to m/e 181 for Perfluorobutene-2)

		(1)	(2)	(3)	(4)
Filament No. 1	4.9 5.0 5.7	17	7.8	6.3	4.8
Filament No. 2	5.3 5.4 4.3	25	9.7	6.3	5.8

*Includes effect due to multiplier

[1] Prior to first vibration test

[2] U-shaped filaments, test electronics

[3] U-shaped filaments, flight electronics

[4] 8 days after (3)

Table 4-4. ABMS Analyzer (Continued)

QUAL UNIT

				(1)	(2)
Sensitivity (amps/torr source N_2)					
Filament No. 1	4.2×10^{-6}	5.2×10^{-6}	5.0×10^{-6}	2.5×10^{-6}	5.6×10^{-6}
Filament No. 2	6.0×10^{-7}	8.6×10^{-7}	8.6×10^{-7}	3.5×10^{-7}	1.5×10^{-6}
Resolution					
Filament No. 1 (N_2 at 5% Valley)	225	215	255	200	200
m/e 181.5 (% Valley)	10.4%	11%	6.3	13.8	12
Filament No. 2 (N_2 at 5% Valley)	207	200	232	NA	200
m/e 181.5 (% Valley)	14%	13%	8.0	21.4	13.5
Mass Discrimination*					
(Ratio of m/e 31 to m/e 181 for Perfluorobutene-2)					
Filament No. 1	1.6	2.1	1.3	1.2	NA
Filament No. 2	3.0	2.8	2.7	2.3	NA

*Does not include effect due to multiplier

(1) New U-shaped filament design

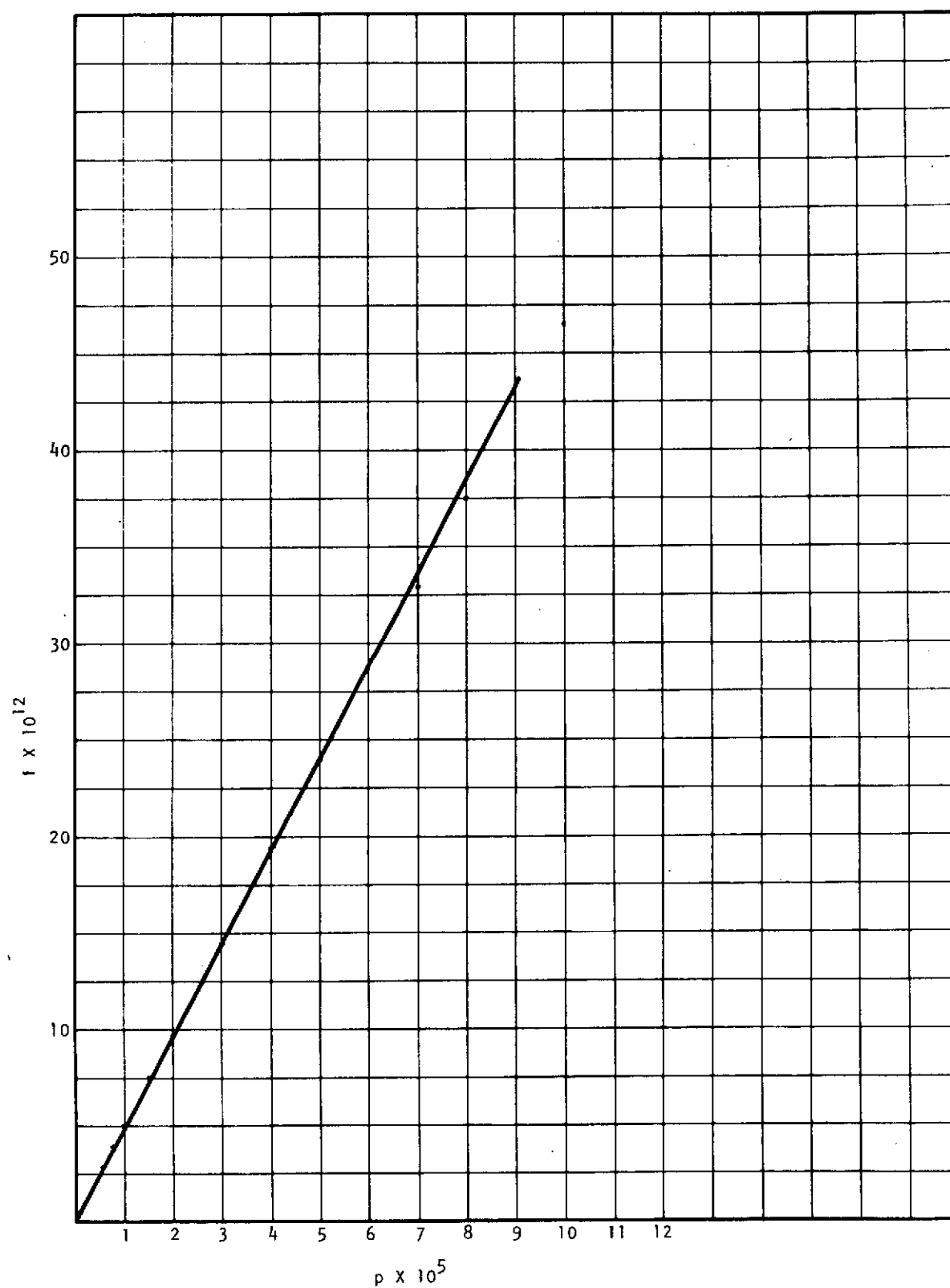(2) Object slit height reduced from 0.150 inch to 0.100 inch.

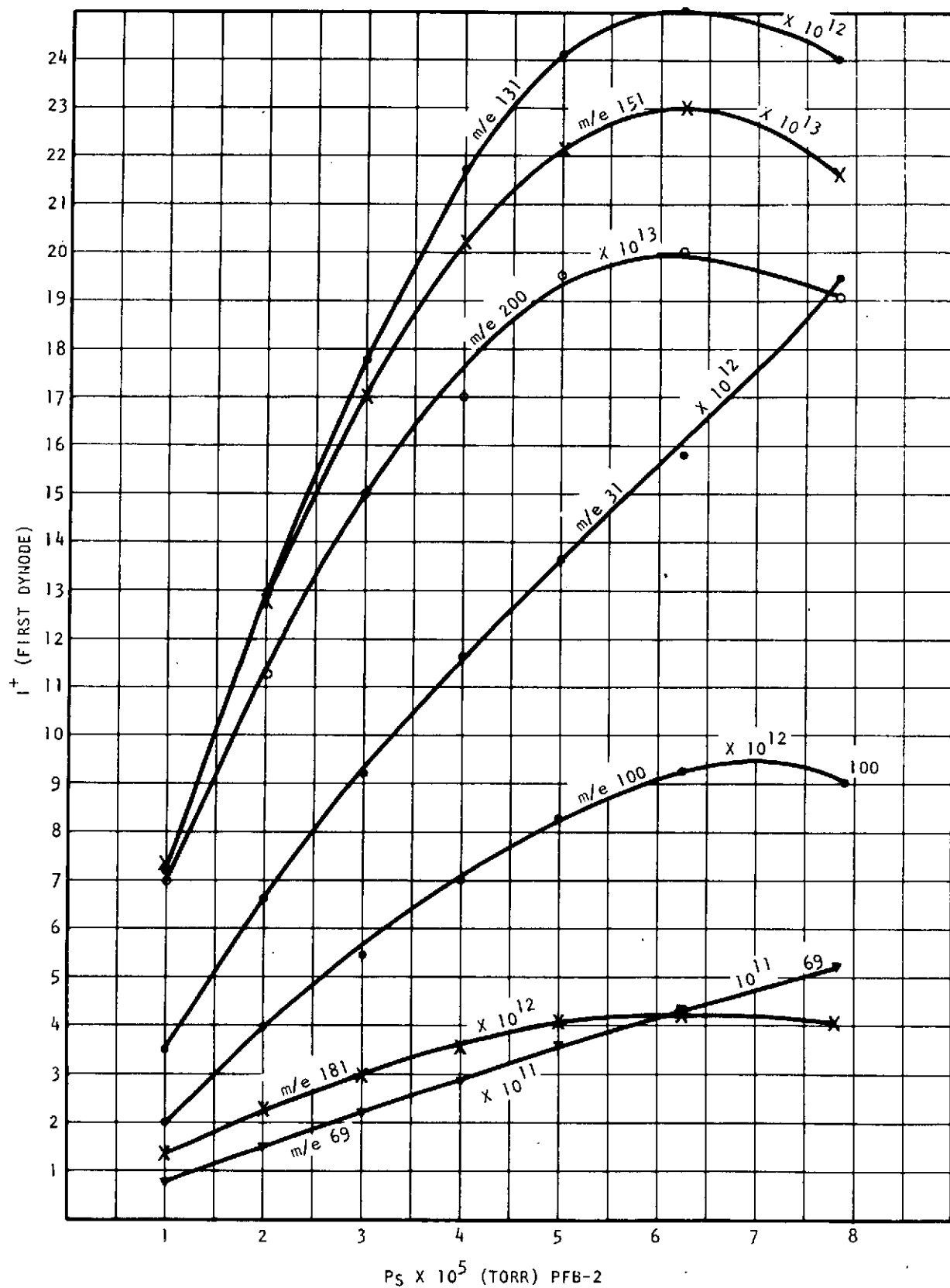Figure 4-5. Source Linearity for N_2 at the First Dynode Versus Pressure

Figure 4-6. Source Linearity for Mass Spectra of Perfluorobutene-2

regained following bakeout. The problem may be caused by a semi-insulating coat of contamination which accumulates charge whenever struck by ions in such areas as the magnetic pole pieces and the entrance region to the magnetic analyzer. In the PTC analyzer the problem was solved by coating the magnetic pole pieces with a thin layer of Aquadag (a colloidal suspension of carbon). Similarly, the Qualification unit was Aquadaged at the pole pieces and the drift tube. The exact cause of this deterioration in the resolution has not been isolated. However, design modifications can be made to help eliminate the problem.

4.2.5 Mass Discrimination

Under normal tuning conditions, the present mass spectrometer has a certain discrimination in sensitivity against the higher masses. This mass discrimination is due to several factors:

1) The Ion Source. There is an inherent mass discrimination in an ion source which scans in voltage. In such an instrument the sensitivity of the ion source is proportional to the square root of the accelerating potential. This has been substantiated in the present instrument by measuring the total ion current as a function of the accelerating voltage.

2) Magnetic Analyzer. Because of the lack of z-focusing in this analyzer, there is a greater probability for the heavier mass ions to strike the magnetic pole faces than there is for the lighter ions. This phenomenon contributes to mass discrimination.

3) Electron Multiplier. The secondary emission characteristic of the multiplier is a function of the ion energy striking the first dynode. Since heavier ions have lower energies, and thus lower gain at the first dynode, the multiplier itself introduces a certain amount of mass discrimination which becomes less with higher multiplier voltage. The effect of gain voltage on mass discrimination is shown in Figure 4-7. Figure 4-8 shows a typical curve of multiplier voltage versus gain.

Nonlinearity of the source with pressure would introduce further ion discriminations since the sensitivity for the higher masses is more pressure dependent than that of the lower masses.

Mass discrimination is measured by the ratio of m/e 31 to m/e 181 for PFB-2. Typically the value is of the order of 2 or 3 when measured at the first dynode. A published spectrum of PFB-2 shows a value of 0.3 for this ratio. The reason for such a low ratio is because it was measured
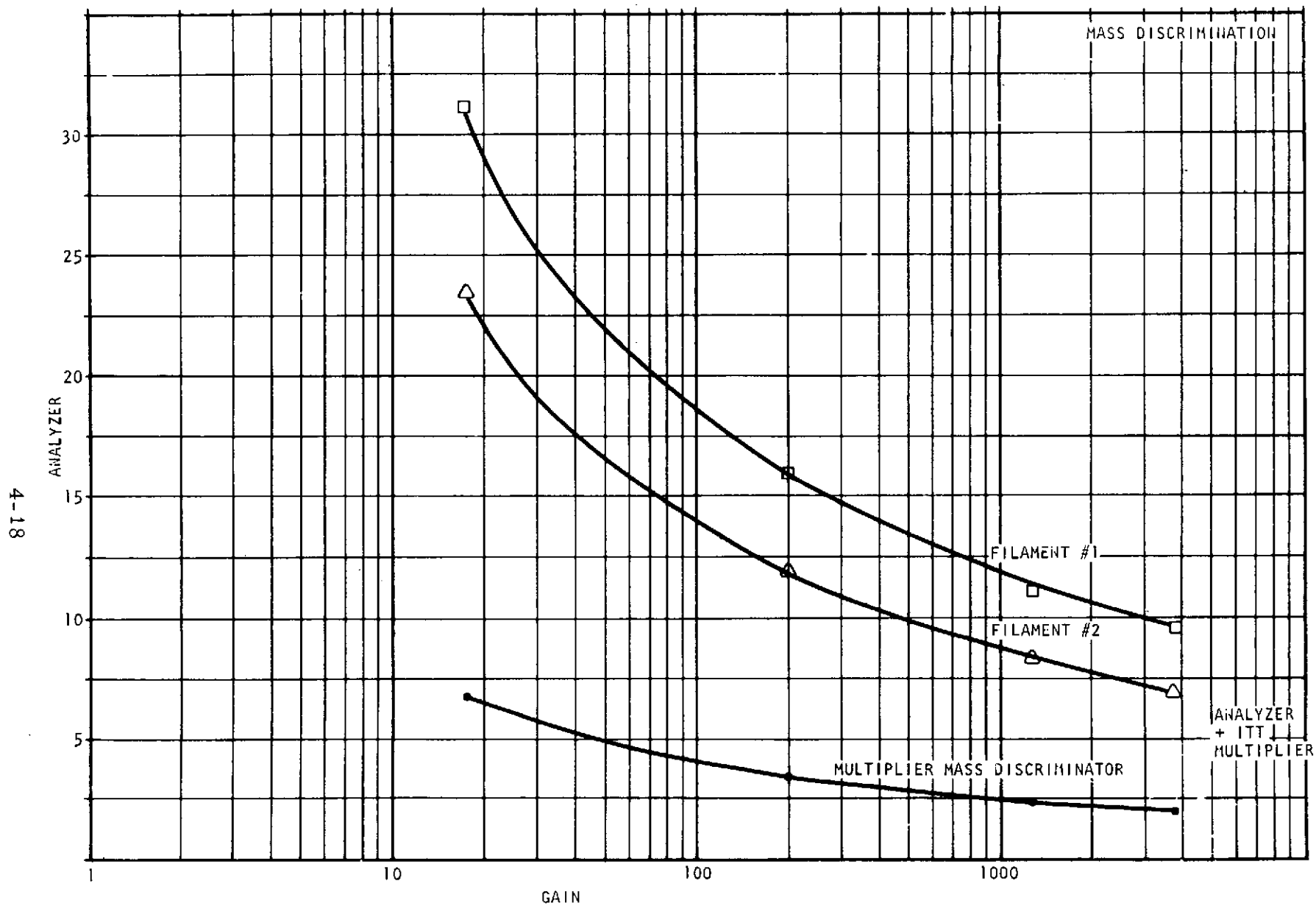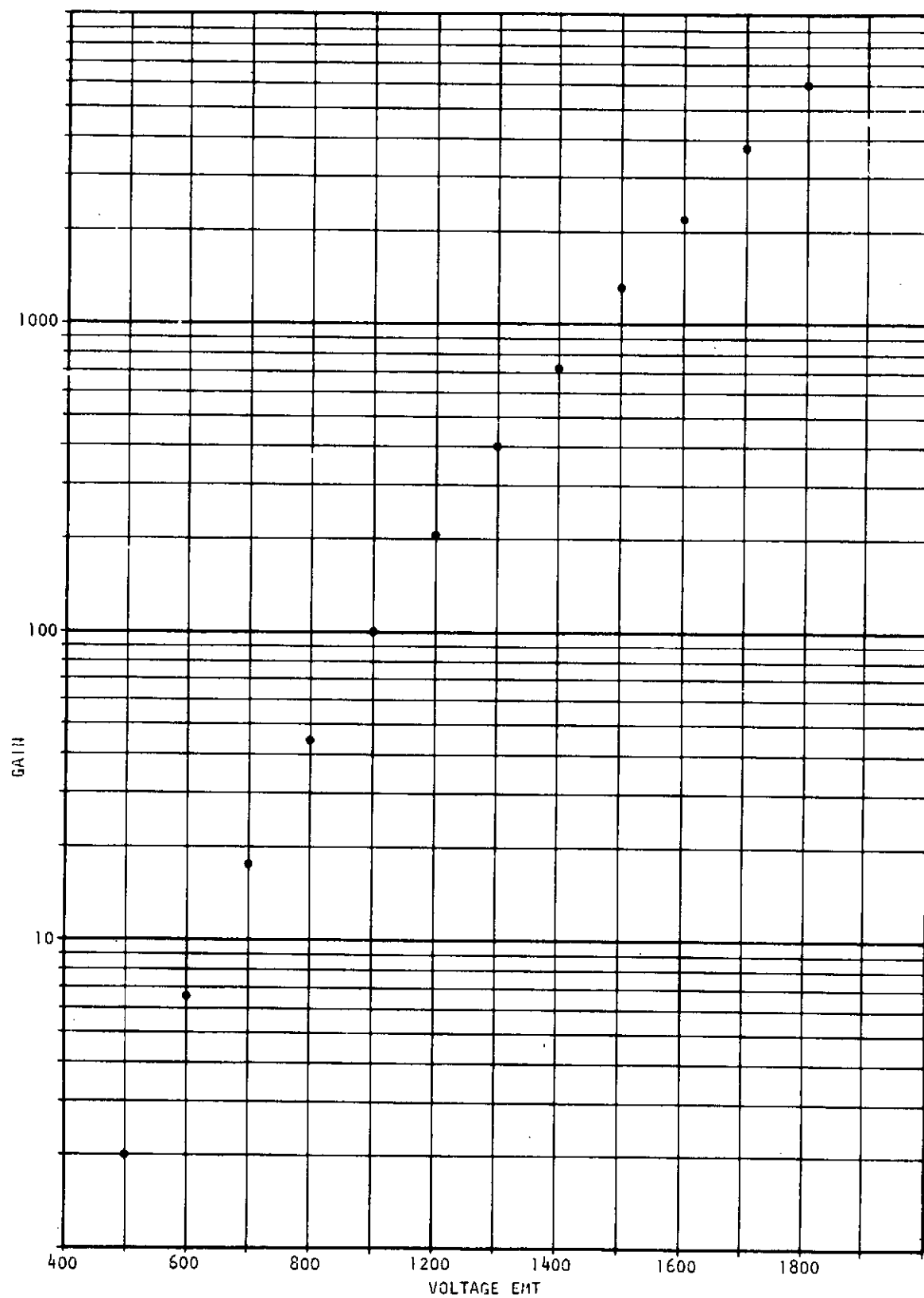
Figure 4-7. Mass Discrimination

Figure 4-8. ITT Multiplier Gain Dependence on Voltage

with a magnetically scanning laboratory mass spectrometer which will eliminate all the sources of mass discrimination discussed above. Thus, the Viking '75 instrument exhibits mass discrimination about 10 times that of laboratory mass spectrometers.

The value measured depends on the approach used in tuning the source. Initially, the source was tuned for optimum resolution at high mass end and sensitivity at the low mass end of the spectra. Some high values for mass discrimination were measured under this condition. See, for example, data for the DTU system in Table 4-4. Subsequently, a compromise was made in tuning procedures to minimize mass discrimination.

4.2.6 Source Pressure, Differential Pumping and Time Constant of the Source

Design analysis for N_2 indicates the source may be operated at pressure up to 1×10^{-4} torr with less than 1 percent error due to space charge. The data for nitrogen tend to substantiate this; the data for PFB-2 indicate that the source pressure should not exceed 1×10^{-5} torr for good linearity. For constant sample flow into the instrument the source pressure is given by

$$Q = C_s (P_s - P_a) = S_p P_a$$

where

$$
\begin{array}{lll}
Q & = & \text{Flow rate} \\
C_s & = & \text{Conductance of the source} \\
P_s & = & \text{Source pressure} \\
P_a & = & \text{Analyzer pressure} \\
S_p & = & \text{Speed of the pump}
\end{array}
$$

The above relation may be expressed as

$$\frac{P_s}{P_a} = \frac{S_p}{C_s} + 1$$

where P_s/P_a is called the differential pumping. A high differential pumping is desirable in that it reduces pump memory effect and also reduces the variation in source pressure due to variations in pump speed. The latter can be shown by differentiating the above expression;

$$\frac{dP_s}{P_s} = \frac{C_s}{(S_p + C_s)} \frac{dS_p}{S_p}$$

Since S_p is of the order of 300 cc/s and C_s is 32 cc/sec at a source temperature of 210°C, then

$$\frac{dP_s}{P_s} = \frac{1}{10} \frac{dS_p}{S_p}$$

Thus, if the pumping speed changes by 50 percent, the pressure in the source will change by only 5 percent. The differential pumping can be increased by increasing the pumping speed and/or by decreasing the source conductance. However, decreasing the source conductance will increase the time constant of the source, which is undesirable.

For the present instrument, the source volume is 2.3 cc and the source conductance is 32.5 cc/sec which gives a time constant of

$$T = \frac{2.3}{32} = 70 \text{ ms.}$$

4.2.7 Temperature

The source is equipped with a nichrome type heater which is vapor deposited on a short ceramic cylinder. The heater is located in the stack of electrodes at the exit from the ion source. A thermistor temperature sensor is located on a ceramic disc on the mounting block. The temperature is normally controlled at $210 \pm 5^\circ$C during organic analysis. For the atmospheric analysis the source is not heated. The thermistor sensor is part of the temperature controller which regulates temperature by controlling the duty cycle of the heater. The existing heater design can operate at 250°C.

4.2.8 Pumping Speed

The analyzer is equipped with a small ion pump which is welded to the magnetic sector housing, (see Figure 4-1). The ion pump was designed for a pumping speed of one liter per second. Typical values of the pumping

speed are of the order of 300 cc/sec for nitrogen at pressures below 10^{-4} torr. Measured values of the pumping speed for various gases are shown in Figures 4-9 through 4-12. Pump current and noise current as a function of pressure are shown in Figure 4-13, and pump current as a function of voltage is shown in Figure 4-14. The ion pump starting voltage as a function of pressure is shown in Figure 4-15. High pressure pumping speeds and time required to pump down from high pressure are summarized in Figures 4-16 through 4-21 for nitrogen, carbon dioxide and hydrogen. These data are summarized in Table 4-5.

A simulated life test was conducted in which the ion pump was operated at 10^{-5} torr of nitrogen continuously. The data are shown in Figure 4-22. The pump exhibited pulsing on day 7 of the test, but this settled down; by day 10, pulses were occurring randomly. On day 22, pulses were occurring at 4 to 7 second intervals. The cumulative charge at day 22 was 288530.7 ma-s. The pump current increased 550 μa at 10^{-5} torr, indicating a short was developing. A 20 ohm short developed between the anode and internal ground of the pump and the test was terminated on day 29. The total amount of gas pumped to day 22 was 5.3 torr liters. These tests were conducted at unusually high pressures and cannot be simply extrapolated to lower pressures. The one point of concern in the pump design is the electrode gap spacing, nominally 0.042 inch. This is relatively short by conventional standards. A larger spacing would be desirable. Pulsing has occasionally been observed in pumps on the analyzer systems but these have been intermittent and have disappeared. The conclusion is that the pump appears to be satisfactory but not ideal from the conservative design viewpoint.

There were some questions that the baffled aperture into the pump was a restriction on the pumping speed measurements. A recent calculation of the conductance of this aperture indicates that this is not the case.

4.2.9 Minimum Detectable Levels

The minimum detectable signal is established from the acceptable signal-to-noise (S/N) ratio and the noise current for the detection electronics system. The design criterion for the Viking '75 system is
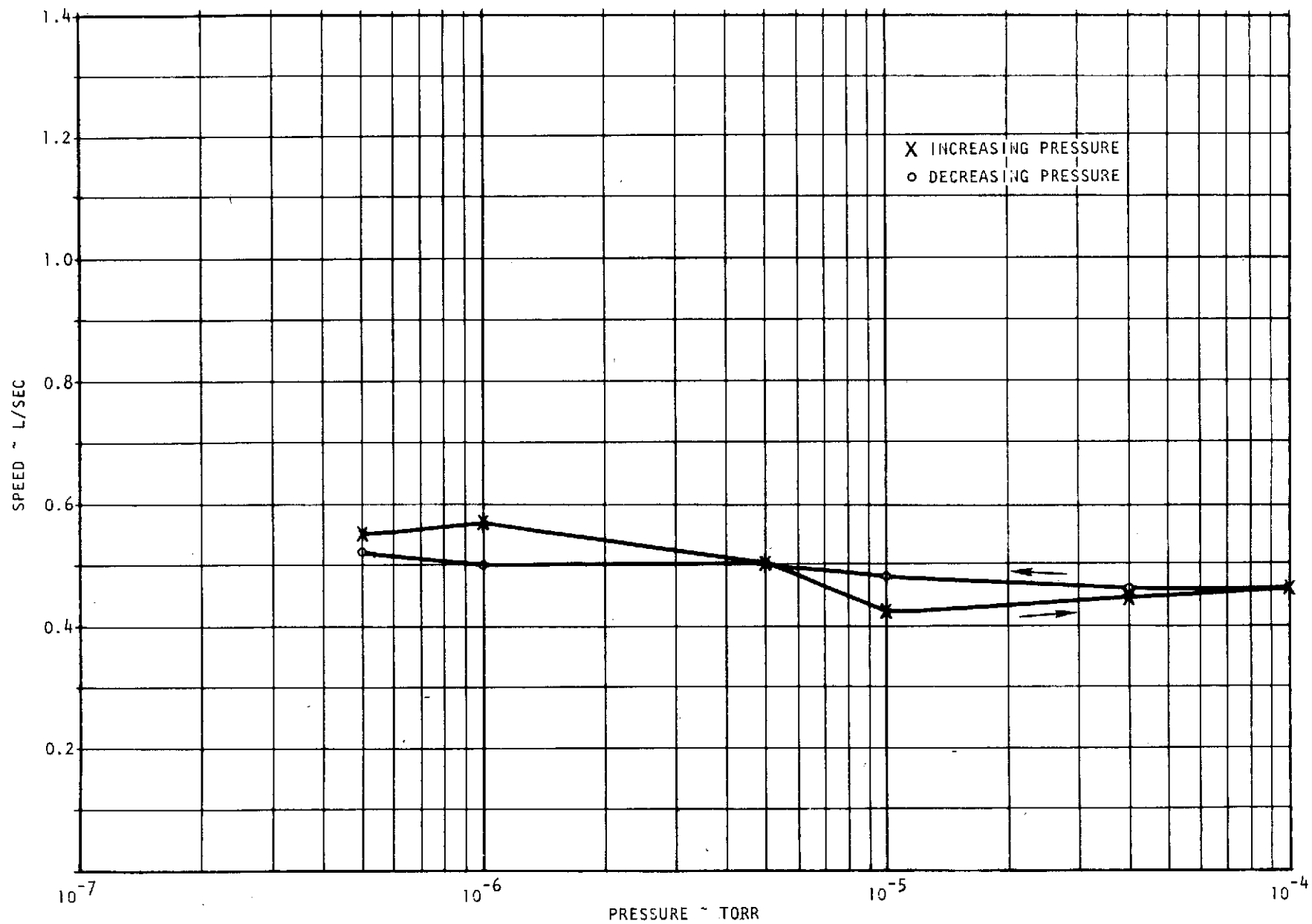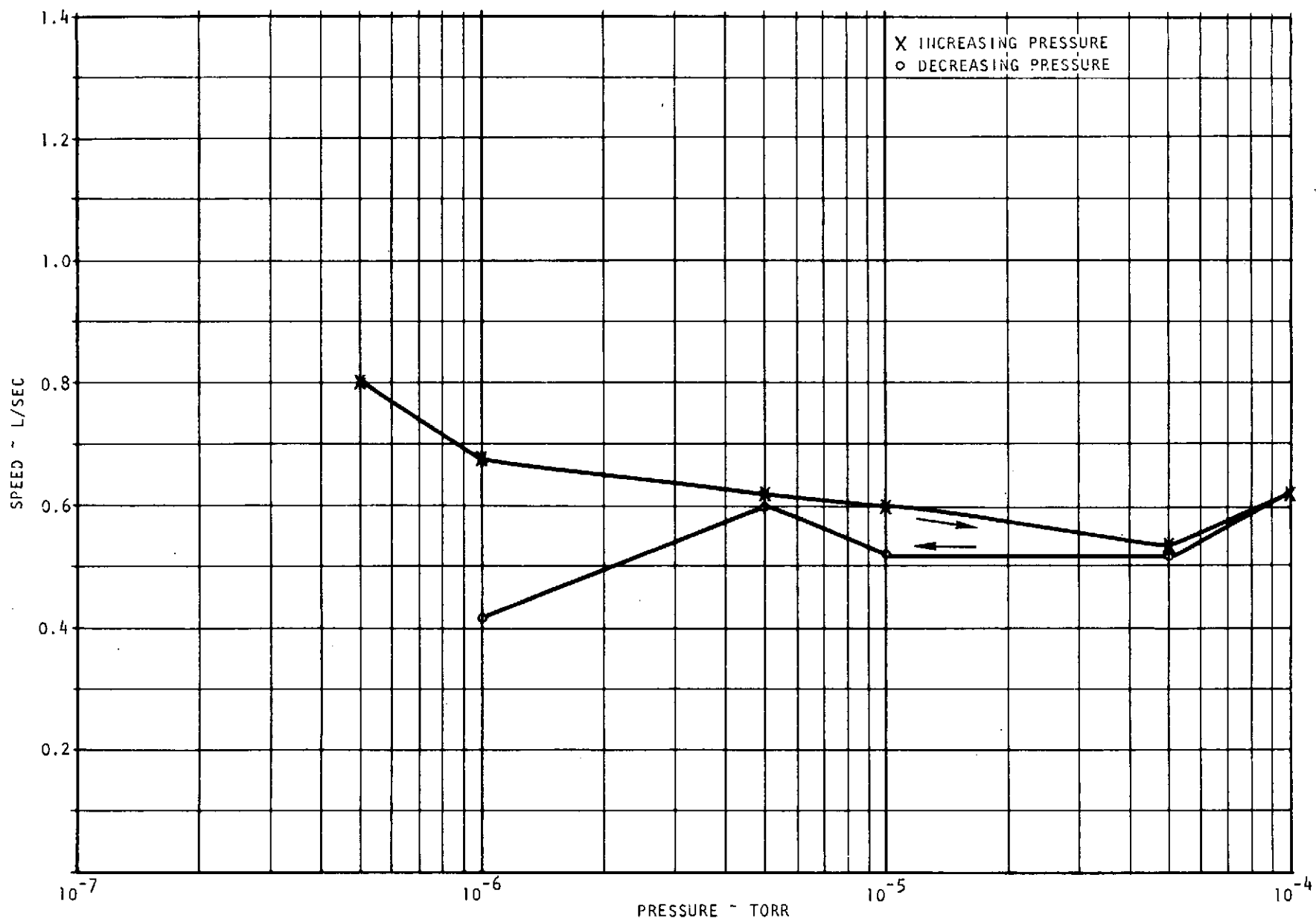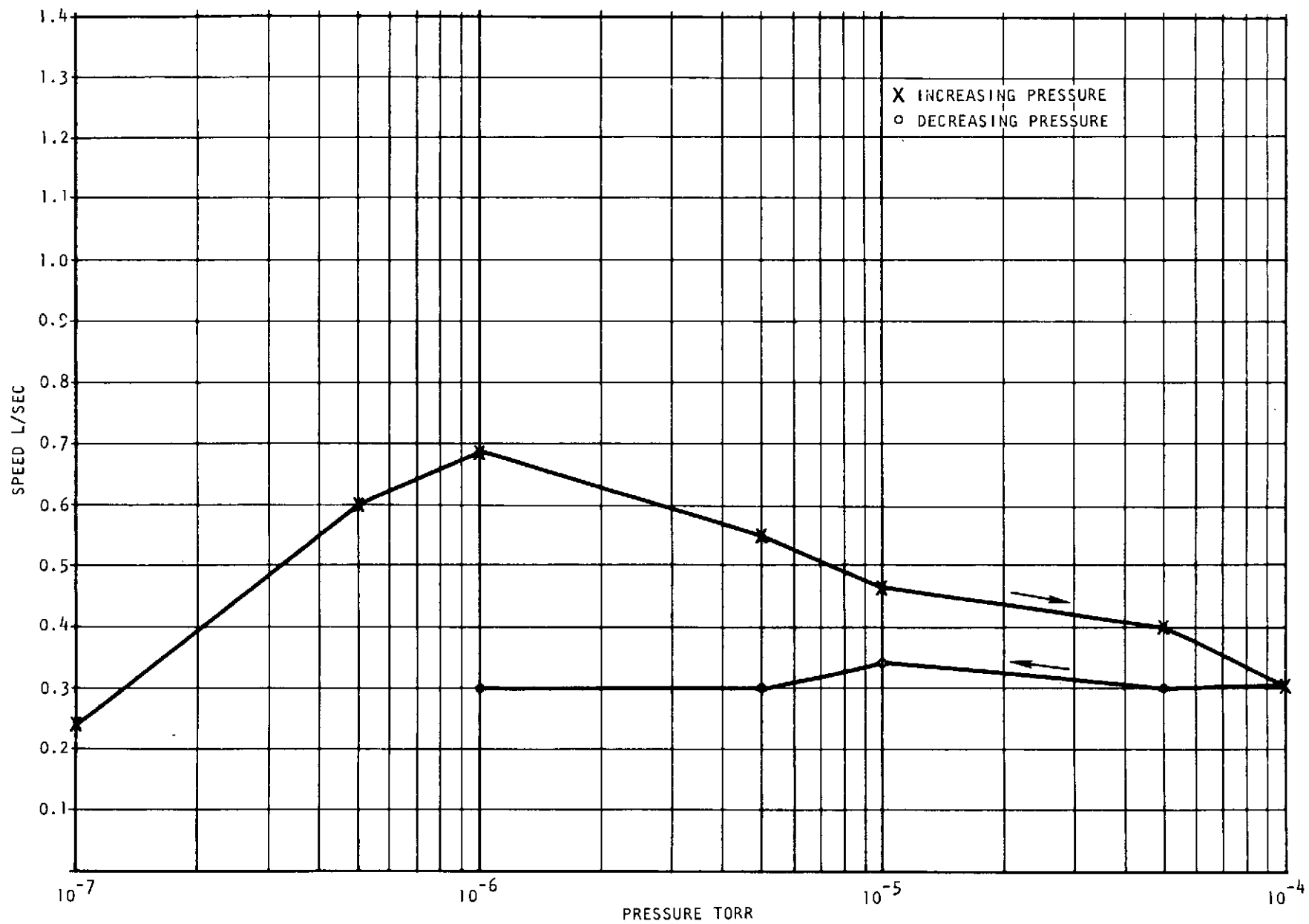
Figure 4-9. Pumping Speed Air

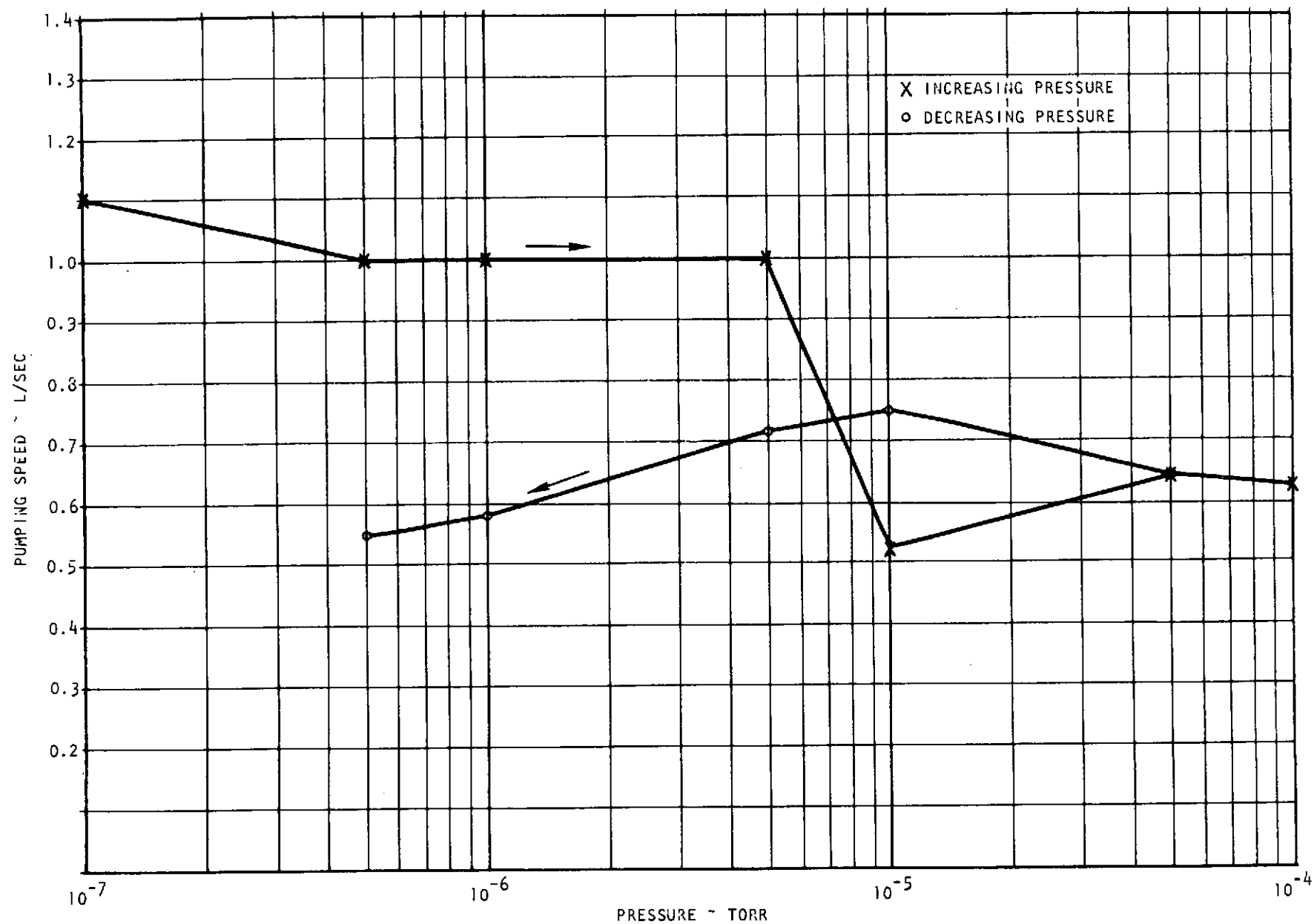Figure 4-10. Pumping Speed CO_2

Figure 4-11. Pumping Speed H_2

Figure 4-12. Pumping Speed Freon C-318 (Octabluorocyclobutane)
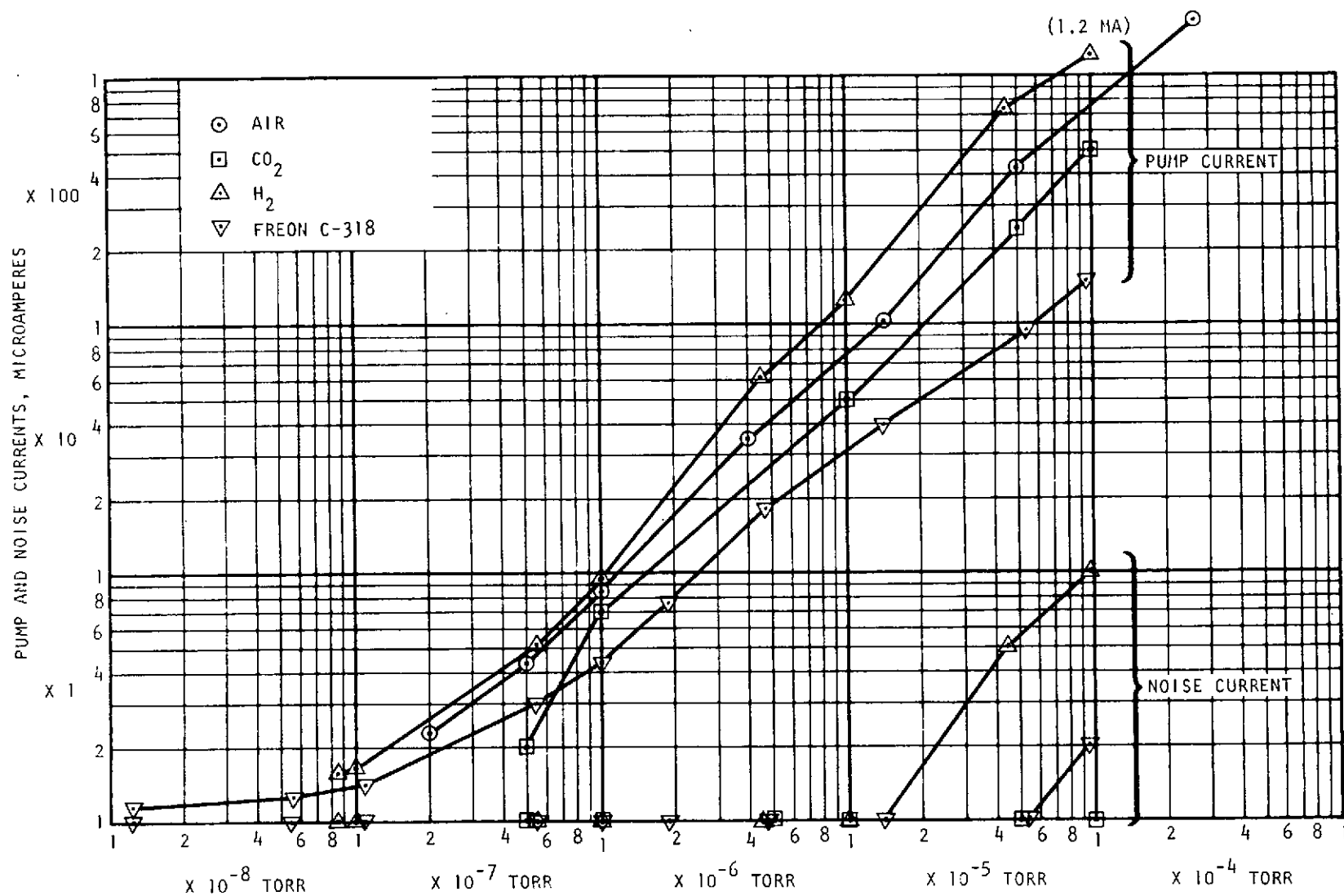
Figure 4-13. Ion Pump Current as a Function of Pressure
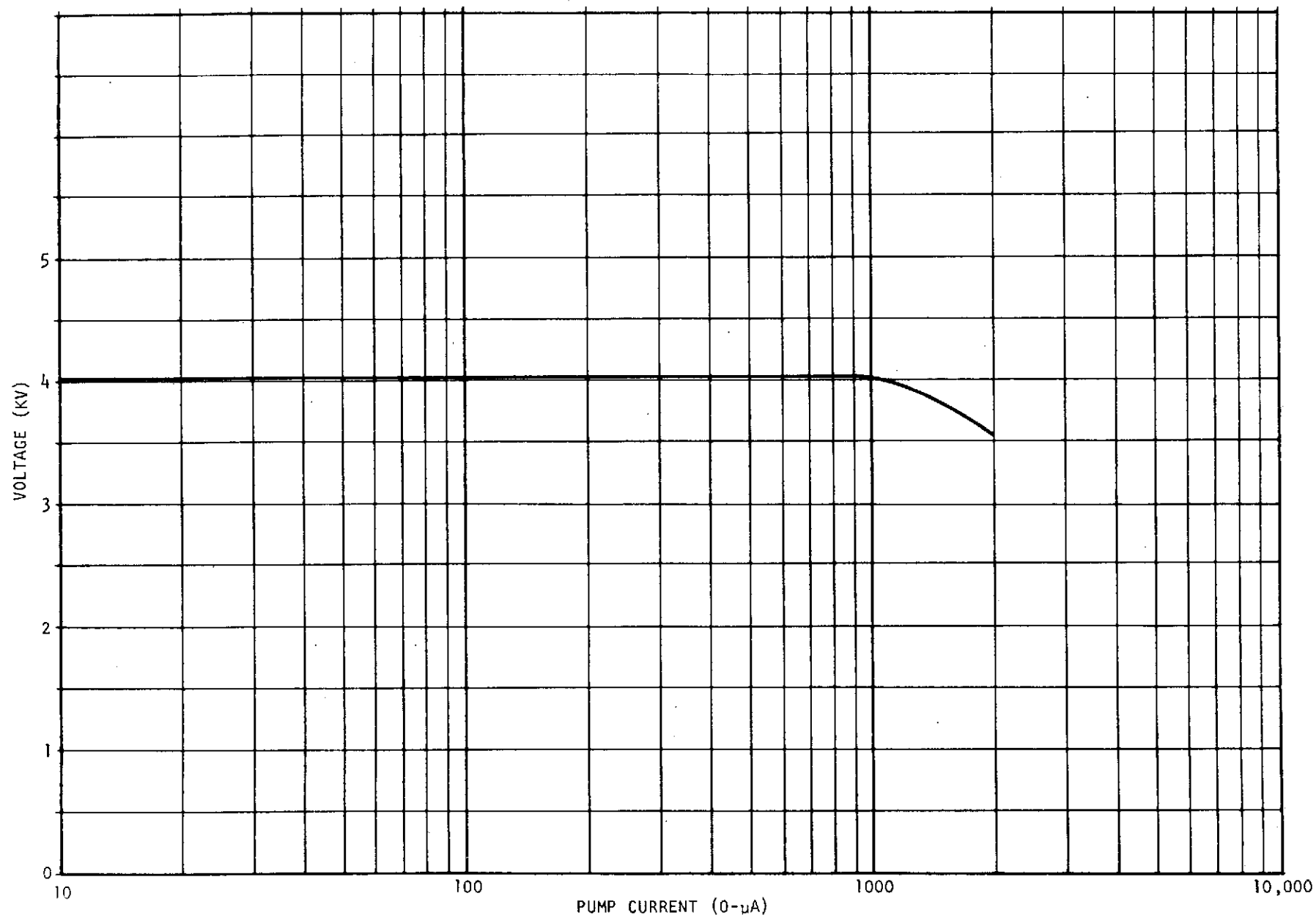
Figure 4-14. Ion Pump Voltage Versus Current for all Gases
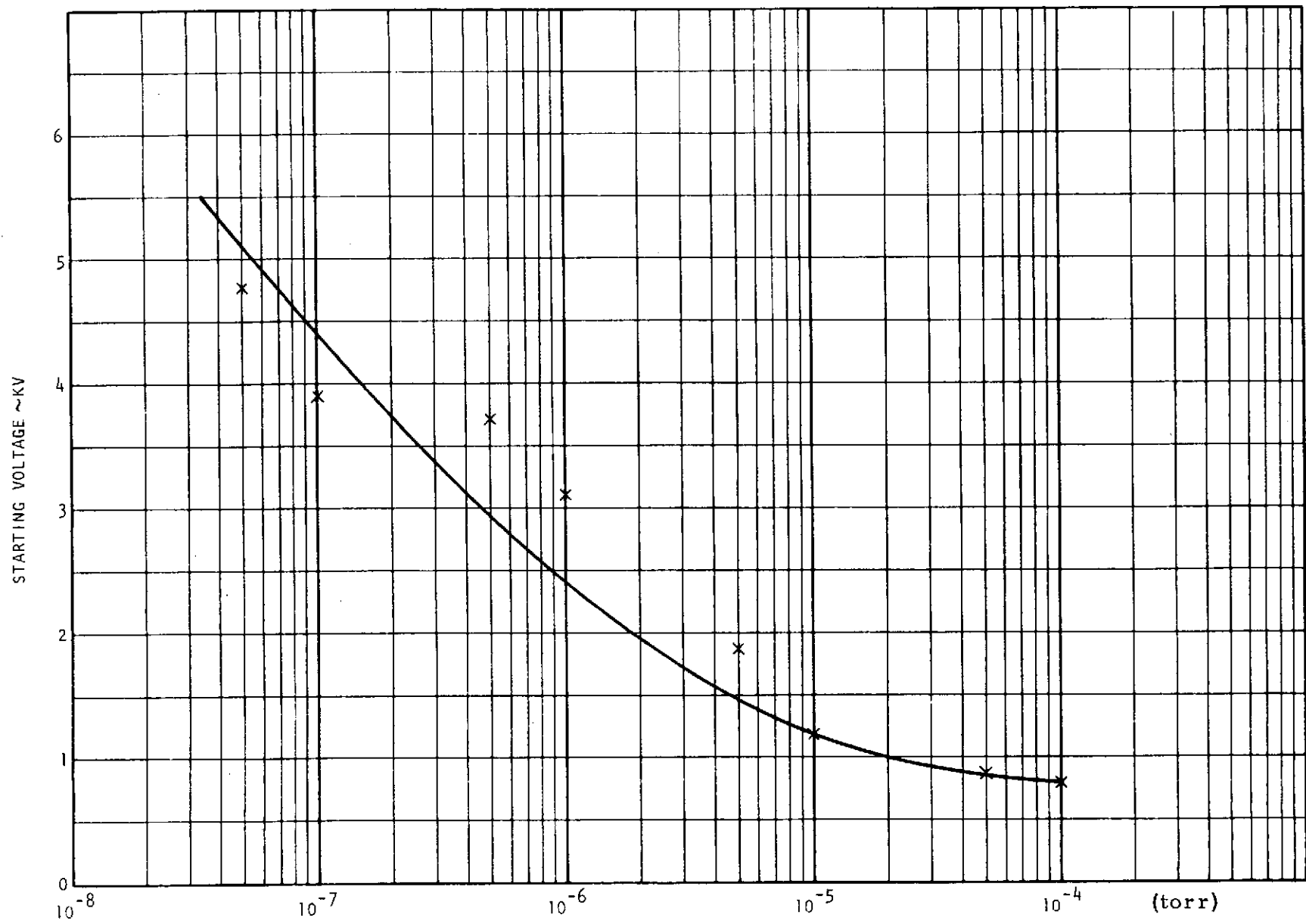
Figure 4-15.   Ion Pump Evaluation, High Pressure Starting Test
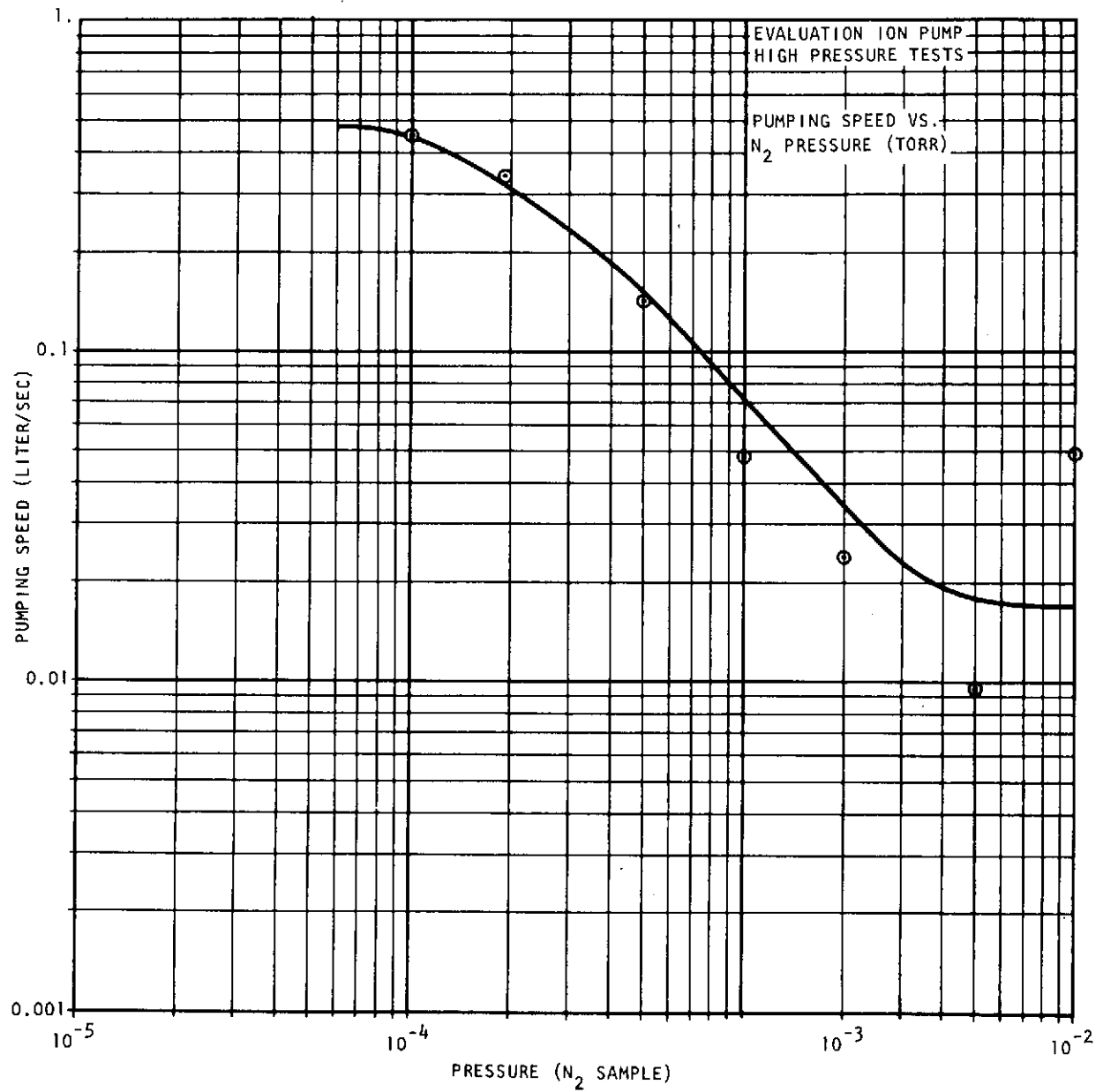
Figure 4-16. Ion Pump Evaluation High Pressure Test,
Pumping Speed Versus N_2 Pressure
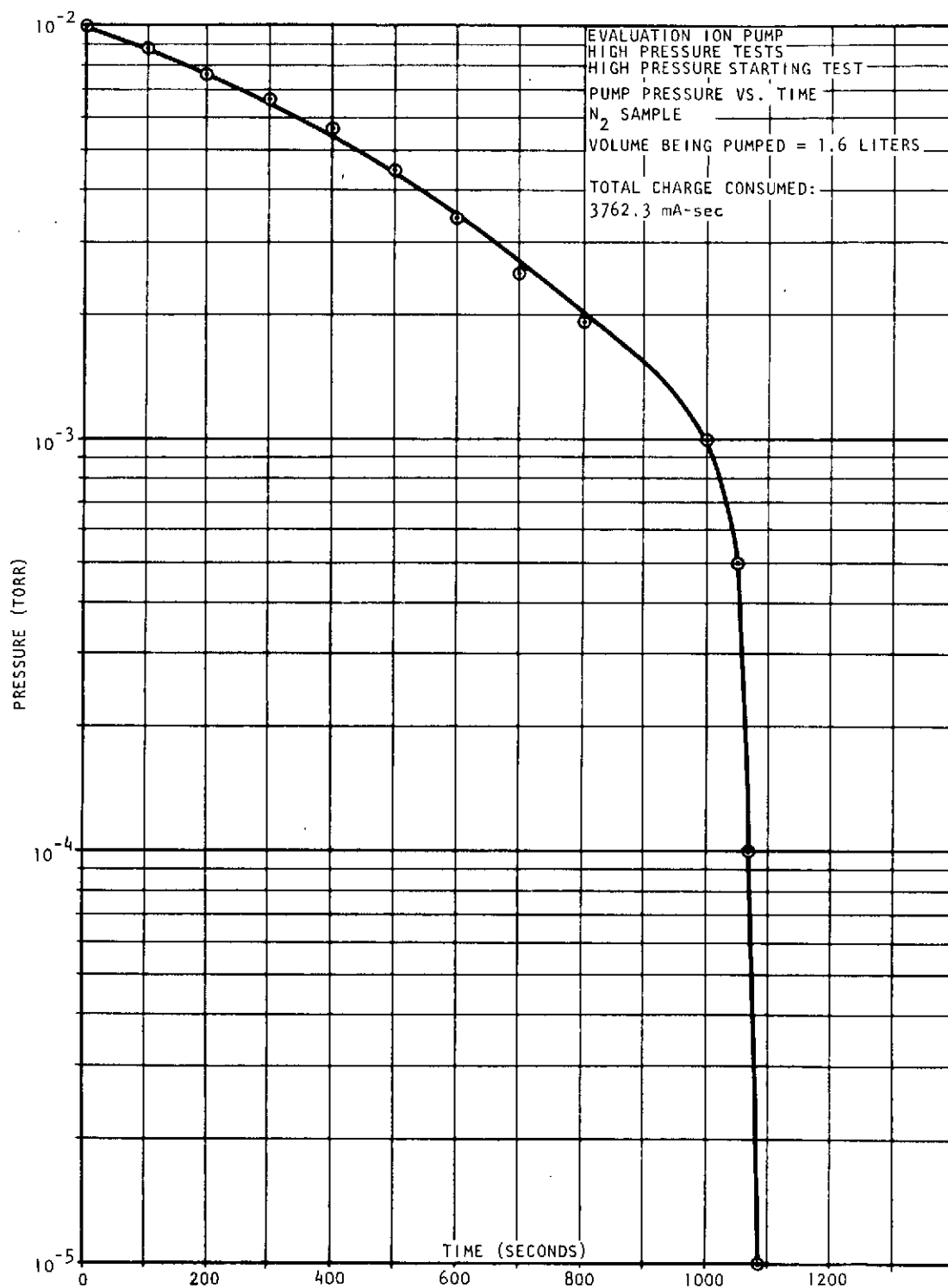
Figure 4-17. Ion Pump Evaluation High Pressure Starting Test
Pump Pressure Versus Time, N_2 Sample
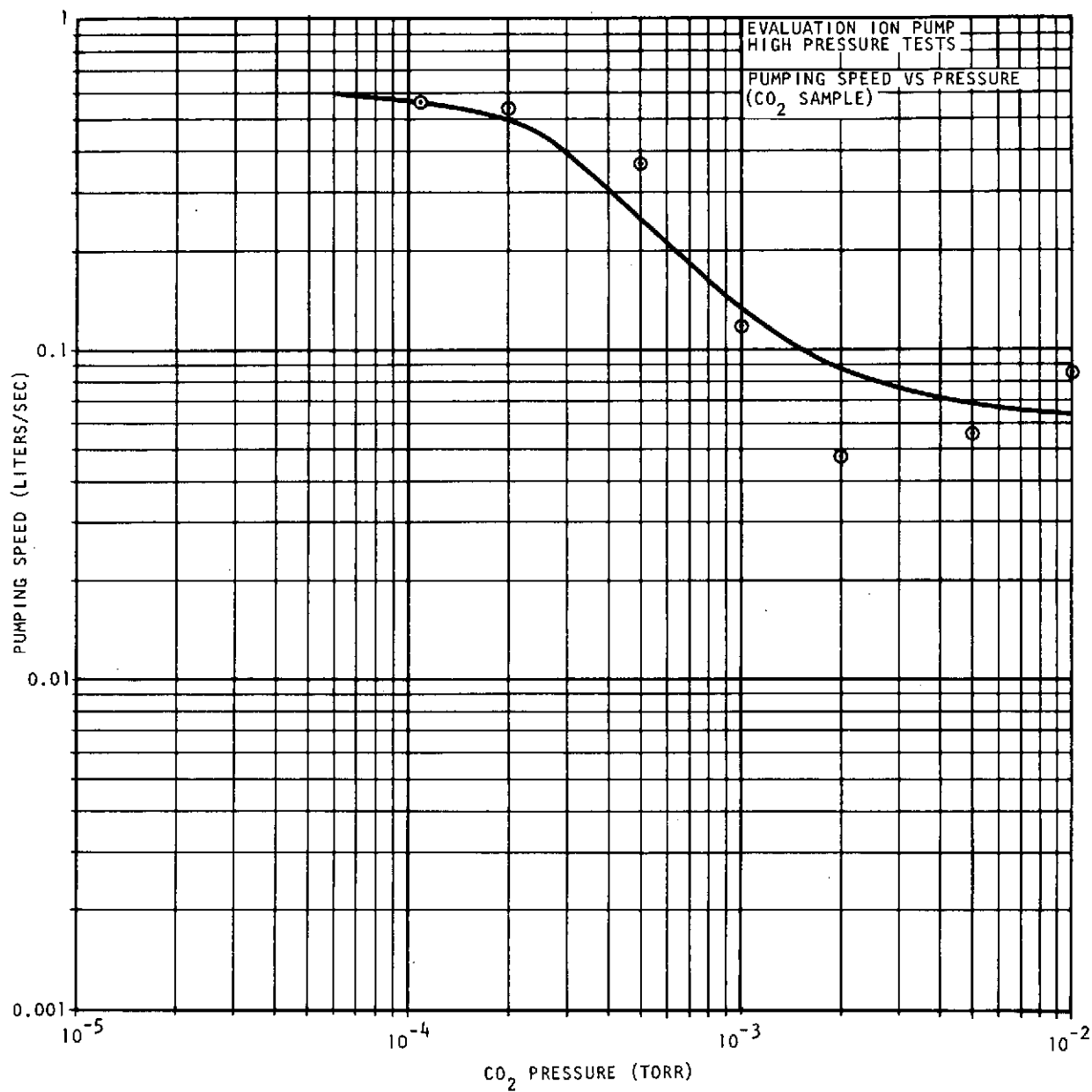
Figure 4-18. Ion Pump Evaluation High Pressure Test,
Pumping Speed Versus CO_2 Pressure
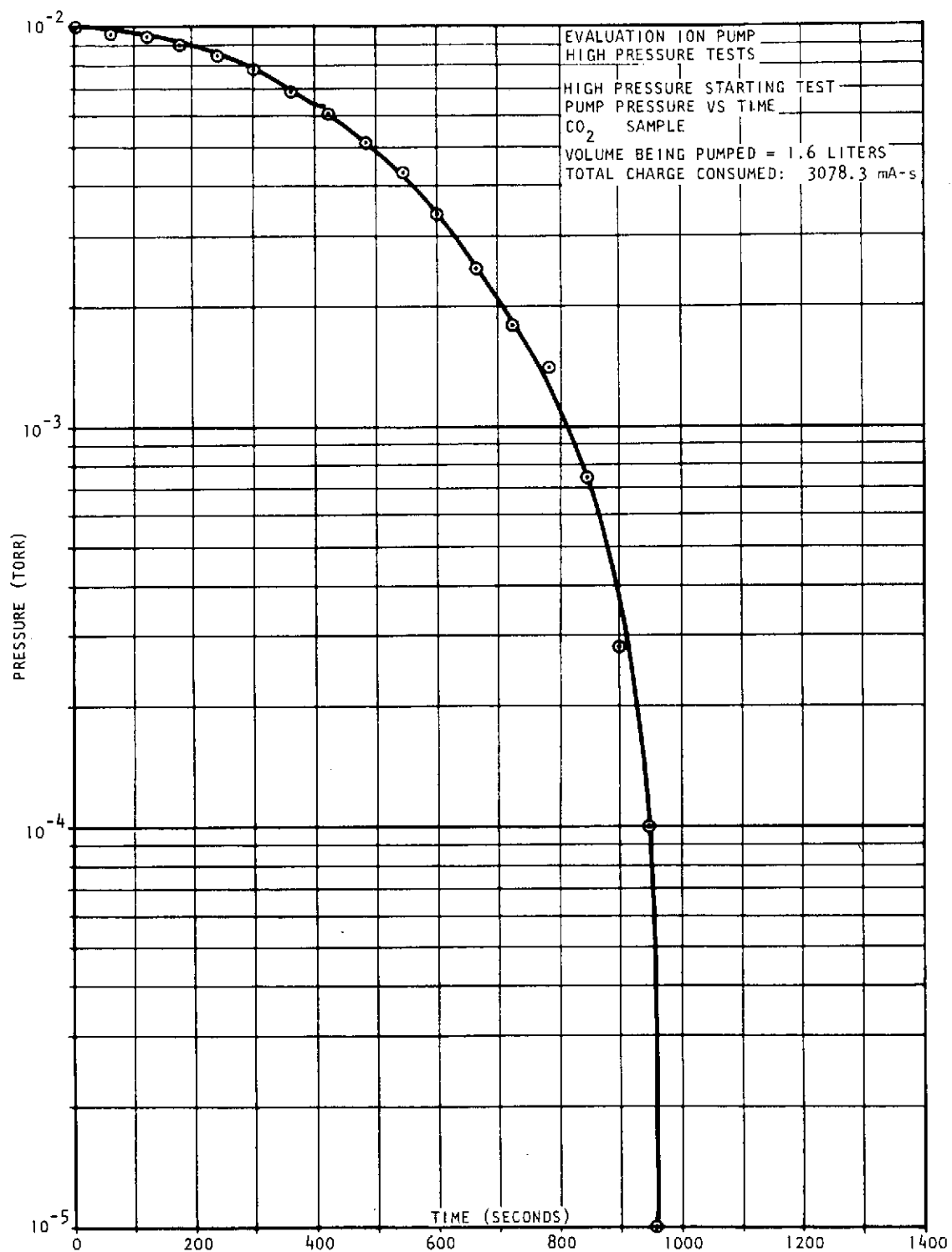
Figure 4-19. Ion Pump Evaluation High Pressure Starting Test
Pump Pressure Versus Time, CO_2 Sample
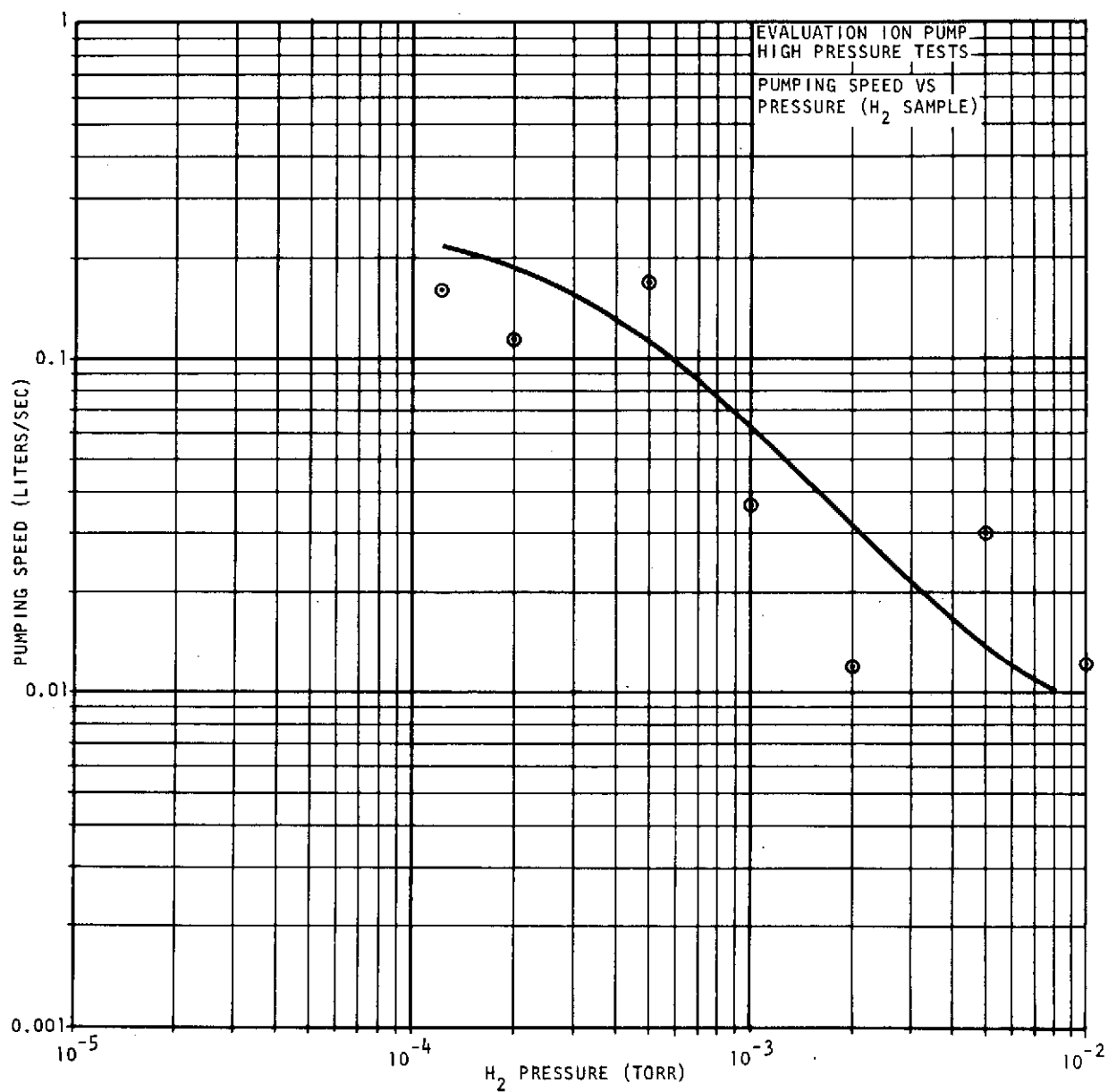
Figure 4-20. Ion Pump Evaluation High Pressure Test,
Pumping Speed Versus H_2 Pressure
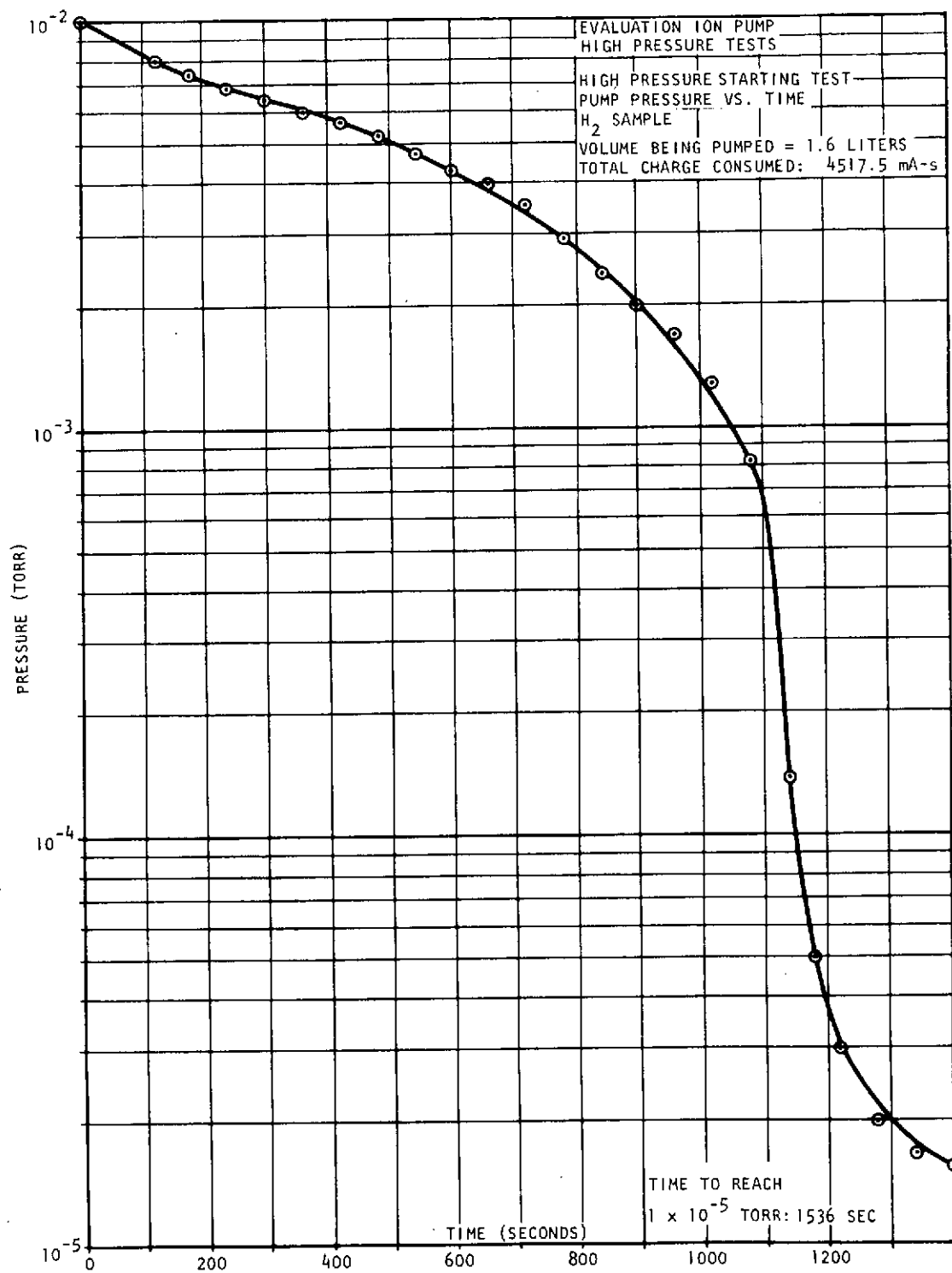
Figure 4-21. Ion Pump Evaluation High Pressure Starting Test
Pump Pressure Versus Time, H_2 Sample

Table 4-5. High Pressure Pumpdown Data

To Reach 4.0×10^{-5} Torr

Starting Pressure (torr)	N_2 Sample		CO_2 Sample		H_2 Sample	
	Charge (mA-s)	Time (s)	Charge (mA-s)	Time (s)	Charge (mA-s)	Time (s)
1×10^{-3}	112.2	60	124.2	65	128.2	160
2×10^{-3}	1025.1	310	436.5	159	345.7	265
5×10^{-3}	2032.3	600	1392.7	451	1479.7	687
1×10^{-2}	3762.3	1080	3078.3	955	4517.5	1536
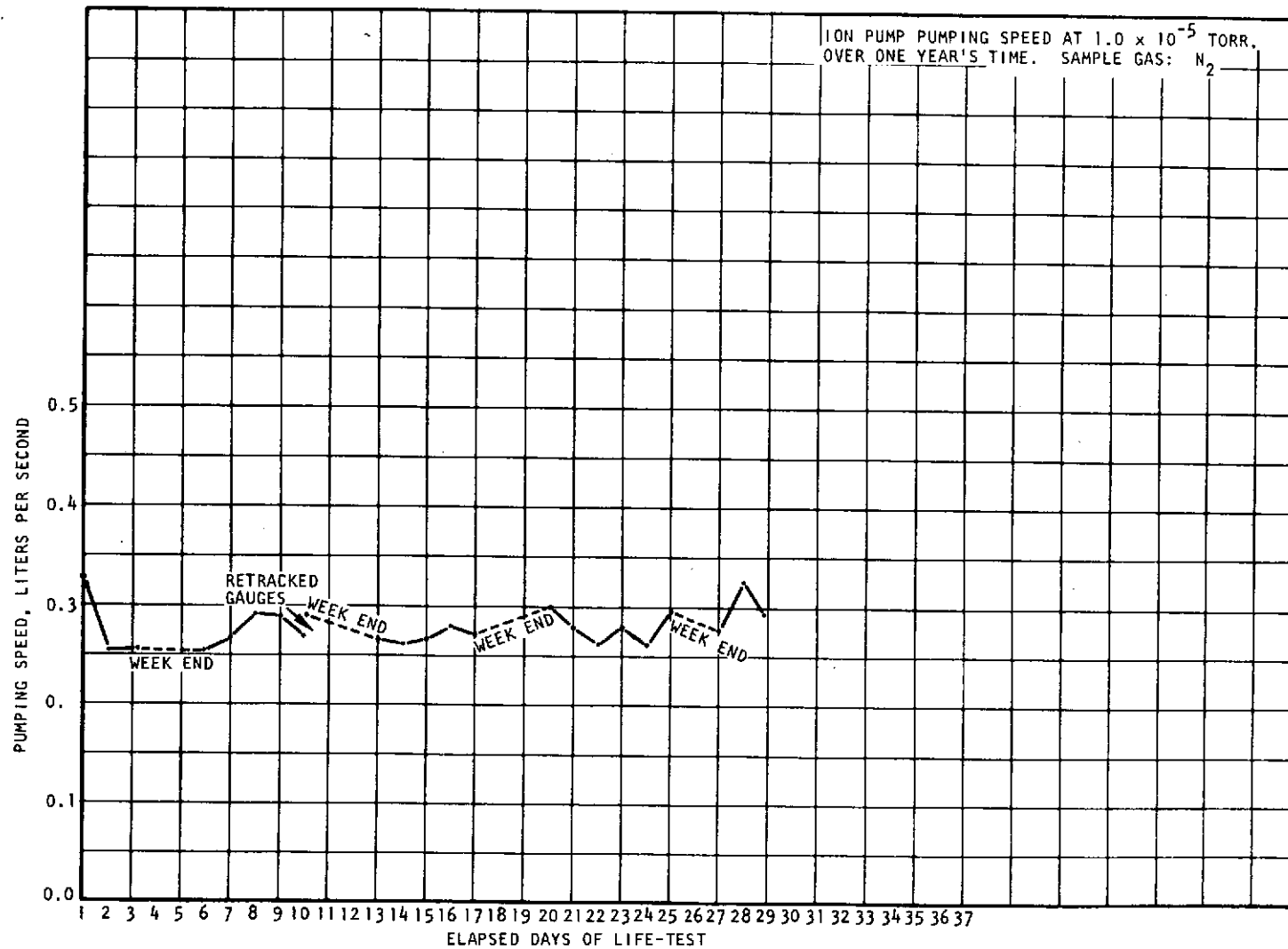
Figure 4-22. Ion Pump Life Test

S/N = 3 at a signal of 10^{-11} amps. At an EMT output of 10^{-11} amps, and an EMT gain of 2000, this electrometer noise current is 1.26×10^{-12} amps which is slightly greater than the 5×10^{-13} amp effective electrometer input noise. The S/N ratio is 4.4, peak signal to rms noise. The minimum detectable signal at an ion source sensitivity of 3×10^{-6} amp/torr and conductance of 32 cc/sec corresponds to a nitrogen flow rate of 0.5×10^{-14} g moles/sec.

For an organic compound in a gas chromatograph peak with a 30-second base peak width and a requirement to detect a 1 percent fragment ion, the total amount of sample required for detection is of the order of 0.01 nanomole. This estimate must be modified for potentially higher noise levels if the bandwidth needs to be increased for the mass range required.

Other factors related to minimum detectable signal are described in the dynamic range section.

4.2.10 Dynamic Range

The dynamic range is principally determined by the minimum detectable signal and the maximum source operating pressure. The minimum detectable signal corresponds to a source pressure of approximately 3×10^{-9} torr. The maximum source operating pressure can be established by accepting the maximum source pressure that can be utilized with linear output, or if some compromise can be accepted in response linearity, the maximum source pressure consistent with the available pumping speed. The maximum source pressure based on pumping speed limitations is of the order of 5×10^{-4} torr. This would imply that the maximum dynamic range in the mass spectrometer would be of the order of $\pm 10^{6}$. The minimum dynamic range determined by source linearity (maximum source pressure equal to 1×10^{-5} torr) would be of the order of 2×10^{4}. In practice, it would probably be desirable to limit the dynamic range to the lower value in order to avoid formation of insulating deposits within the analyzer.

The dynamic range for the resolved ion current electrometer is 10^{6}. The electron multiplier gain control circuitry allows the EMT to operate

at gain range of a factor of 20 which increases the output signal dynamic range to 2×10^{7}.

Factors limiting the dynamic range for output signal from adjacent mass numbers are: electron multiplier memory, logarithmic amplifier characteristics, and tail on the peaks. For an output pulse of 10^{-6} amps of 20 ms duration, the signal from the ITT multiplier decays by a factor of 10^{3} in 5 ms, and by another factor of 10^{3} in the succeeding 100 ms. The time between adjacent mass numbers decreases with increasing mass number. At mass 200 for example, the time between mass numbers is roughly 17 ms; a mass number adjacent to a large signal pulse would be detectable only if its amplitude were greater than 10^{-3} to 10^{-4} that of the large signal. Figure 4-23 shows the nearest peak number for which the 10^{6} dynamic range is available as a function of mass number
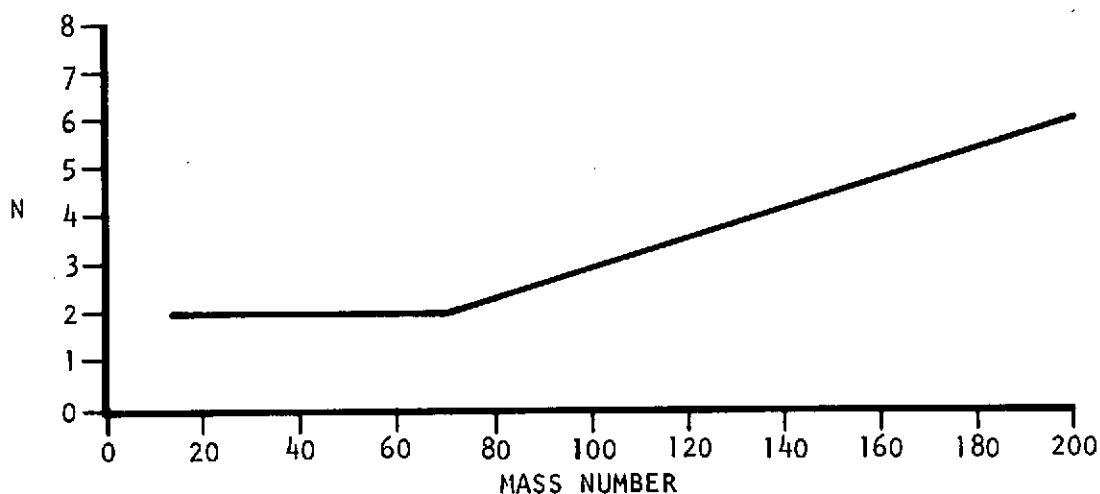

Figure 4-23. The Number N of the Closest Peak for Which the Dynamic Range is 10^{6} as a Function of Principal Peak Mass Number

Figure 4-24 shows the output signal dynamic range for mass numbers following a large signal.
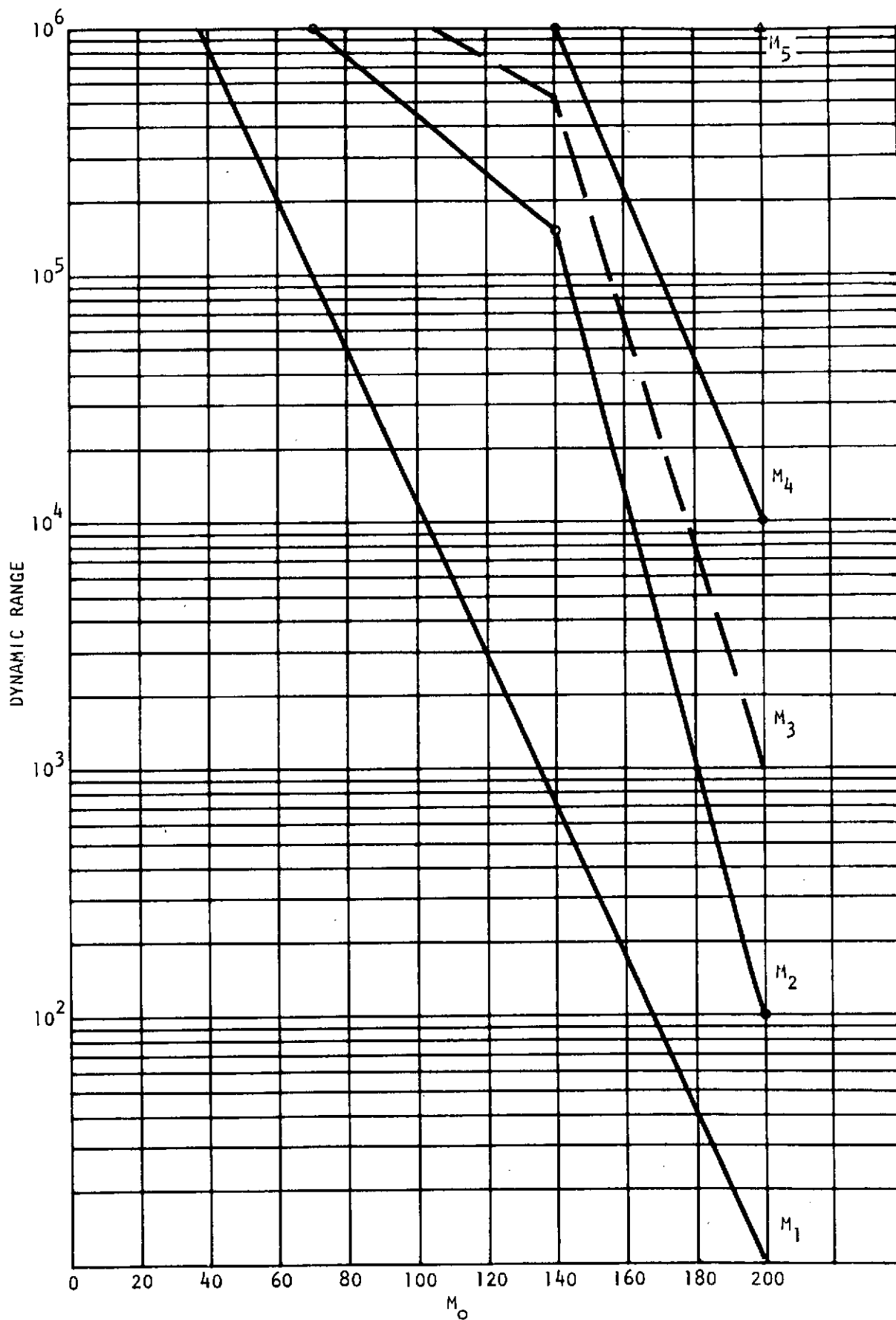
Figure 4-24. Dynamic Range of Peaks Following Principal Peak M_o

One additional feature of the log amp operating characteristics is that on return from a rapidly decaying signal the amplifier response time is such that the amplifier undershoots the actual signal. Recovery from this condition requires an interval of time which can overlap adjacent mass numbers and cause small signals adjacent to large ones to be undetected.

4.2.11 Background Levels and Pump Memory Effects

The observed background levels in the mass spectrometer are low. The major peaks observed are always low mass ions, m/e 18, 20, 28, 40 and 44. There is generally no detectable background at mass numbers greater than 44. Since the mass range of interest for the amino acid analysis is from m/e 50 to 240, there should be little problem with mass spectrometer background.

Pump memory effects have been observed in successive samples of nitrogen and perfluorobutene-2. As was previously discussed, the Qual system has a differential pumping of about 10 while the ABMS and the DTU units have a differential pumping of 7. A test was conducted on the ABMS analyzer to determine the existence of pump memory. Pump memory lasting about 10 minutes was observed. However, it should be remembered that the PFB-2 load was a factor of 40 larger than the largest load expected from the GC and also that the differential pumping was 7 instead of the present 10.

4.2.12 Sample Interfaces

The mass spectrometer interfaces with two sample systems through two valves. A restrictor is placed in series with the valve that interfaces with the atmospheric inlet system. The interface with the hydrogen separator is valved. The GC effluent passes through the effluent divider, where a selected portion of the effluent is vented. The effluent going to the mass spectrometer passes through the hydrogen separator, where the hydrogen carrier gas is removed. The organics stripped of the hydrogen carrier gas enter the mass spectrometer through the valve. The system is shown in Figure 4-25.

The effluent divider permits the effluent to be split in the ratios 1:1, 1:3, 1:20, 1:400 and 1:8000. (The figure does not show the 1:3 divider

4-41
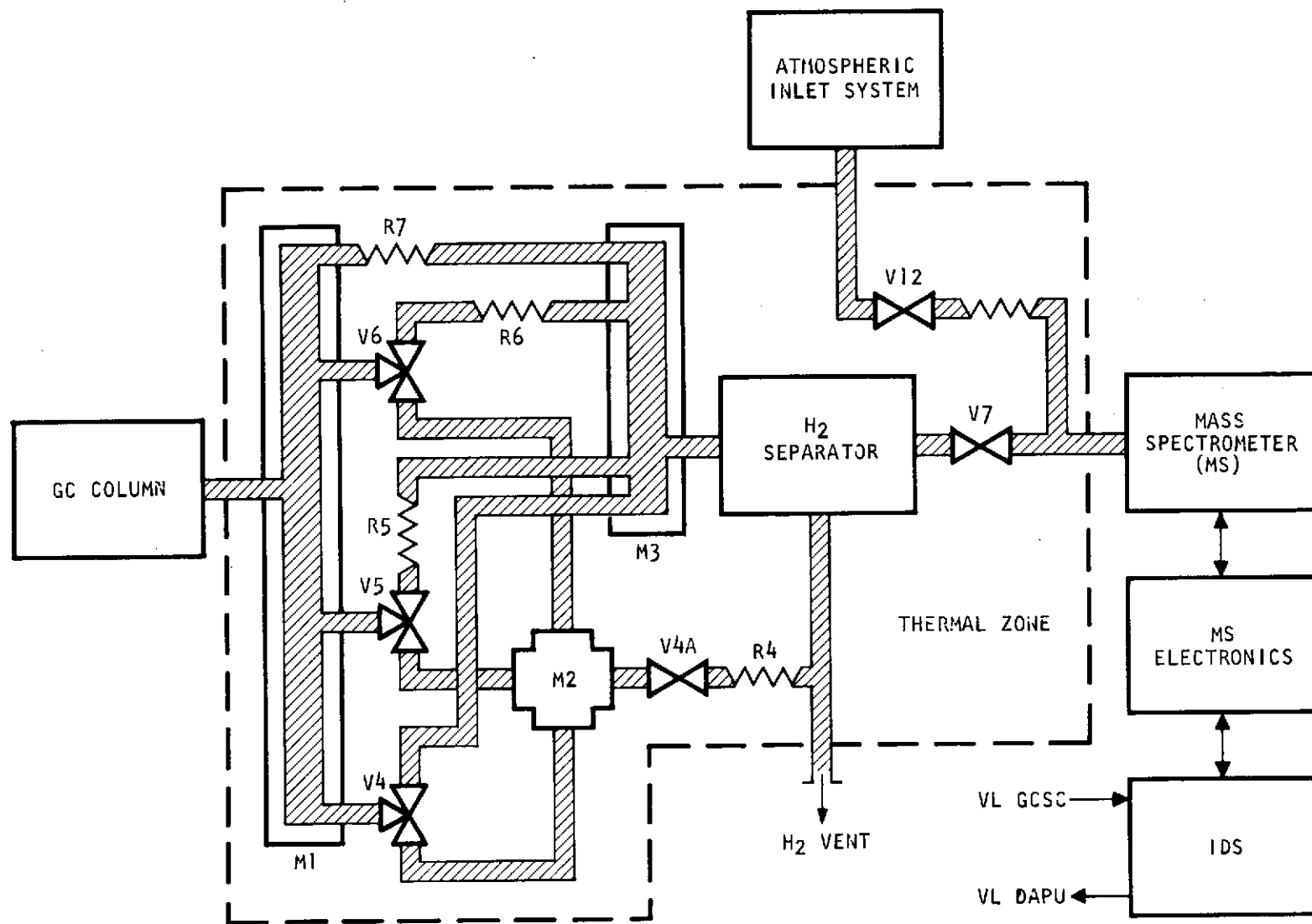
Figure 4-25. Sample Interface

loop.) The split level is controlled by a high level, low level discriminator circuit operating from the ion pump current. At the start of chromatogram the highest divider ratio is selected. On signal, the split ratio is reduced to obtain the necessary sensitivity for detection of the GC peaks.

The hydrogen separator is a palladium silver tube which acts as the anode of an electrochemical cell. Hydrogen diffuses through the anode and is oxidized to water in a molten alkali-metal hydroxide electrolyte. Water is reduced at the cathode and hydrogen evolved to the vent system. Minimum operating temperature of the cell is reported to $175^{\circ}C$. The efficiency of the separator is high; virtually all the hydrogen is removed at the maximum GC flow rate of 2 standard cc/min.

4.2.13 Low Voltage Ionization

For organic analysis, an electron energy of 70 ev is employed in the Viking '75 system. In the atmospheric analysis, both 70 ev and 45 ev ionization energies are used. The 45 ev capability is primarily included to eliminate the interference of doubly ionized argon with the measurement of neon at m/e 20. Ionization of organics at 45 ev does not substantially reduce fragmentation. Voltages of the order of 10 volts are required to obtain only molecular ion peaks. The sensitivity decreases by at least one to two orders of magnitude at these ionization energies, and it does not appear practical to utilize low voltage ionization for organic analysis with the Viking '75 analyzer.

4.2.14 Total Ion Current Monitor

The total ion current monitor is a circular electrode located at the exit from the object slit in the ion source assembly. This electrode intercepts a portion of the ion beam and is used to monitor GC peak. The output of the electrode is fairly sensitive to the scan voltage; it decreases roughly by the square root of the accelerating voltage. At system test level with flight electronics, the TICM current decreases by a factor of 3 as the voltage scans down exponentially from m/e 12 to m/e 200 peaks.

The response of this electrode to source pressure for N_2 is shown in Figure 4-26.

4-43
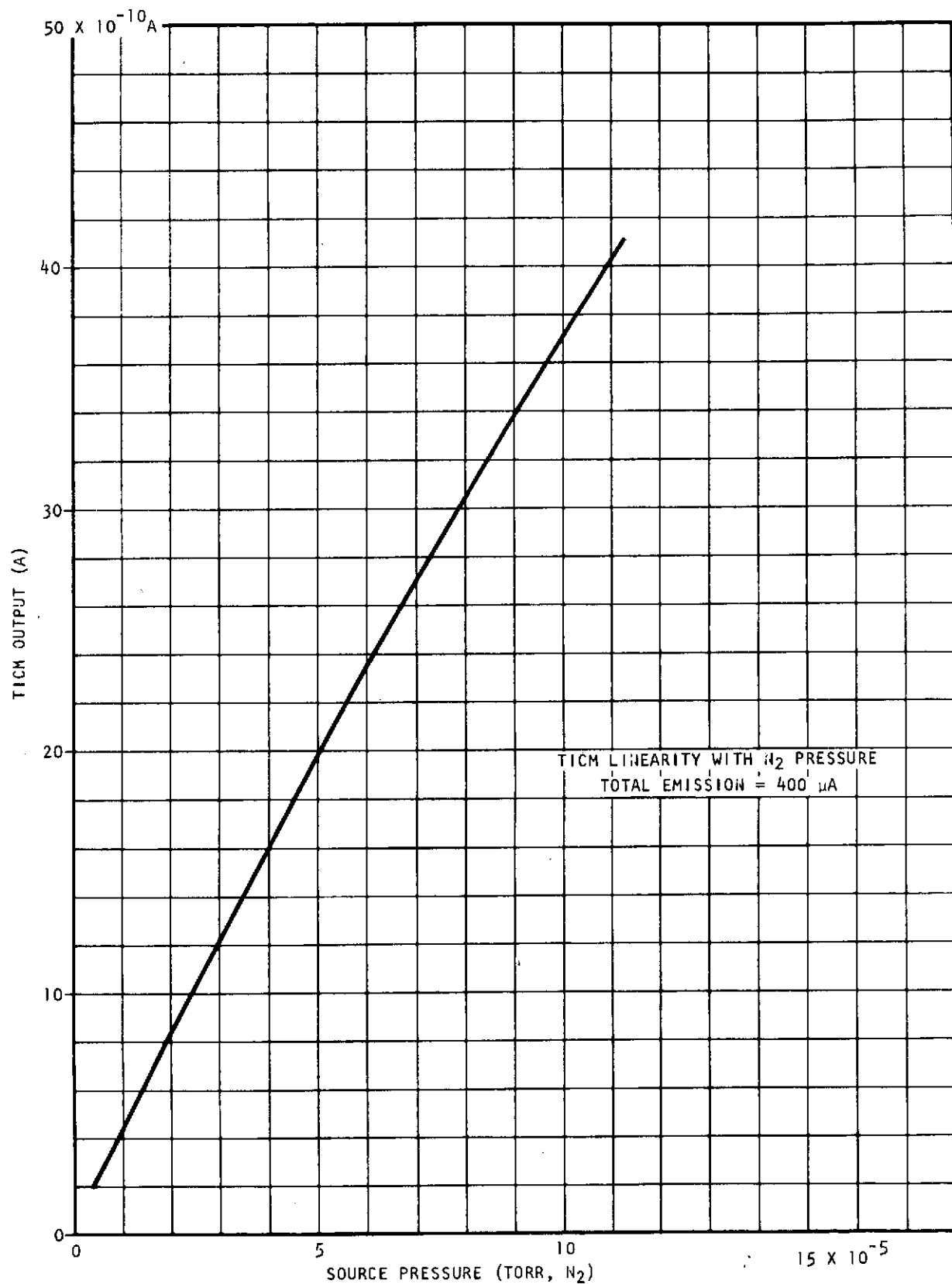
Figure 4-26. TICM Output as a Function of Source
Pressure at 400 μa Emission

4.2.15 Physical Parameters

4.2.15.1 System Weight

Mass Spectrometer Analyzer	6.0 lb
Electronics	9.5 lb
Electronics Tray	3.5 lb
Total M.S. (excluding G.C. portion which is ~ 10 lb)	19.0 lb
Instrument Electronics System	
Portion of system used by MS	(0.82 lb)
Total Tray Assembly	9.0 lb
Instrument Data System	5.4 lb

The weight of the mass spectrometer analyzer and the electronics essential to its operation are summarized in the first part of the table. Certain power supplies and controls which are contained in the instrument electronics tray are used by the MS system. An estimate of the weight of these components is indicated in brackets in the second part of the table. It is not possible at the present time to assess what portion of the Instrument Data System to assign to mass spectrometer operation. The value is the total weight of the system.

4.2.15.2 System Volume

The mass spectrometer analyzer and its electronics are contained on a tray 10 3/4 inches by 13 inches; this tray also contains the Viking '75 gas chromatograph and atmospheric inlet system. The volume occupied by the analyzer is 10 3/4 inches by 6 inches on one side of the tray. The electronics are contained in the opposite side of the tray in a 2-inch high module which fills the whole tray area (10 3/4 inches by 13 inches). The volume of the system is estimated at 500 cu in.

4.2.15.3 System Power

Current operating power is estimated at 27.5 watts with the ion source at 210°C. During heatup of the source the heater draws approximately 25 watts of power continuously. It takes approximately 20 minutes to heat the source to 210°C from lab ambient.

4.2.16 Electronic Error Analysis

The error analysis presented in this section summarizes the critical initial and worst case long term (temperature and load life changes) electronics error.

In assessing overall system performance in terms of sensitivity, linearity, resolution, mass discrimination and mass marking, all electronic parameters capable of producing performance degradation must be considered. The critical electronic parameters are, therefore:

a) RIC electrometer characteristics

b) TIC electrometer characteristics

c) Ion Pump electrometer characteristics

d) Pressure overload and underload discriminator trip points

e) EMT supply output voltages

f) Ion source bias potentials

g) Ion source emission current

h) Ratio of total electric sector potential to ion accelerating voltage and ripple on electric sector potential and ion accelerating voltage

i) Ratio of upper and lower split lens potentials to ion accelerating voltage and ripple on split lens potentials

j) Voltage monitor representation of ion accelerating voltage

k) Overscan capability of ion accelerating voltage to assure mass range coverage.

Table 4-6 provides a summary of electronics errors in the above parameters as derived from the circuit analysis results.

Table 4-6. Summary of Electronic Circuit Errors

1. RIC Electrometer: Expected worst case dc errors in the output representation of input current as referred to the input current, see Figure 4-27.
Ideal Output: $V_o = (6.51 + 0.5437\, I_{in})$.

AC Response: Double pole ($671\ \mu s$ and 1.79 ms) at input and single pole ($187\ \mu s$) following log elements.

Equivalent Noise Input: $<10^{-13}$ amps

Dynamic Range: 10^{-12} to 10^{-6} amps

NOTE: For currents from 10^{-10} A and temperature from -32 to $+60^{\circ}$C, worst case error is $<\pm20\%$ referred to input current (typical error $<\pm6\%$).

2. TIC Electrometer: Expected worst case dc errors in the output representation of input current as referred to the input current, see Figure 4-27.

Ideal Output: $V_o = + (12.5 \pm 0.435\, \ell nI)$

Equivalent Noise Input: $<10^{-13}$ amps

Dynamic Range: 10^{-12} to 10^{-6} amps

NOTE: For currents from 10^{-10} to 10^{-6} amps and temperature from -32 to $+60^{\circ}$C, worst case error is $<\pm20\%$ referred to input current (typical error $<\pm6\%$).

3. Ion Pump Electrometer:

Ideal Output: $-(7.2 + 0.435\, \ell nI_i)$

DC Error: $\pm3\%$ typical, $\pm10\%$ worst case maximum for current from 10^{-6} to 10^{-2} amps and temperature from -32° to $+60^{\circ}$C.

Equivalent Noise Input: $<10^{-9}$ amps

Dynamic Range: 10^{-6} A to 10^{-2} amps

4. Pressure Overload Discriminator: Determines upper limit of analyzer pressure.

Nominal Upper Trip Point: May be set to any voltage in range of 2.72 to 3.72 v.

Initial Upper Trip Point Setting Accuracy (IP electrometer output): $\pm.01\%$

Trip Point Stability (IP electrometer output): ±20 mv.

Table 4-6. Summary of Electronic Circuit Errors (Continued)

5. Pressure Underload Discriminator: Determines lower limit of analyzer pressure.

    Nominal Lower Trip Point: May be set to any voltage in the range of 1.255 to 1.655 v.

    Initial Lower Trip Point Setting Accuracy (IP electrometer output): ±.01%.

    Trip Point Stability (IP electrometer output): ±16 mv.

6. EMT Supply Voltage

	Initial Setting Accuracy	Stability (%)	Ripple (%)
Nominal Voltage	±0.01	±0.1	<0.0025
Low/Nominal Voltage Ratio	±0.01	±0.1	<0.0025
High/Nominal Voltage Ratio	±0.01	±0.1	<0.0025

    NOTE: Nominal voltage may be set to any voltage from 500 to 2450 v.

7. Ion Source Bias Potentials:

Ion Source Element	Setting Range (V)	Initial Accuracy Stability (V)	Short Term (%)	Long Term (%)	Ripple (%)
Mounting Block:					
High Energy Mode	15 to 60	<1.0	0.1	1	0.5
Low Energy Mode	15 to 40	<0.5	0.1	1	0.5
Filament Reference:	65 to 105	<1.0	0.1	1	0.5
High Energy Mode	40 to 80	<0.5	0.1	1	0.5
Low Energy Mode					
Electron Accelerator	250 to 350	<2.0	0.1	1	0.5
Filament Shield	0 to 22	<0.25	0.1	1	0.5

8. Ion Source Electron Emission Current:

    Initial Setting Accuracy: ±0.01%

    Short Term Stability: ±0.1%

    Long Term Stability: ±1.0%

Table 4-6. Summary of Electronic Circuit Errors (Continued)

9. Ratio of Total Electric Sector Voltage to Accelerating Voltage:

    Nominal Value: May be set to any value in the range of 0.10 to 0.18.

    Initial Setting Error: ±0.01%

    Short Term Ratio Stability: ±0.01%

    Worst Case Change of the Ratio due to Regulator Response, Aging, and Temperature (based on Nominal Ratio of 0.14): ±0.046%

    Worst Case Change in Ratio from one end to the other of one complete Mass Scan due to Finite Loop Gain (based on Nominal Ratio of 0.14) ±0.02%

10. Ratio of Negative Electric Sector Voltage to Accelerating Voltage:

    Nominal Value: May be set to any value in the range of 0.05 to 0.09.

    Initial Setting Accuracy: ±0.01%.

    Short Term Ratio Stability: ±0.025%

    Worst Case Change of the Ratio due to Regulator Response, Aging, and Temperature (based on Nominal Ratio of 0.07): ±0.078%

    Worst Case Change in Ratio from one end to the other of one complete Mass Scan due to Finite Loop Gain. (Based on Nominal Ratio of 0.07): ±0.048%

11. Ratio of Positive Elective Sector Voltage to Accelerating Voltage:

    Nominal Value: May be set to any value in the range of 0.05 to 0.09.

    Initial Setting Accuracy: ±0.01%

    Short Term Stability: ±0.01%

    Worst Case Change of the Ratio due to Regulator Response, Aging, and Temperature (based on Nominal Ratio of 0.07): ±0.025%

    Worst Case Change of the Ratio from one end to the other of one complete Mass Scan: ±0.015%

12. Ratio of Upper and Lower Split Lens Voltages to Accelerating Voltage:

    Nominal Values: Either ratio - may be set to any value in the range of 0.8 to 1.0.

Table 4-6. Summary of Electronic Circuit Errors (Continued)

Initial Setting Accuracy: ±0.01%

Short Term Stability: ±0.005%

Worst Case Change of either Ratio due to Regulator Response, Aging, and Temperature (based on Nominal Ratio of 0.07): ±0.02%

Worst Case Change of the Ratio from one end to the other of one complete Mass Scan: ±0.01%

13. Voltage Monitor Representation of Accelerating Voltage and Mass to Change Ratio assuming constant V_{ace} x m/e = 28000.

U***	Range (V)		Worst Case Low Voltage Error (U)	(V)	Worst Case High Voltage Error (U)	(V)
22 - 10	1275 - 2825		±0.026	±1.51	±0.0096	±2.712
73 - 22	385 - 1275		±0.104	±0.55	±0.0215	±1.25
153 - 73	183 - 385		±0.192	±0.16	±0.074	±0.39
254 - 153	1100 - 183		±0.308*	±0.13**	±0.159	±0.19

* ±0.228 (U) amu at m/e = 200 U (amu)

** ±0.09 v at m/e = 200 U (amu)

*** U = former abbreviation was amu
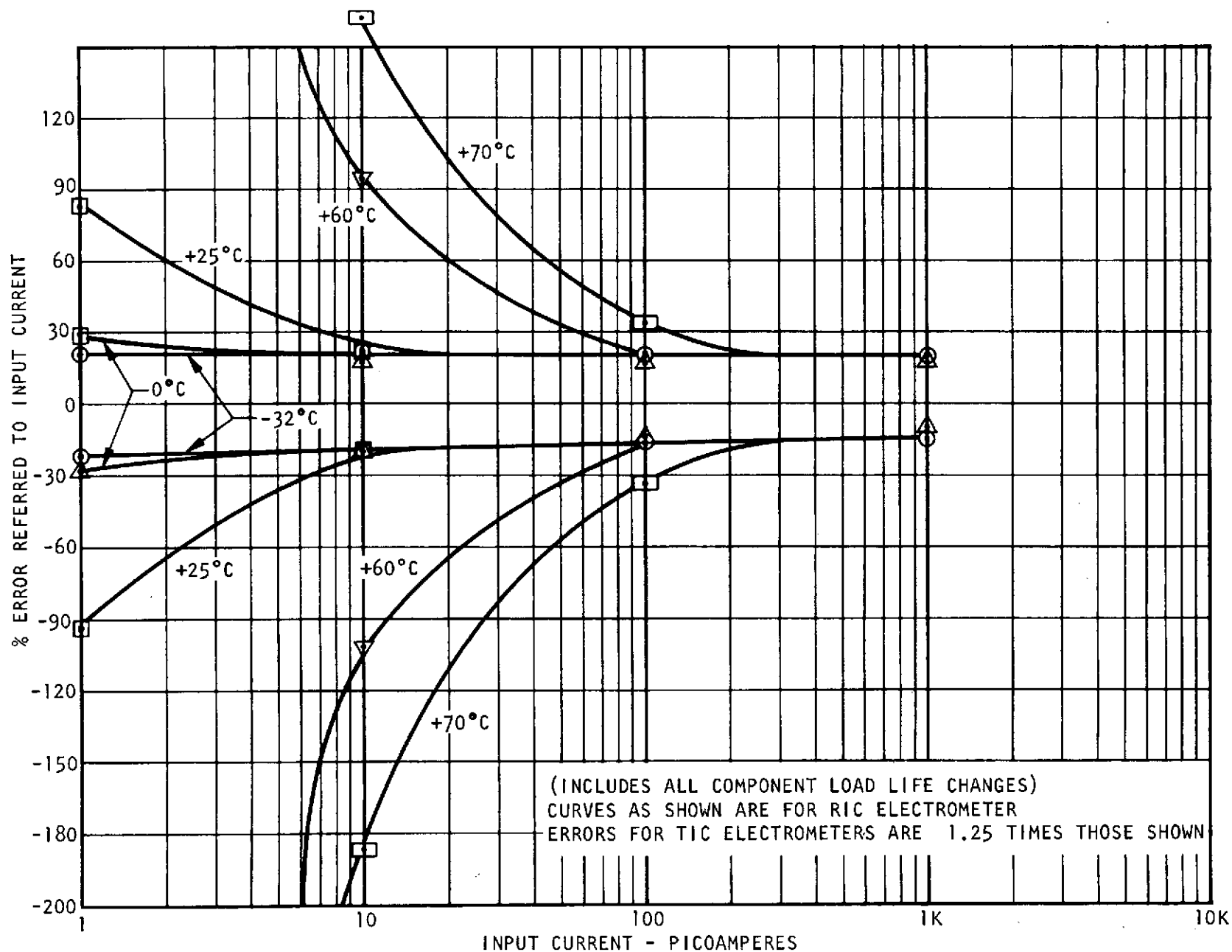
Figure 4-27. Worst Case Error Limits for RIC and TIC Electrometers

5. SUPPORTING COMPONENTS

The addition of an MS to the Wet Chemistry experiment, to assist in identification of the amino acids, requires the same systems analysis for its interface with the GC system as was originally performed for the GCMS of Viking 1975. The important difference between the two systems, apart from the amino acid derivatization, occurs at the interface between the GC column, the GC Detector (GCD) and the MS. The present Wet Chemistry requirement calls for the GC column effluent to be analyzed by both a GCD and an MS, whereas the Viking '75 GC/MS only uses an MS analysis. So although the GCMS interface is similar, this difference in requirements introduces several new questions that need to be resolved. However, operation of the Wet Chemistry/MS interface in an identical manner to the current GCMS, by using the MS total ion current as a GCD, has considerable merit and will be part of any future GCD tradeoff study.

The areas that need further definition are: (1) the effluent from the GC needs to be analyzed by both the GCD and the MS; (2) the present GCD requires a hydrogen-helium mixture which is not compatible with the present carrier gas removal system that is required for efficient MS operation; (3) the selection of the best separator operating temperature, which in turn determines the overall efficiency for the removal of hydrogen; and (4) protection against the possible over-pressurization of the MS ion source. Items 2, 3 and 4 are interconnected problems.

The areas identified in the preceding section can be accommodated by an analysis of only two components — the flow divider network and the hydrogen separator. In the following sections each of these components is studied in some detail to select a design for the Wet Chemistry GC/MS interface.

5.1 THE DIVIDER NETWORK

The major decision concerning the interface is the determination of a system that allows the effluent from the GC to be analyzed efficiently by both the GCD and the MS. It would appear that the ideal approach would be to use one of the analyzers in the flow-through mode, allowing the GC effluent to pass through it to the other analyzer. Obviously, the MS cannot be used in this manner because of its high vacuum mode of operation,

so the GCD would have to be the flow-through analyzer. The current GCD on the Wet Chemistry system is the hydrogen flame detector, which con - sumes the sample. As the flow-through mode appears to be impossible for the present system design, the effluent from the GC will need to be split between the two analyzers. However, with the addition of the MS to the Wet Chemistry system, the original GCD study should be re-evaluated to determine if another GCD is more suitable for the new conditions.

The second tradeoff concerns the Wet Chemistry GC gas. At pres- ent the Wet Chemistry experiment uses a helium carrier gas containing 40 percent hydrogen, with the flow rate of 6 cc/min, for transporting the amino acid derivatives. This flow rate is increased by an order of magnitude just prior to entry into the GCD to optimize the detector operation. The MS cannot handle the full GC flow rate, so the carrier gas needs to be preferentially removed using a gaseous separator. A separa- tor, identical to the one used on the Viking GC/MS would be adequate. This separator removes 99.999 percent of the hydrogen gas flow, allow- ing the amino acids to dominate the gas flow entering the ion source. How- ever, this type of separator will only remove hydrogen from the gas stream, so the carrier gas for flight operation will need to be changed from a helium/hydrogen mixture to pure hydrogen. The hydrogen flame GC de- tector (GCD) requires helium and oxygen in addition to the hydrogen to operate efficiently. In addition, the operation of the GCD is such that the helium will need to be added to the hydrogen gas flow going to the GCD jet, and the oxygen is added to the GCD via a separate path. This means that all three gas supplies need individual systems. Ideally, the helium will be added to the hydrogen at a point just prior to the GC detector where the flow rate increase presently occurs. Therefore, in all further dis- cussions of the Wet Chemistry GC carrier gas, the use of 100 percent hy- drogen will be assumed together with the requirement for two extra gas bottles containing, respectively, helium and oxygen for GCD operation only. This requirement further highlights the need to re-evaluate the GCD.

From the above discussions, if the present GCD is used, the hydrogen carrier gas and the amino acids emerging from the GC will be divided between the two paths in the ratio of R where:

$$R = \frac{\text{Flow in GCD path}}{\text{Flow in MS path}} = \frac{\text{Molar sensitivity GCD}}{\text{Molar sensitivity MS}} \geq \frac{10^{-10}\text{moles}}{10^{-11}\text{moles}} \geq \frac{10}{1}$$

This division of flow must not have any severe mass discrimination. For laminar flow through a narrow tube the volumetric flow rate is independent of mass, so this first divider can simply be a pair of balanced restrictors. The two flow rates will be set so that 5.4 cc/min will flow into the GCD line and 0.6 cc/min will flow into the MS input line.

The design for the GC detector flow line is now relatively simple. The majority of the effluent for the GC flows through the 5.4 cc/min flow restrictor. Just prior to the detector, helium gas will be injected into the hydrogen carrier gas flow, and the total helium/hydrogen flow rate will be increased to ensure efficient operation of the hydrogen flame detector.

The MS flow line is more difficult; the hydrogen carrier gas flow that transports the amino acids needs to be reduced considerably before it enters the MS ion source. The further reduction in the size of an amino acid peak that would result from utilizing another divider network is very inefficient, unless it has been determined that the amino acid peak about to enter the MS is above a minimum level. This minimum level can be sensed by either the GCD or the MS total ion current monitor, which then feeds back a signal to a divider network. The detector response will need to be reasonably fast as a flow of 0.6 cc/min through a 1/16 inch-diameter tube will have a velocity of 0.6 cm/sec. For a 5-second wide large peak, the maximum peak value will take about 5 seconds from the time a minimum signal is measured at the MS, to its arrival at the ion source. This allows ~3.0 centimeters of tubing between the divider and the MS which is rather impractical. An apparently better method would be to take a signal from the GC detector and insert a delay line in between the 0.6 cc/min restrictor at the MS line entrance and the ion source. The GCD gas line has an order of

magnitude faster flow than the MS line and therefore has a flow velocity of
$\gtrsim 6$ cm/sec. For this case, within about 2 to 3 seconds of the carrier gas
entering the first divider, a GCD generate pulse could operate the second
divider, which would be situated at a delay line length of ~ 6 cms from the
initial flow divider in the MS line. This would allow efficient removal of
extraneous amino acid, thereby protecting the ion source against overload.
This second divider could be the present GCMS design in which different
ratio conductances can be inserted in the flow path, so that the extraneous
portion of the amino acid flow into the MS can be dumped to the external
atmosphere. The present GCMS restrictor ratios will probably need to be
changed, but this will be carried out later in the study. From the compon-
ent point of view it would be better if the first flow divider incorporated the
variable divider and would therefore perform both divider tasks. In prac-
tice this would mean slight changes in the amount of amino acids entering
the GC detector line, as the first divider ratio would need to be suddenly
changed when a large amino acid peak was sensed. This would complicate
the interpretation of the chromatogram. A computer program should be
able to sort these changes out knowing the different divider ratios used dur-
ing the peak period. However, while this system appears attractive, at the
present moment it is complicated, and the baseline will be the apparently
simpler two divider system that can be merged together at a later stage if
necessary.

The hydrogen gas flow rate into the MS is still much too large, des-
pite the two flow dividers that have been inserted into the system. The need
for a very efficient gaseous separator before the flow enters the MS is there-
fore important.

5.2 THE SEPARATOR

The removal of the hydrogen carrier gas from the effluent flowing in-
to the ion source of the MS should not present a problem. The current de-
sign of palladium separator, in use on the Viking '75 GCMS, appears to
have a hydrogen removal efficiency and life expectancy in excess of the re-
quirements for Wet Chemistry operation.

The flight separator lifetime expectancy has been found to be greater
than 2000 hours for various temperature, voltages and cycling rates. Its
efficiency for hydrogen removal, at various operating temperatures, is shown

in Figure 5-1. The proposed operating temperature is about 220°C, which should provide a hydrogen removal efficiency of 99.9995 percent. The fast decrease in hydrogen removal efficiency below 220°C, shown in Figure 5-1, can be improved if required, by varying the concentration of the sodium hydroxide electrolyte. The effect on the analyzer and ion source pressure for various separator efficiencies or temperatures can be determined from Figure 5-2. The ion source which has a pumping speed of ~160 cc/sec for hydrogen should operate under normal conditions with a hydrogen partial pressure of $<10^{-6}$ torr for the same temperature and conditions. These figures are well below the maximum permissible levels, indicating that, with the exception of some questions regarding chemical effects, the GCMS separator has acceptable operating characteristics for inclusion in the Wet Chemistry system. The only doubts about its operation are the effect that large amino acid peaks may have on the separator operating characteristic and the converse effect of the separator affecting the amino acids. Current thoughts based on limited GCMS data indicate that there should be minimal effects in both cases. Tests with a commercial separator to evaluate these effects have been carried out and are reported in Section 7 (Laboratory Investigation).

The region between the MS and the separator will also be identical to the GCMS design. The gas flow after the separator will be in the molecular flow region and little in the way of peak broadening has been seen to occur during the passage of the peaks into the ion source for the current GCMS system. This section of flow path will also be maintained at 220°C and will incorporate a valve to act as protection against MS overload.

5.3 CONCLUSION

The analysis of the interface region between the GC column, GC detector and MS has produced a provisional design and identified the need for further GCD appraisal.

The present design is based on the MS having an order of magnitude more sensitivity than the GC detector and on the GC detector identifying and operating the divider mechanism to stop overloading of the ion source. Little in the way of new technology needs to be developed and only the divider ratios need to be determined at a later date. This part appears to be quite satisfactory.

Anode-24" long 6 thou I.D.-12 thou O.D. 75/25 palladium/silver
tube on PTFE mandrel with 12" long 35 thou I.D. - 43 thou O.D.
cathode in a sodium hydroxide electrolyte.

$$\frac{H_2 \text{ Out Sep}}{H_2 \text{ In Sep}}$$

$$\times 10^{-6}$$

OPERATING REGION

IDEAL O.R.

SEPARATOR TEMPERATURE °C
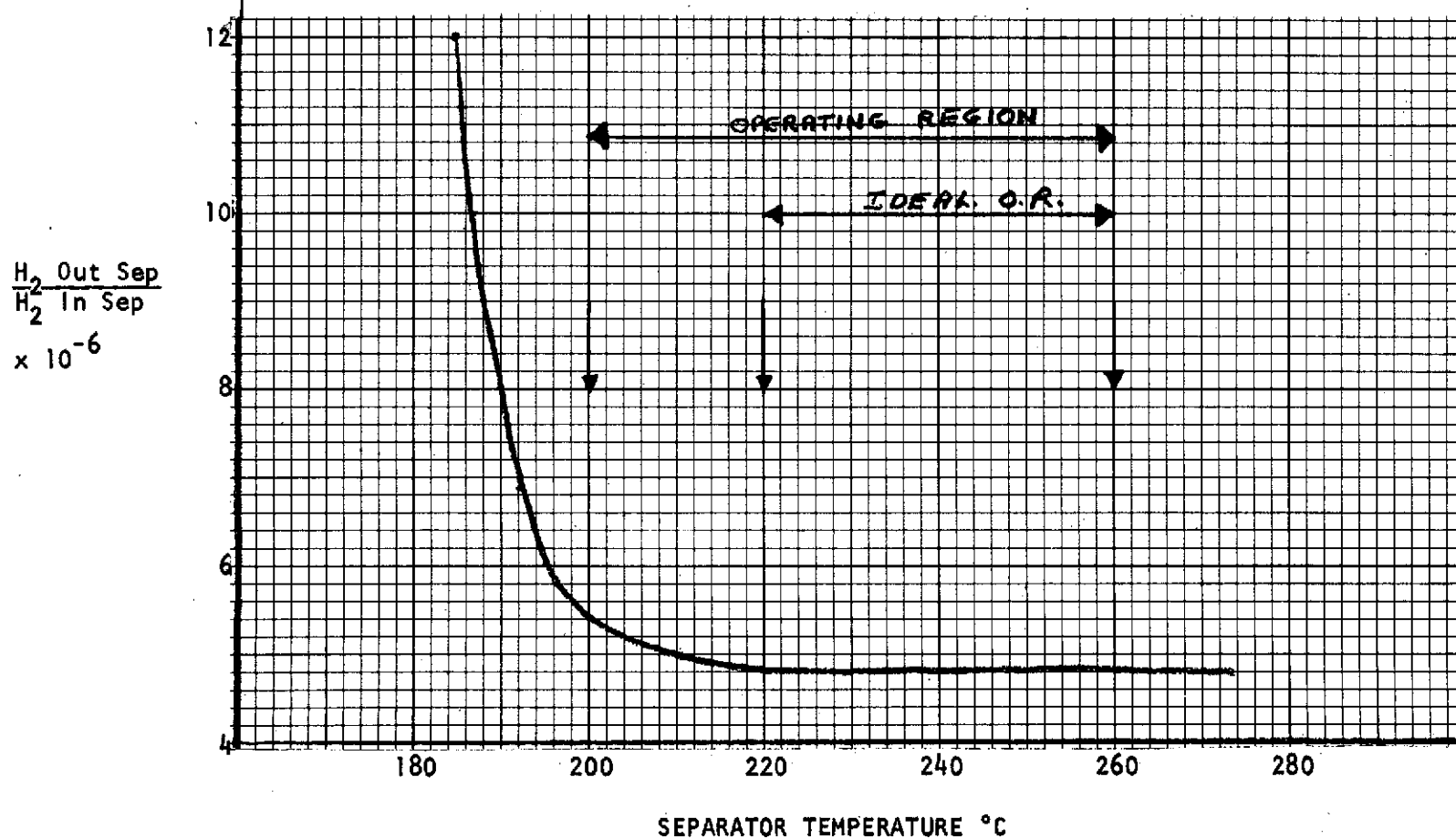
Figure 5-1.   Separator H_2 Rejection Ratio With Temperature
(From Dencke, Rushneck and Shoemaker, Anal. Chem.
44, p. 1753, 1972.)

y-axis label: $\dfrac{H_2 \ \text{Out Sep.}}{H_2 \ \text{In Sep.}}$*

Curves: 1000 cc/sec, 500 cc/sec, 100 cc/sec MS PUMPING SPEED

SEPARATOR TEMPERATURE - 190 °C

200 °C

$\geq$220 °C

MS PRESSURE IN TORR
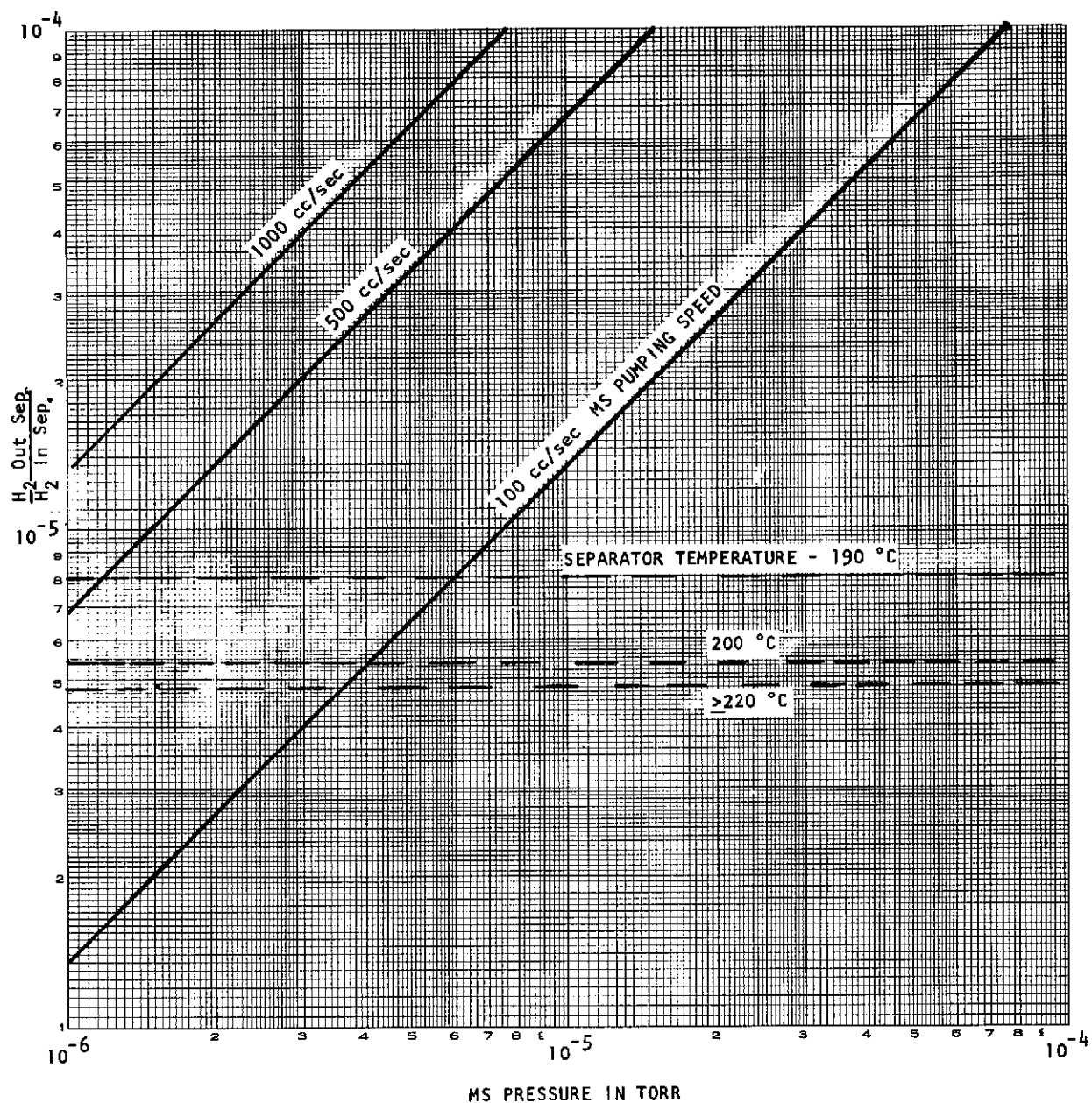
*If a 10:1 divider is used divide required pumping speed by 10.

Figure 5-2. MS Pressure Relative to Separator Hydrogen Rejection Ratio, Pumping Speed* and Separator Temperature

The operation of the MS in conjunction with the present GCD that necessitates the removal of helium from the carrier gas has added a bottle of helium to the system, together with a pressure regulator and flow restrictor. This, in addition to the oxygen bottle, stipulates the need for two extra gas supplies in addition to the hydrogen. The above system analysis demonstrates that the need for a flow-through detector is not as important as it originally seemed; however, the advantages to the system obtained from the removal of the helium and oxygen bottles, indicate that a future tradeoff study on the various GC detectors, based on the new requirements, still appears necessary.

6. WET CHEMISTRY/MASS SPECTROMETER (WCMS) INSTRUMENT SYSTEM DESIGN

The following sections contain an analysis of each of the major operational parameters affecting system design. A conceptual instrument system design is presented, and the engineering interfaces and parameters are discussed. This is followed by a comparison of the WCMS requirements and the Viking '75 MS performance capabilities. The final section presents a discussion of recommended future instrument development and modifications.

6.1 INSTRUMENT SYSTEM PARAMETERS

6.1.1 Mass Range

A list of the specific amino acid derivatives that are required to be identified by the WCMS is shown in Table 6-1 and Figure 6-1. The sensitivity of the Viking '75 MS does not appear to be adequate, at low ionization energy (15 ev), to allow idnetification of the percent ion of these derivatives. The only ionization energy that will be used, therefore, is the most efficient iionization energy of 70 ev. The majority of the specified amino acids have been analyzed at 70 ev by the NASA/Ames facility and the cracking patterns of each of the amino acids are shown in Figures 6-2 and 6-3. The cracking patterns of the amino acids at this energy show a minimum of the parent ion peak. In addition, the mass range that appears to provide unequivocal identification of the amino acid derivative can be seen to cover the range of 55 to 220 amu. The low value of the range is determined by butyl and CF_3 derivative which are important as they confirm the presence of an amino acid derivative. The maximum value is determined by the a-amino adipic, ε-amino caproic, aspartic and glutamic acid derivatives.

6.1.2 Resolution and Sensitivity

In general the sensitivity of the '75 MS appears adequate for Wet Chemistry operation. However, improvements in the value of this parameter may be required to provide either better amino acid evaluation to be carried out or to compensate for tradeoffs whereby other parameters may be improved at the expense of sensitivity. The components that affect sensitivity will therefore be studied in some detail to determine their

Table 6-1. Specification Amino Acids

A. Mandatory Detectable Amino Acids

1. Alanine
2. Valine
3. Isoleucine
4. Leucine
5. Glycine*
6. Proline
7. Aspartic Acid
8. Methionine
9. Phenylalanine
10. Glutamic Acid
11. Beta Alanine*
12. Norvaline
13. Norleucine
14. α - Amino - η - Butyric
15. Lysine
16. Pipecolic Acid
17. α - Amino Isobutyric*

B. Design Goal Detectable Amino Acids

1. Ornithine
2. ϵ - Amino Caproic Acid*
3. δ - Amino Valeric Acid*
4. γ - Amino Butyric Acid*
5. α - Amino Adipic Acid
6. Alloisoleucine
7. β - Amino - η - Butyric
8. β - Amino - Isobutyric
9. N - Mehtyl-Alanine
10. Isovaline

*Denotes that the amino acid is not optically active.

ideal operating range for Wet Chemistry operation. The parameter of re-solution is more difficult to determine, as the controlling factor of the flight GC column has not been selected. It is therefore difficult to evaluate the required resolution, as only a few GC chromatograms from potential flight columns (in which a large number of the amino acids have been iden-tified from a single elution) exist. This type of data for the flight column may not be available for some time. Until the relevant data are available a resolution of one mass unit at mass 240, with a valley of 5 percent, will be assumed. However, it is possible that the present MS system resolu-tion of $m/\Delta m$ of 200 at a 20 percent valley is adequate.
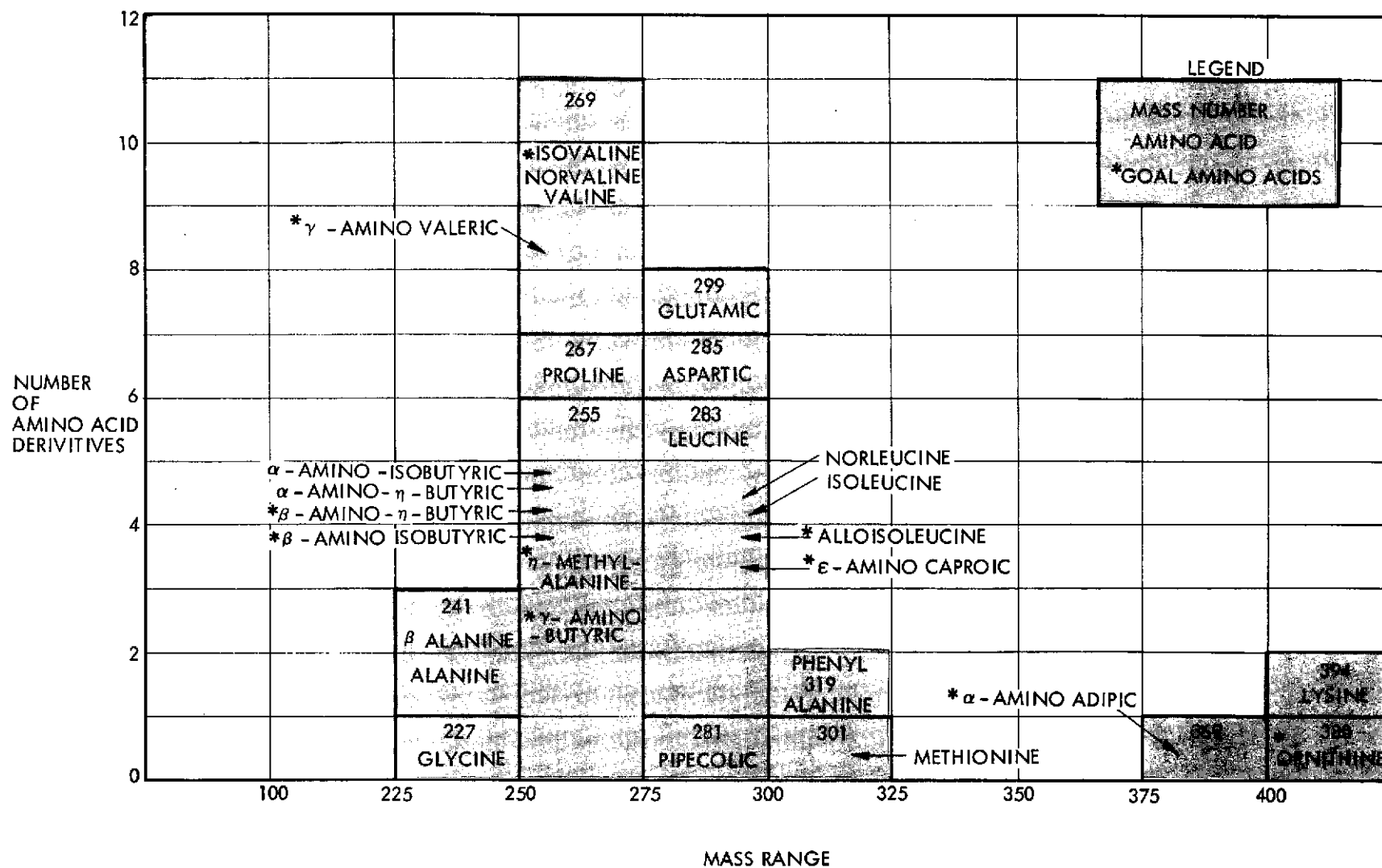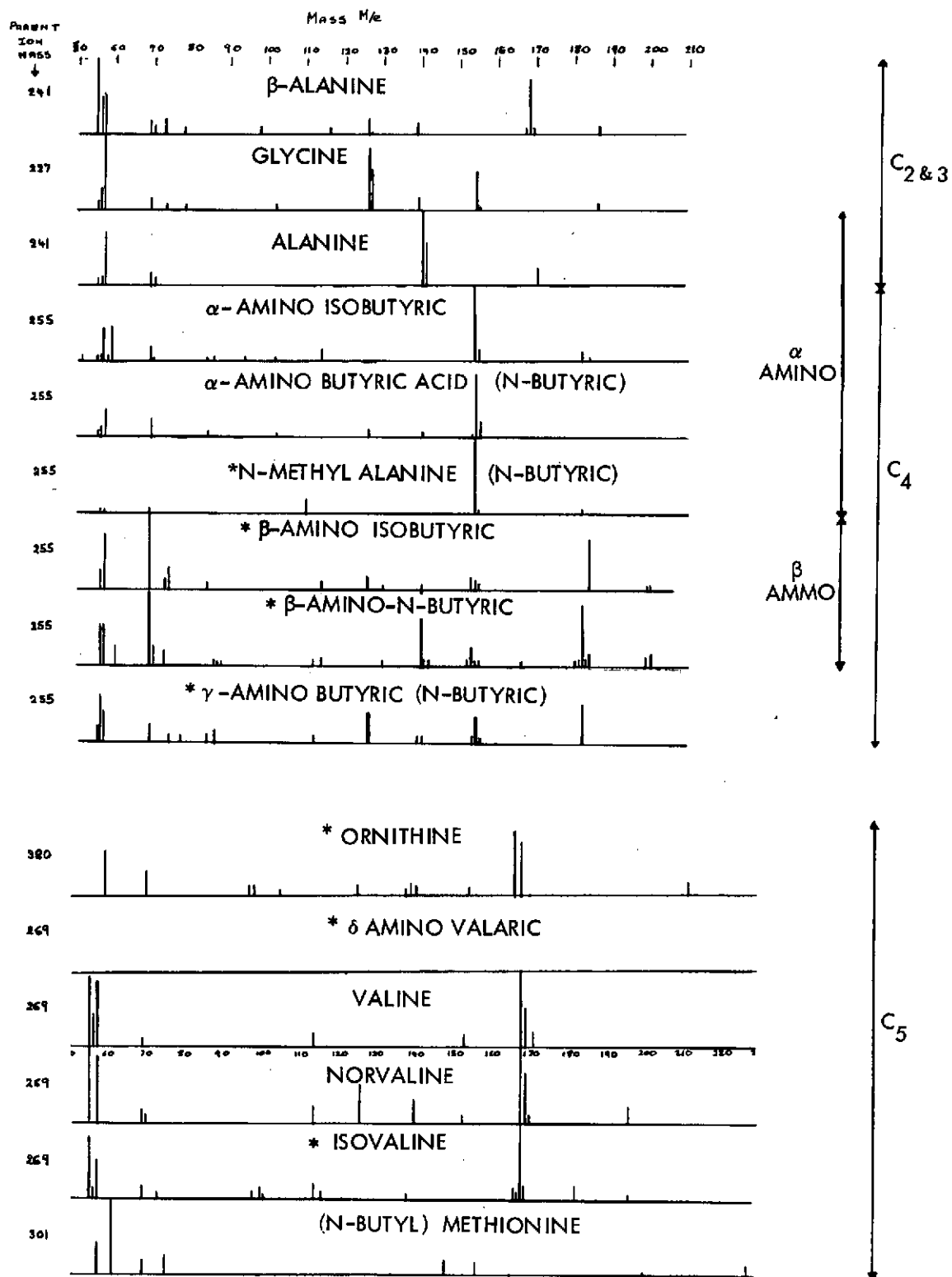
Figure 6-1. Amino Acid Derivative Mass Numbers

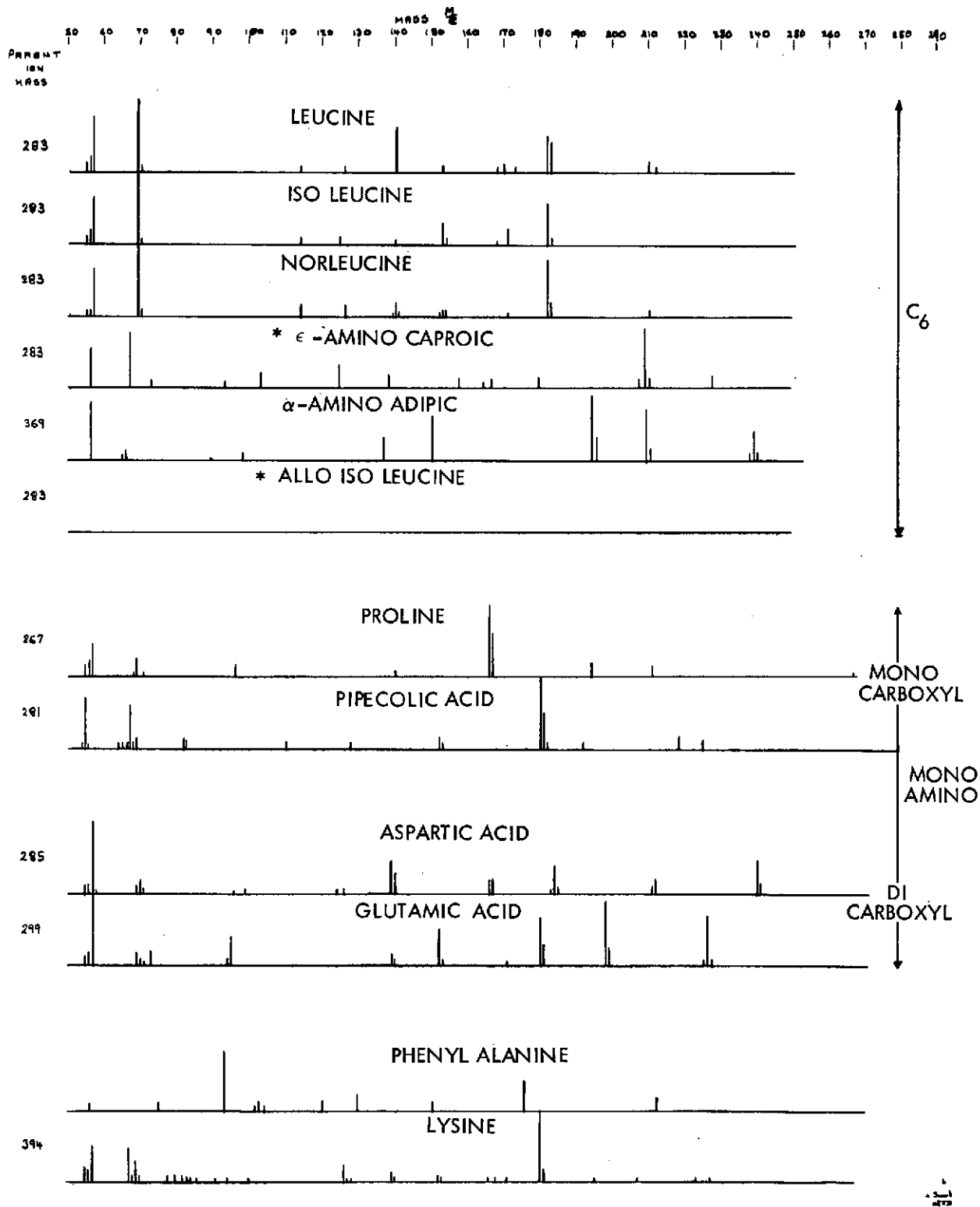Figure 6-2. Mass Spectra Cracking Patterns for the
Mandatory and Goal* Amino Acids

Figure 6-3. Mass Spectra Cracking Patterns of the
Mandatory and Goal* Amino Acids

6.1.2.1 <u>Sensitivity</u>

In this study and in many reports relating to the GCMS, two definitions of sensitivity are used. The definition in terms of amps/torr is an absolute value and provides the ion current generated for a specific gas partial pressure in the ion source. A second definition of amps/torr cc/sec provides the ion current generated as a function of ion source gas throughput. This value is related to the ion source gas conductance which is dependent on the mass of the ion, the geometry of the system, and the operating temperature of the ion source. In addition both of the above definitions are dependent on how the ion current is measured. The true ion current can be measured on the first dynode of the electron multiplier (EM), provided that the correct voltage distribution to reduce secondary emission is applied to the EM electrodes. An amplified ion current can be obtained from the output of the EM and therefore represents the total MS output current for a particular ion mass. These different methods of quoting the MS sensitivity are described in Table 6-2.

The Viking '75 GCMS system requirement for the sensitivity states that for ionizing electrons with an energy of 70 ev, the MS shall have a sensitivity exceeding 8.0×10^{-5} amps/torr cc/sec for the nitrogen peak. In addition, this figure shall apply to ion source operation at temperatures exceeding 200°C in a scanning mode, for the filament of highest sensitivity. The measured flight value is 3.0×10^{-6} amps/torr measured at the EM first dynode. This can be converted to amps/torr cc/sec by dividing the previous figure by the ion source conductance for N_2 of 42 cc/sec at 210°C (Table 6-2). The figure measured for the flight units is therefore 7.1×10^{-5} amps/torr cc/sec, which is very close to the required value.

The absolute sensitivity of the MS system is governed by the ion source efficiency, losses in the analyzer sections, the EM gain, the electrometer sensitivity and the general system noise. Each of these parameters will be studied to determine their best operating value for the WC/MS system.

Ion Source

The ion current that is generated as a function of GCMS ion source pressure is shown in Figure 6-4. It can be seen that above a pressure of

Table 6-2. The Definition of Sensitivity as a Function of Pressure Throughput and EM Output

Parameters Included in Measurement of Sensitivity / Output Current Measured at:	MS Sensitivity		Sensitivity Conversion Factor
	Current Measured at EM as a Function of:		
	Ion Source Pressure	Ion Source Throughout	
1st Dynode EM	3.0×10^{-6}	7.1×10^{-8}	Divide amp/torr by the ion source conductance at ^{o}C for the particular gas. This results in amps/torr cc/sec.
Output of EM (Gain 10^3)	3.0×10^{-3}	7.1×10^{-5}	
Units	Amps/torr for $m/e = X$	Amps/torr cc/sec at $T^{o}C$ for $m/e = X$	

*Electron energy 70 eV $m/e = x$

3×10^{-5} torr, the ion current becomes nonlinear with the increasing mass. This nonlinearity of output current from the ion source with pressure is due to many additive processes. The loss of ion current can be caused by beam space charge effects, gas collisions, and surface charging. This latter process causes the deflection of the low velocity heavy ions from the ion beam near the ion source exit aperture, by internally generated electrostatic fields. These fields can be produced very easily in the case of organic analysis by the buildup of charge on insulating films which are formed on the internal surfaces of the ion source. The insulating film is probably produced by heavy organic volatiles that have condensed out on the surfaces, and the charge is generated from the large number of charged ions produced during the fragmentation of the heavy gas molecules. Another of the processes that could produce the nonlinearity is the loss of low velocity heavy ions by collision with the high pressure neutral background gas. It can be concluded that the effect of these processes may be reduced by increasing the energy of the ions with a higher accelerating voltage. The precise value of pressure at which the current becomes nonlinear may alter if the ion source voltages are adjusted to favor operation at higher mass numbers.
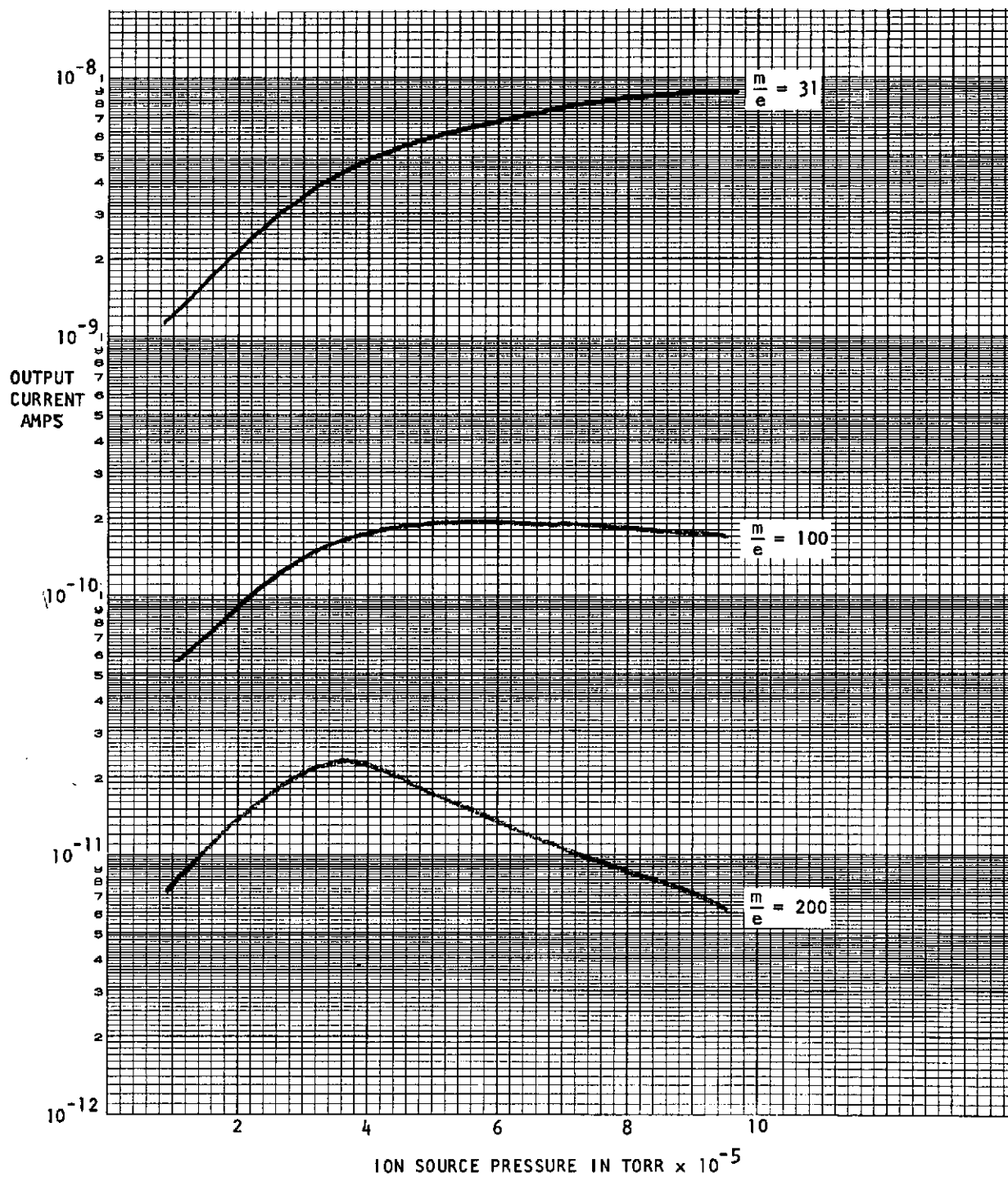
Figure 6-4. Ion Current Output With Ion Source Pressure
(Obtained from Perkin Elmer Viking 1975-MS-CDR)

For Wet Chemistry operation, the mass range of maximum interest is between m/e values of 100 to 200. In this region little appears to be gained by operating the ion source above 5×10^{-5} torr as no increase in ion current is produced for an increase in ion source pressure. In addition, for the higher masses approaching 200, a loss in sensitivity occurs above 4×10^{-5} torr. The current GCMS is more interested in the lower mass range, where an increase in ion current _is_ obtained for an increase in ion source pressure. The nonlinearity effects are then corrected for in the data reduction.

This method appears to offer little to the Wet Chemistry operation and the additional signal can be better used by the gas chromatograph detector (GCD). In addition, this nonlinearity may become more severe when neutral amino acid (AA) compounds with m/e of 200 to 400 are present. If the current ion scan range of 12 to 200 mass units is utilized, then the ions in the region of m/e 200 will have very low accelerating voltages. This, coupled with a high gas pressure of large molecules with masses 200 to 400 amu, may result in an even greater nonlinearity of output current with pressure, together with the additional loss in sensitivity. This problem may be improved by using the same voltage scan range that is used at present for the 30 to 160 amu portion of the mass range for the proposed Wet Chemistry mass range of 55 to 240 (an m/e value of 200 may be adequate). As the m/e = 240 voltage will now be the larger voltage that was applied to the m/e = 160, a larger magnet will be required to keep the present magnetic radius of curvature. The acceleration voltage applied to the mass fragments is proportional to the square of the magnetic field, so to keep this radius of curvature, the magnetic field will be increased by $(240/160)^2 = 2.3$. Even with the improvements in permanent magnets, since the GCMS was originally designed and the fact that the large magnet may not have the linear increase in weight that this change appears to demand, this type change does not appear feasible. Another possibility is to change the method of scanning from electrostatic to magnetic. Improvement in the hysteresis effects that have caused problems in the past have been reduced and this method should have much lower mass discrimination, as a higher acceleration voltage can be used for the high mass ions. However, this is a major change in design and can only be produced at high

cost. Nevertheless, it should be evaluated if an increase in sensitivity at the higher mass numbers is required.

Another possible way of improving the sensitivity for the high mass region may be produced by varying the distributions of voltages on the various ion source electrodes. These voltages can be changed over a narrow range to improve the ion current for different portions of the mass scan. However, the capability for tuning the existing design is severly limited and causes less than optimum performance in many respects. In the ion source, for example, there is considerable difference in sensitivity between the two filaments because potentials are not changed when the filaments are switched. So changes in the voltage distribution will be needed when operation at a different filament is programmed. As a minimum improvement, it is suggested that the electron focus and repeller voltages be switched when switching between the two filaments. This would permit optimum alignment of both electron beams with respect to the repeller and would result in improved resolution and sensitivity with either filament. In the present system, compromise settings to achieve acceptable performance from both filaments results in considerably less than optimum performance with either filament. The modifications required are primarily in the operation control logic.

The Analyzer Section

The analyzing section consists of an electric sector which provides energy selection and a magnetic sector which separates different m/e values. The effect of changes in the aspect ratio of the electric sector have been studied at Perkin Elmer and have indicated that improved resolution might be obtained if the beam were somewhat off center in the sector. In the narrow gap of the present design, the beam cannot be moved very far without striking the sector plates; this considerably restricts the degree to which the system can be tuned. Charging problems to date have not been identified in this part of the instrument, but increasing the spacing between the sector plates would reduce the possibility of this occurring. In addition, the overall conductance of the system would be slightly increased The main benefits that would be gained from such a change, would be the increase in resolution and sensitivity which would result from the improved tuning capability. The modifications required would involve increasing

the height as well as the width of the sector in order to maintain aspect ratio, so that the overall sector dimensions would increase. The weight penalty would not be severe. The deflection voltages would need to be increased for the wider gap and this appears to involve relatively minor electronics redesign.

The present instrument does not have any Z directional focusing prior to the ions entering the magnetic sector. It would appear that the sensitivity can be improved by including a Z-axis focusing lens (Einsel Lens) in the drift tube. A theoretical analysis of the effect of Z-axis focusing shows that transmission of all ions can be increased by at least a factor of two, and that mass discrimination can be reduced by about 50 percent. Some experiments have been performed in the existing system in which a negative potential was applied to the beam alignment slit; transmission of all ions was increased by a factor of 2.5 to 3 at the optimum voltage. Mass discrimination was not significantly changed. This is not in any sense an idealized situation. There were no ground plane electrodes which would normally be employed and the positioning of the lens was fixed. As an approach to minimal design changes, the beam alignment slit could be used as a sort of Z-axis focusing lens. The only redesign effort would be in the scan supply to provide the necessary voltage. This new voltage requirement might be typically 50 to 60 percent of the present scan voltage. Since the scan supply should be redesigned to reflect the change in mass range, the additional effort would not be extensive.

A higher level of effort would be to implement a separate Z-focus assembly within the drift tube area at an optimum position. This would be a three-electrode system requiring a larger diameter for the drift tube in order to assure field uniformity. This would involve mechanical redesign of the drift tube. The resulting system would fit within the existing instrument configuration. If this level of effort is undertaken, it should include the bellows to permit better alignment of the ion optical path. It should also be noted that the Berry curvature may be somewhat altered by the Z-axis focusing. Present assessment of the situation is that the effects would be minor. Principal impact of any major change in the Berry curvature would be a change in the curvature of the image slit shape, or the addition of beam straightening electrodes in the region between the exit from the magnetic sector and the image split plate.

In addition to the Z focusing it has been determined at Perkin Elmer that the beam does not enter the magnetic analyzer at the same position for all masses. This results in one portion of the mass range operating at a disadvantage with respect to the other. The addition of a bellows in the drift tube would provide additional flexibility that would give some control over the entrance of the beam into the magnetic sector. It would permit some lateral or Y-axis tuning of the image slit plate. This involves a modest amount of redesign in the drift tube area. Changes in the magnetic sector that would improve the system sensitivity have already been discussed in the previous section dealing with the ion source.

Electron Multiplier

The present EM in the GC/MS operates at a gain of $\sim 10^3$. The system sensitivity is quoted as 3.0×10^{-6} amps/torr at 210°C with a maximum ion source pressure of 3×10^{-4} torr. At this maximum pressure the absolute maximum current at the first dynode of the EM would be $\sim 10^{-9}$ amps which would result in an EM anode current of $\sim 10^{-6}$ amps. The present ion source appears to be nonlinear above a pressure of 3×10^{-5} torr for the high mass compounds (m/e 100 to 200). For WCMS operation this high mass region is of particular interest, and operation above a maximum pressure of 3×10^{-5} torr therefore does not appear to have any advantages. However, if the ion source maximum pressure is lowered, it does mean that a gain of 10^4 could be used for the EM, with no increased risk of destroying the EM due to an excessively large dynode current. This increase in gain has several advantages. The effective increase in sensitivity resulting from the increase in EM gain means that the MS is more sensitive than the GC detector system, and therefore requires only a fraction of the total GC effluent to complete an AA analysis. If both systems are required to detect the minimum value peak, the Wet Chemistry GCD will receive the majority of the GC effluent, which means that no increase in the current GCD system sensitivity requirement is needed despite the inclusion of the MS in the system. In addition, the total mass discrimination that has been measured in the EM system for the larger masses (~ 180 amu) relative to nitrogen decreases from a factor of 12 at a gain of 10^3 to ~ 8.5 at a gain of 10^4. It appears that the percentage of the masses discrimination in the total system that is directly relatable to the EM is due to the low velocity

heavy ions producing a reduced secondary electron emission yield from the EM dynodes. The increase in overall EM voltage to produce the higher gain also increases the velocity of the incoming ions and therefore improves this situation. In addition, this effect would probably be reduced still further if the proposed scan voltage change was incorporated.

System Noise

The minimum detectable signal is determined by the EM and electrometer system noise. The main noise signal at the output of the EM is due to ion statistics and is expressed by:

$$I_{rms} = 100K \left[2e\, \Delta f\, Io \right]^{1/2} amps$$

where

Io = EM output DC current

K = EM noise enhancement constant (measured in lab = 2)

e = electron charge

f = system bandwidth 125 Hz.

The resultant theoretical noise current and signal noise ratio, as a function of EM output current for constant bandwidth, is shown in Figure 6-5. This noise current is the calculated ion statistical noise plus the much smaller electrometer noise input current of 5×10^{-13} amps. The graph shows that for an input into the electrometer of 3×10^{-12} amps, the signal to noise ratio is one. For an input of 10^{-11} amps the signal to noise ratio is 2.2 which means that this figure is just about the minimum detectable signal. This noise level can be decreased by operating with a narrower bandwidth. This, however, does not seem feasible if the system resolution is to be maintained.

Electrometer

The electrometer is basically adequate for the WCMS system operation; however, the unit does suffer from large errors at low currents over the present wide temperature operating range of -32 to +60°C. If this temperature range was stipulated for the WCMS, then 10^{-10} amps would be the minimum operating point. To reach a value of 10^{-11} amps, an operating temperature range of -25° to +25°C is required; therefore, this temperature range will be the baseline for electrometer operation on the WCMS.
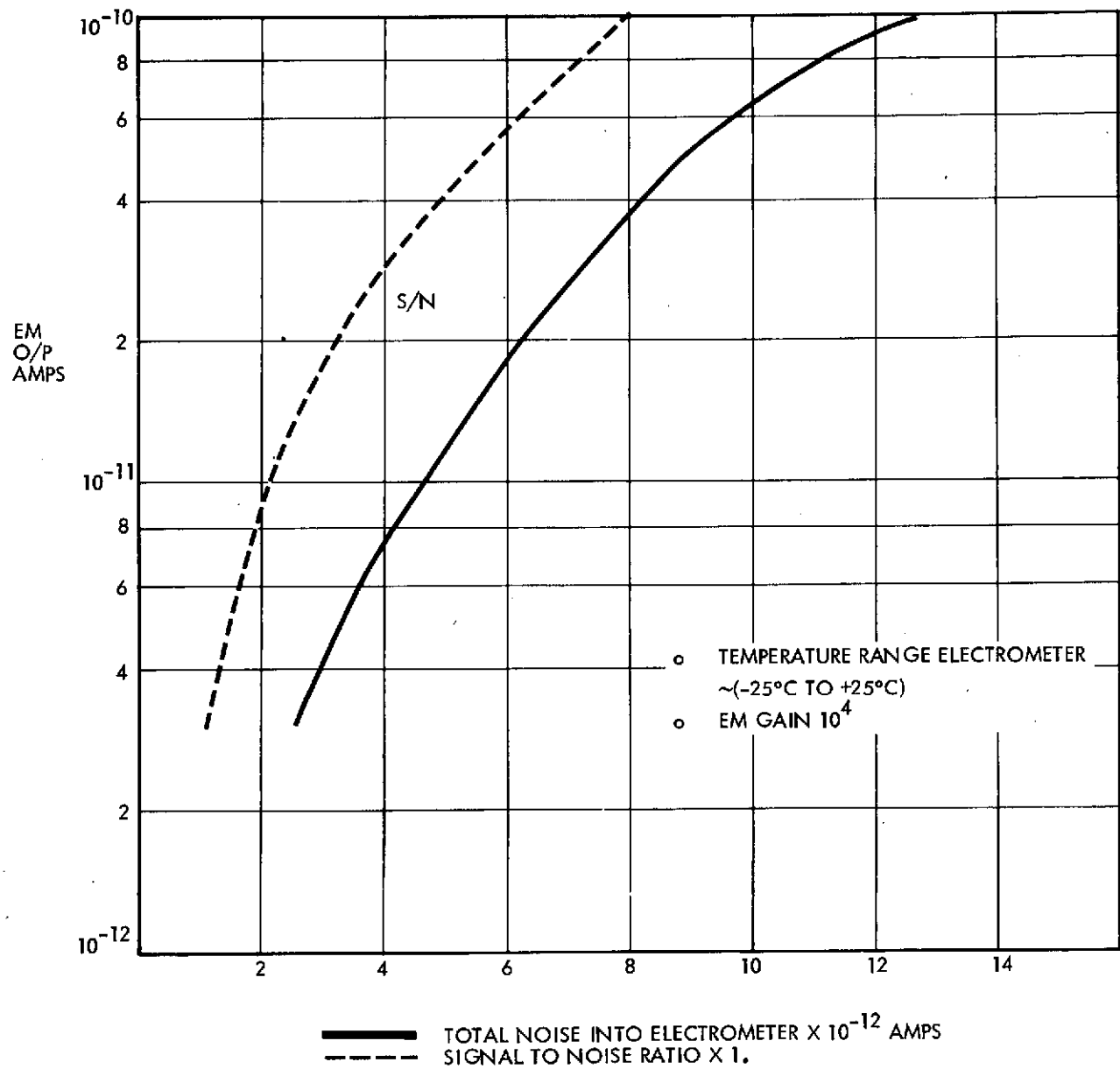
Figure 6-5.   Total Noise into Electrometer With EM Output Signal

Overall System Sensitivity

The above discussion has outlined the new system requirements that allow the current MS of the GCMS. to maintain an adequate sensitivity for operation with the Wet Chemistry instrument. These requirements are listed in Table 6-3, and together with the previously discussed improvements to the system to increase the sensitivity, provide a good summary of the current situation.

The sensitivity level that is required for the MS to operate satisfactorily with the WC experiment is shown in Figure 6-6. In this figure are shown the two levels of sensitivity that were actually obtained from the flight MS instrument, for m/e values of 28 and 181. Also shown are the levels of sensitivity that are required to detect 10^{-11} and 10^{-10} molar peaks, with widths from 5 to 30 seconds. These projected values assume an EM gain of 10^4 and the ability to detect a mass fragment that contains 1 percent of the total current generated during a 1-second period with a minimum signal to noise ratio of 2.5. The measured values of sensitivity for the masses of 28 and 181 fortunately span the mass range into which the majority of the mass fragments from the AA derivatives fall. It can be seen that the sensitivity for GC peaks between 15 and 30 seconds wide containing 10^{-11} moles is about a factor of 2 below the required sensitivity level for high mass operation. The sensitivity, in general, is therefore just about acceptable for the proposed mode of operation. If one or more of the methods discussed previously of improving the sensitivity is included, the total system should be adequate.

Table 6-3. Current and Projected Values for Sensitivity and Resolution

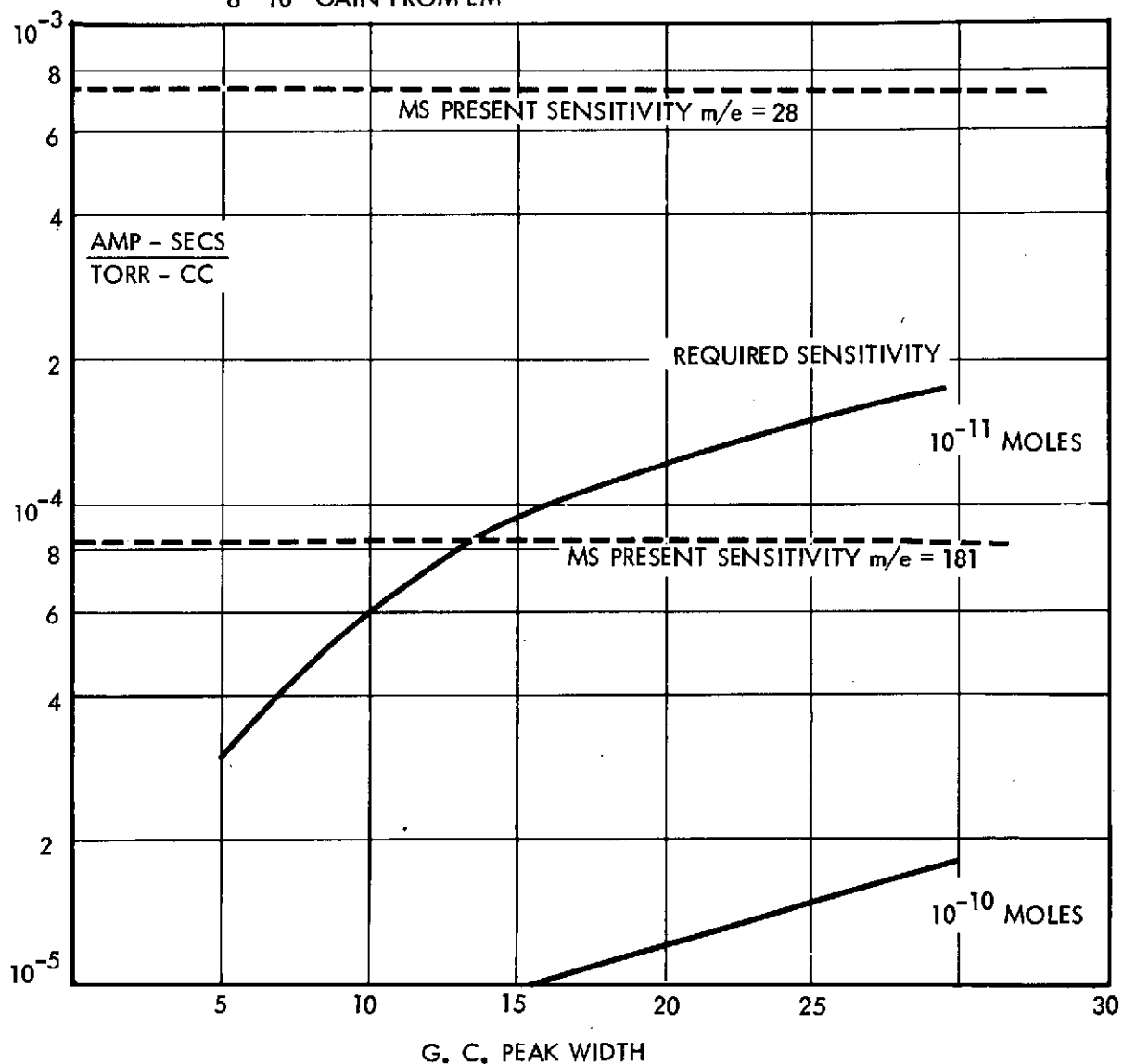| Parameter	Current Value	Comments	Projected Requirements	Suggested Modification to Achieve Projected Value
Sensitivity Amps/torr	3.0×10^{-6}	• In parallel operation with hydrogen flame detector • EM gain 10^4 • Electrometer operating temperature range $\pm 25^\circ C$ • Elution peak must be detectable by GCD	6.0×10^{-6}	• Z focusing • Bellows in the drift tube
Resolution $\Delta m/m$	200 at 20% valley	• Possibly adequate but due to unknowns • a) Flight GC elution characteristics b) Present system charging affects aim for projected value	240 at 5% valley	• Present voltage for mass 200 used for 240 • Decrease slit to 0.0015 inch • Improve pumping capacity • Bellows in line

Figure 6-6. Required MS Sensitivity With GC Peak Width

The sensitivity requirement for the Wet Chemistry experiment is 0.1 to 50 nanomole for each amino acid. The mass spectrometer can detect 10^{-11} moles and on the basis of the above requirement only 10 percent of any peak containing 10^{-10} moles needs be diverted for MS analysis. This allows the GCD to receive approximately the whole of the 10^{-10} molar peak for analysis. In this manner a 50 nanomole peak will be divided so that 5×10^{-9} moles will pass to the MS. This can be analyzed by the mass spectrometer, but for the case of a 5-second peak width it will produce a pressure of 10^{-4} torr in the ion source. This level of signal will need to be reduced before injection into the ion source, as an ion source gas pressure $>3 \times 10^{-5}$ torr can only degrade the signal. The dynamic range of the MS under these conditions will be 10^{-11} to 10^{-9} moles. If the background response of the system allows greater sensitivity than outlined by the above figures and it is desired, then the system will need to be re-evaluated so that both detectors are exposed to the whole sample.

6.1.2.2 Resolution

The parameters of resolution and sensitivity are interrelated, which in practice means that there is a high probability that an increase or decrease in one of these parameters results in the opposite effect in the other. This effect usually limits the improvements that can be made to an existing system. The first part of this discussion describes those modifications to the Viking '75 analyzer that are required to improve the present resolution to a value closer to the worst case resolution of $M/\Delta M = 240$ with 5 percent valley. The second part presents some of the factors which cannot be readily qualified that are affecting the performance of systems presently in test at Perkin-Elmer and suggests some additional modifications, which are fairly extensive, to remedy some of the design deficiencies.

Increased Resolution

Modifications which will increase the resolution and maintain sensitivity are considered in the following paragraphs.

The resolution of the existing instrument is approximately $m/\Delta m = 200$ at 20 percent valley. The resolution is primarily determined by the velocity spread which is a function of the voltage drop in the ionizing region and the accelerating voltage. In order to obtain comparable resolution at m/e 240 the magnetic field strength must be increased so that mass 240

ions would be focused at the same velocity as m/e 200 in the existing design. The alternative is to decrease the beta spread ($\Delta V/V$) in the source and accept some reduction in sensitivity. The best compromise between these two alternatives is to increase the magnet energy to its maximum stable value, about 7 percent below the saturation level, to achieve an MV product for the system of 33000. This will permit mass 240 ions to focus at an accelerating voltage of 137 volts which is nearly equal to the accelerating voltage for m/e 200 in the existing design. The velocity of m/e 240 will be about 10 percent less than that of the mass 200 ions, and in theory the voltage drop in the ionizing region should be decreased about 10 percent to achieve the same beta. In practice, the resolution could be achieved by tuning the instrument within the range of voltage variation currently available in the source. The resulting resolution should be close to that achieved in the present system. No difficulty is anticipated in operation of the magnet at the higher energy.

To increase the resolution to 5 percent valley at mass 240, the slit dimensions and the beam aberrations must be reduced. The calculated beam width in the present system derives from the object slit width, the image defect aberrations (uncorrected second order effects), the Berry curvature, and defects due to mechanical misalignments.

In the existing instrument

$s_o = s_i = 0.002$ inch   The object and image slit width

$y_i = 0.0005$ inch   The second order terms

$B = 0.0015$ inch   Berry curvature

$a = 0.002$ inch   Mechanical misalignments

The resolving power is given by

$$RP = \frac{rm/2 \ (1 - M_m)}{s_o + (s_i M_m + y_i + B + a) \ (1 - V/100)}$$

M_m = magnification of the magnetic sector = -0.678

V = percent valley between adjacent peaks

If a reduction in a of 50 percent could be obtained, the desired resolution could be achieved by narrowing the slits to 0.0015 inch and accepting a 25 percent reduction in sensitivity. In order to improve the mechanical alignment capability, it is suggested that a bellows be included in the drift tube region. This has been discussed in the previous section on sensitivity and is a relatively minor modification, which could result in considerable improvement in performance. Without this flexibility for tuning, the slit dimensions must be reduced to 0.0009 inch and a 55 percent decrease in sensitivity sustained.

Apart from the design changes for improving performance specifications, there are other considerations that should be noted regarding the ability of the current design to reliably perform to specifications. While there is emphasis on maintaining the existing design intact to the greatest possible degree, certain practical considerations may dictate more substantial changes. There are two broad areas that have accounted for a great deal of time-consuming test and retest, and ultimately have resulted in serious compromises in performance. These are poor stability and insufficient flexibility in tuning. Each of these areas is discussed below with recommended modifications.

Stability

The history of the Viking analyzer provides ample evidence of instability. It is usually manifested as a decrease in resolution at the high mass end of the spectrum. The basic instrument is capable of a resolution typified by less than 10 percent valley between m/e 181 and m/e 182. When performance deteriorates, the valley may increase to 30 to 40 percent. In nearly every instance the cause of deterioration has been traced to charge-up of surfaces within the analyzer, usually within the magnetic sector. Specific and careful stability tests have not been very successful in isolating, clarifying or quantifying this effect, and it continues to plague instrument test. The single most successful method of dealing with this problem has been to coat the magnetic sector surfaces with Aquadag (a colloidal suspension of graphite). In some instances multiple coatings have been required and even then deterioration has recurred. There is a serious question regarding the durability of the Aquadag coat and the reliability of flight instrumentation utilizing this surface coating.

Typically in high resolution instruments two approaches are used to minimize surface charging effects: (1) the number of ions striking surfaces in the analyzer region is reduced to an absolute minimum; and (2) the criticality of ions striking a particular surface is minimized.

Several design factors are important in minimizing ion current striking the analyzer surfaces:

1) Increase the magnetic sector gap. The gap in the existing design is 0.100 inch; it is the narrowest point along the analyzer path length. Many ions strike the magnetic sector pole pieces. Increasing the gap would reduce this number and increase sensitivity at the same time. The disadvantage is that the increased gap would demand a larger analyzer magnet.

2) Add a baffle in front of the magnetic sector to intercept those ions that would otherwise strike the pole pieces. This would also cut off some ions that would otherwise be transmitted. The advantage, however, is that this surface is less critical because the transmitted ions pass by it more rapidly and are less affected by surface charges.

3) Reduce the object slit height. This will limit the range of Z-axis initial conditions and eliminate many ions that would otherwise strike analyzer surfaces. While there is some attendant loss in sensitivity, this is not too severe.

4) Add a Z-axis focus lens at the alpha focus between the electric and magnetic sectors. This will improve Z-direction transmission of ions as discussed earlier.

By properly implementing all of these steps, it is possible to devise a design in which a fairly small fraction of ions entering the analyzer are not transmitted, and these will all strike the vertical baffle in front of the magnetic sector. Even with these improvements some ions will strike analyzer surfaces, and the potential for surface charging still exists. The following changes could further reduce the possibility of deleterious effects:

1) Those surfaces receiving the preponderance of ions should be heated. The vertical baffle and the image slit fall into this category. By keeping them hot absorption of compounds which may form insulating surfaces is reduced. Of course, power demands for heating would be a few watts.

2) Increasing the speed of the ion pump to reduce the analyzer pressure and thereby the number of gas molecules striking surfaces. The present Viking ion pump has a speed of only a few hundred ccs/sec and is extremely small by conventional mass spectrometer standards. Typical high resolution laboratory instruments use several hundred liter per second pumps, even though

their gas loads are not 10^3 larger. The net result is that the Viking analyzer may experience peak analyzer pressures of 10^{-5} torr. It would be feasible to increase the ion pump speed to a few liters per second. Any increase above this would be too costly in weight and ineffective because of the conductance limitations in the analyzer. There is an existing design for a 4 liter per second ion pump which has flown on Skylab 1. It weighs approximately 4 pounds.

3) The discussion thus far has referred to ions striking surfaces that are out of the central plane. Ions also strike the outer and inner radial boundaries of the magnetic sector, and the end of the sector around the image slit. While these surfaces may charge up, the effect can be minimized by displacing them as far as is reasonable from the optical axis. This would lead to some enlargement of the analyzer housing, but the weight penalty would not be serious.

4) One of the factors affecting the degree to which surface charging deteriorates performance is the velocity of the ions as they pass the charged surface. This is evidenced by the data that show a more rapid fall off in resolution with increasing mass than can be accounted for by beta effects alone. Therefore, in theory the effects of charging can be reduced by increasing the ion energy. This necessitates a larger analyzer magnet since either the radius of the magnet of the field strength must be increased in proportion to the square root of the velocity. This is not an appealing approach since energy does not increase very rapidly with weight for a magnet.

In summary, there are several possible improvements that can potentially be made in the existing Viking analyzer to improve stability. Taken in aggregate they represent fairly significant design changes with associated power and weight penalties. While this is not particularly desirable, neither is the alternative, and therefore they should be considered.

The effect of "tuning" the system was covered in the section on sensitivity. Since the parameters of resolution and sensitivity are closely related there is a natural tradeoff if one parameter is improved at the expense of the other. One of the possible system "tuning" possibilities not covered in that section was compensation for Berry curvature. The existing design provides a certain amount of correction for Berry curvature in that the slits are curved in the image slit plate. The radius of curvature was determined experimentally at JPL using the "Bell Jar" system. However, no two magnets are completely identical and the

6-21

fringe fields may vary slightly from unit to unit. For these reasons it would be desirable to have some capability for correcting this aberration within the system tuning procedure. Furthermore, if a Z-axis lens is built into the drift tube to improve ion transmission, there may be significant change in the image plane. It is proposed that a lens systems in the region between the exist from the magnetic section and the image slit plane be used to straighten the beam. This would permit adjustment of the image defect for each individual unit during tune up of the system.

Discussion

As explained at the beginning of this report, the generation of more data together with a more detailed analysis is required before the real requirements for resolution can be deduced. The present resolution may be adequate but the modifications suggested in this study should enable a better resolution to be obtained, if it is required. On the basis of the above information a value for the resolution of the instrument will be tentatively stated requiring an $M/\Delta M = 240$ with a 5 percent valley.

6.1.3 Mass Spectrometer Scan Time

Data generated in the past by the Wet Chemistry experiment indicate that the nominal range of peak width obtained from GC chromatograms is from 3 to 30 seconds. It is possible that by varying the operating parameter of the GC the duration of the peak widths can be increased. It is felt that a nominal range of 5 to 30 seconds would not degrade the GC capability while not imposing severe demands on the electronics. The present Viking MS has a scan time of 10.3 seconds over the mass range of 12 to 200. It is desirable to have at least two scans per peak but in the present case this would mean a minimum peak width of 21 seconds, which is not compatible with efficient GC operating conditions. It appears that a 5-second scan time would be feasible for the Viking '75 MS without producing a major impact on the response time of the electronics and in addition is a minimum operating point for the Wet Chemistry GC. When the operating components and parameters for the GC have been optimized the MS ideal scan time should be re-examined.

6.1.4 Operating Temperature

The volatile amino acid derivatives eluted from the GC column need to pass through considerable plumbing before they reach the GC detector and the MS for analysis. The temperature of this interface region needs to be high enough to stop any condensation of the components. The maximum temperature that is required to efficiently elute the high boiling point amino acids is dependent on the GC column that is used. The current two columns that are being investigated for use with the Wet Chemistry experiment are Carbowax M and Dexil 400. For maximum efficiency in eluting the amino acids the Dexil requires a maximum temperature of $1250^{\circ}C$. However, the Carbowax M maximum temperature is $210^{\circ}C$ and the present Viking '75 ion source has an operating temperature of the same value. If the Dexil is operated at this lower figure, the high boiling point compound takes much longer to elute and a loss in resolution would occur. However, it would appear that if Dexil is used this loss in efficiency could be tolerated.

The other component that has a major impact on the operating temperature is the palladium leak. This is analyzed in Section 5.2 where an operating point of $220^{\circ}C$ is suggested. It would appear from the above discussion that a temperature of $220^{\circ}C$ would be the best compromise temperature for the interface between the GC and the MS and for the MS ion source.

6.1.5 Vacuum Requirements

The MS of the current Viking '75 GCMS and of the proposed Wet Chemistry GCMS both have a vacuum pumping operation that is different from the normal laboratory system. Because of this difference, a brief description of the flight MS is performed to clarify the operational mode of these flight systems. The MS vacuum requirements for the flight system are then analyzed by studying the operation of the ion source and analyzer sections individually, as they both have quite different requirements. The output from the GC that enters the MS consists of two steady background components of the GC hydrogen carrier gas and column bleed, plus two transient components. These transients are a background signal of "junk peaks" from the Wet Chemistry amino acid derivatizer and the

real signal composed of the amino acid peaks. As this total effluent from the GC passes through both the MS ion source and analyzer, each of these components is analyzed in terms of the four gaseous input parameters. A summary of the effect of these four parameters on the operation of the system is shown in Table 6-4.

6.1.5.1 General MS Operation

A percentage of the gaseous output from the GC columns is directed into the ion source of the MS, where a small fraction is ionized by the electron beam. The efficiency of ionization is directly dependent on the gas pressure inside the ion source and a typical operating pressure is usually in the region of 10^{-4} torr. In the laboratory the ion source pressure would be regulated by removing the residual neutral gas with a high speed pump. The ionized portion of the gas, which contains all the usable information, is directed out of the ion source and into the analyzer section, where the various m/e components in the beam are separated out. The analyzer section requires a vacuum of approximately 10^{-6} torr to completely eliminate losses from the beam, due to ion collisions with the residual gas molecules, so this section usually has a separate high speed pumping system.

For space applications the analyzer pump performs the vacuum pumping for both the ion source and analyzer sections, to save power and weight. The ion source is maintained at a higher pressure with respect to the analyzer by allowing the neutral gas from the ion source to pass into the analyzer in a controller manner, through low conductance apertures. However, in this mode of operation it is much more difficult to maintain the ideal pressure conditions for both the ion source and analyzer sections. This process is called "differential pumping", and it allows an equilibrium flow condition to be maintained in the MS.

The total throughput Q (torr cc/sec) of gas into the ion source, at a pressure P_1 torr, is pumped through the ion source/analyzer aperture which has a leak rate of S_1 scc/sec. The same throughput Q enters the analyzer at a lower pressure P_2 torr, which is being pumped at a rate of S_2 scc/sec.

Table 6-4. An Example of the Vacuum Conditions for the MS Operating with Wet Chemistry

| | | Gas Throughput Torr cc/sec | Ion Source | | Analyzer | |
	From the GC	Into the MS	Conductance cc/sec	Pressure Torr	Conductance cc/sec	Pressure Torr
Hydrogen Carrier Gas-Separator at 220°C	3.4×10^{-4} (6 cc/min)	3.4×10^{-5}	~160	2.2×10^{-7}	~600	6×10^{-8}
Column Bleed for Average m/e=100	1.7×10^{-4} (10^{-9} gms/sec)	8×10^{-5}	~25	3.2×10^{-6}	~400	2×10^{-7}
Amino Acid or "Junk Peak"	3.4×10^{-3} (10^{-9} M over 5 sec)	3.4×10^{-4}	~18	2×10^{-5}	~400	8×10^{-7}
TOTAL		4.5×10^{-4}		2.3×10^{-5}		10^{-6}

$$Q = P_1 \times S_1 = P_2 \times S_2$$

$$\frac{P_1}{P_2} = \frac{S_2}{S_1}$$

The pressures in the ion source and analyzer sections can be regulated by the choice of the ratio of ion source conductance S_2 to the total pumping speed of the system. The conductance S cc/sec of an aperture whose length is less than all cross sectional dimensions can be approximated to:

$$S = K_1 K_2 \sqrt{\frac{T}{M}}$$

where K_1 is a dimensional constant,

K_2 is the clausing factor for transmission,

T is temperature in $^\circ$K,

M is the molecular weight.

The conductance of the ion source for various gases, together with an estimate of analyzer pressure for a normal ion source operating pressure is displayed in Table 6-5.

6.1.5.2 Ion Source/Analyzer Investigation

As previously mentioned, the ion source operation will be studied as a function of the four input components of hydrogen carrier gas, GC column bleed, system "junk" peaks and the amino acid peaks. The first three components represent the noise background from which the amino acid peaks need to be resolved. The column bleed from the GC columns that are likely to be used with the Wet Chemistry system has been found to be $< 5 \times 10^{-9}$ gms/sec.

The other unknown is the magnitude and width of the GC "junk peaks". These peaks will produce MS fragmentation patterns, which hopefully will be identifiably different from the amino acid patterns. One of the reasons for a concern over them in this context is their possible overloading of the pressure in the ion source. Because of their unknown characteristics, they will be assumed to be similar in size and shape to the amino acid peaks.

Table 6-5. Ion Source Conductance and Analyzer Pressure
for Various Compounds

	Compounds		
	$\underline{H}_2$	$\underline{N}_2$	Heavy Organics 100-400 amu
Ion Source Conductance S_1 cc/sec	160	42*	22 - 11
System Pumping Speed S_2 cc/sec	~600	~300*	~300
S_2/S_1	~4	~8	~15 - 30
The Resulting Pressure in the Analyzer for a Pressure of 3×10^{-5} torr in the Ion Source	8×10^{-6} torr	4×10^{-6} torr	2×10^{-6} to 10^{-7} torr

*Quoted flight unit values.

6.1.5.3 Ion Source Requirements

The ion source requirements will be studied as a function of the previously mentioned four input components. The worst case column bleed of $\sim 5 \times 10^{-9}$ gms/sec is equivalent to a gaseous throughput of 8.0×10^{-4} torr cc/sec for an average mass of ~100 amu. This will be divided before entering the MS in the ratio of 10:1, and only 8.0×10^{-5} torr cc/sec will enter the ion source. This throughput of gas will produce an ion source pressure of 3.2×10^{-6} torr, for the present value ion source conductance. In practice this throughput of gas will not be a constant, but will decrease with a decrease in the column temperature, during the column programmed heating.

The remaining three input components will be studied for a wide range of operating values. However, before this is carried out, a brief study will be made of current data obtained from the MS flight units. In Figure 6-7 is shown the ion current produced as a function of ion source gas pressure for several compounds with different molecular weights. The indication is that for high mass organics ≥ 100 amu, the response
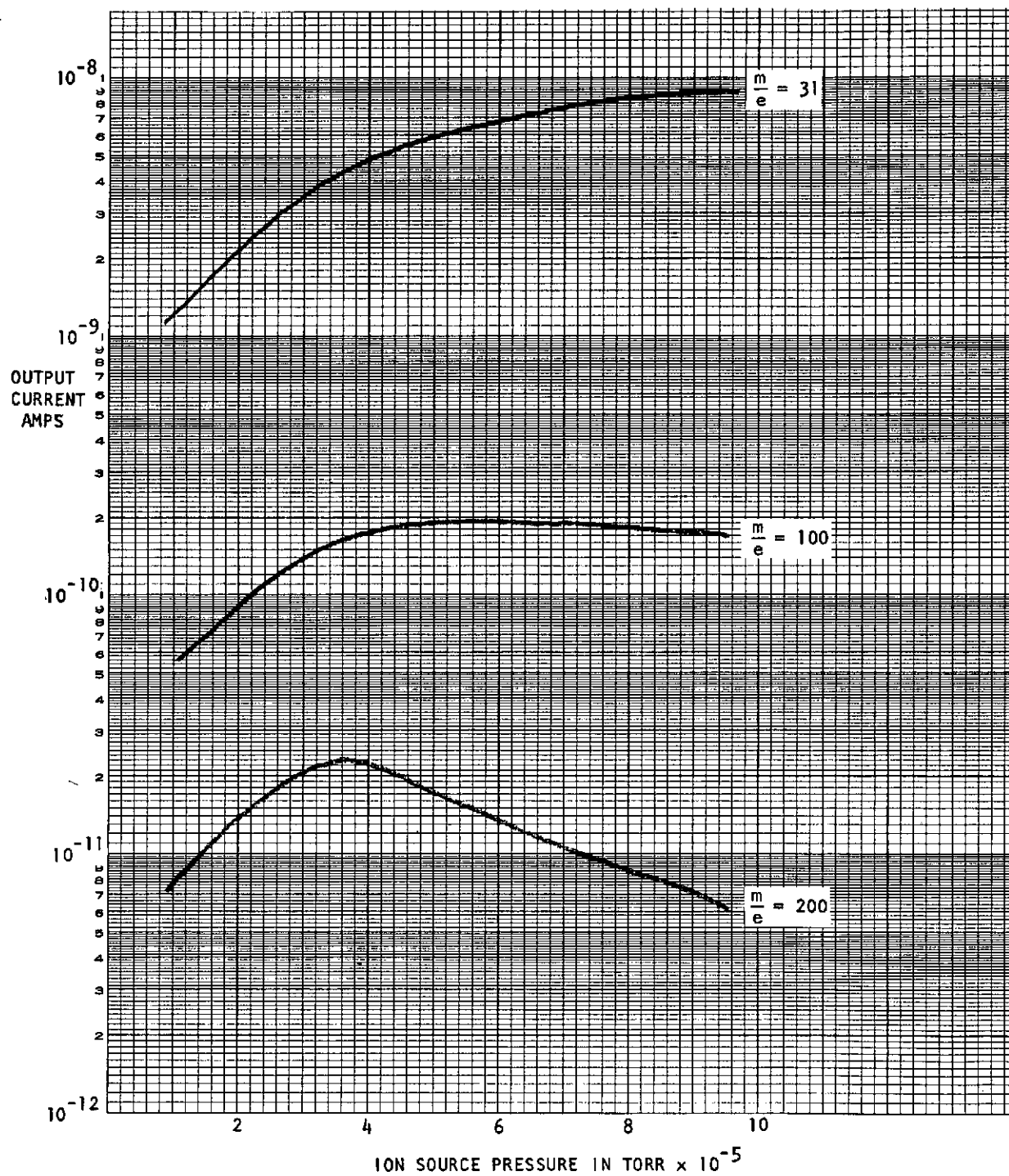
Figure 6-7. Ion Current Output With Ion Source Pressure
(Obtained from Perkin Elmer Viking 1975-MS-CDR)

6-28

becomes nonlinear at about 3×10^{-5} torr and above this value the situation deteriorates rapidly. However, this critical pressure may increase after the ion source voltages are altered to achieve a high sensitivity at large mass numbers for GCMS operation. The results of an analysis of the ion source pressure, as a function of junk peak or amino acid derivative mass number, GC peak widths and molar concentration are displayed in Figure 6-8. From this figure it can be seen that in order to keep the ion source pressure below 3×10^{-5} torr, for amino acids or junk peaks with a mass greater than 200, a 5-second peak cannot contain more than 10^{-10} moles, and a 30-second peak 10^{-9} moles. It should be noted that the molar peak values represent the level actually injected into the MS, which is not necessarily the value for the GC output. This is related to the suggestion that a flow divider be used to split the GC effluent between the MS and the GC detector. This divider will allow 90 percent of the flow to go to the GC detector and the remaining 10 percent will enter the MS ion sources.

The ion source pressure produced by the GC hydrogen carrier gas flowing into the MS can also be estimated. This pressure is in addition to the amino acid peak pressure, and will constitute a continuous background level to which the AA or junk peak pressure is an additive transient. The present ion source conductance is 42 cc/sec for N_2 which produces a pumping speed of ~160 cc/sec for H_2. This pumping speed is close to the total pumping capacity available to the whole system, so for hydrogen there appears to be little in the way of a pressure differential between the ion source and the MS analyzer. (See Table 6-5.) As hydrogen has this high pumping speed, the ion source pressure can be obtained directly from the analyzer pressure characteristics. The ion source pressure for hydrogen can be obtained from the plot of analyzer pressure with separator efficiency for different pumping speeds, which is displayed in Figure 6-9. The separator temperature is planned at the moment to be $220^{\circ}C$, which should produce an ion source hydrogen pressure of 3.5×10^{-6} torr, for a pumping speed of ~160 cc/sec. In addition, the use of the divider after the GC column with the previously mentioned ratio of 1:9 would reduce the hydrogen background to $< 10^{-6}$ torr in the ion source. This is especially desirable as ion pumps similar to the one on the MS tend to re-evolve previously buried hydrogen when exposed to a high pressure during operation.
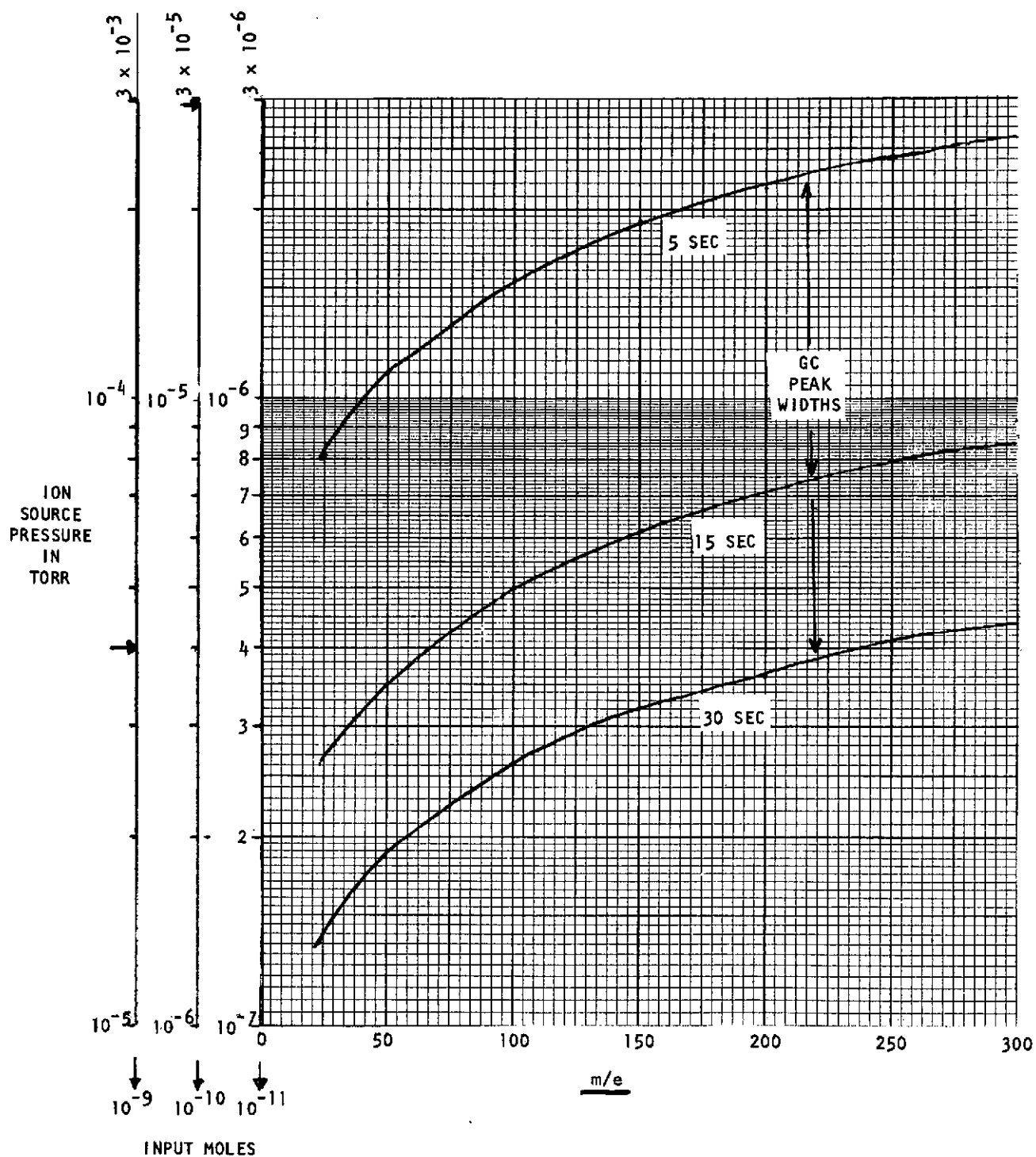
Figure 6-8. Ion Source Pressure as a Function of Mass, Peak
Width and Molar Input. (At present to avoid mass dis-
crimination a maximum pressure of 5 x 10^{-5} torr is
suggested.)

Axis labels:
- Y-axis: $\dfrac{H_2 \text{ Out Sep.}}{H_2 \text{ In Sep.}}$
- X-axis: MS PRESSURE IN TORR

Curve labels: 1000 cc/sec, 500 cc/sec, 100 cc/sec MS PUMPING SPEED

SEPARATOR TEMPERATURE - 190 °C

200 °C

≥220 °C
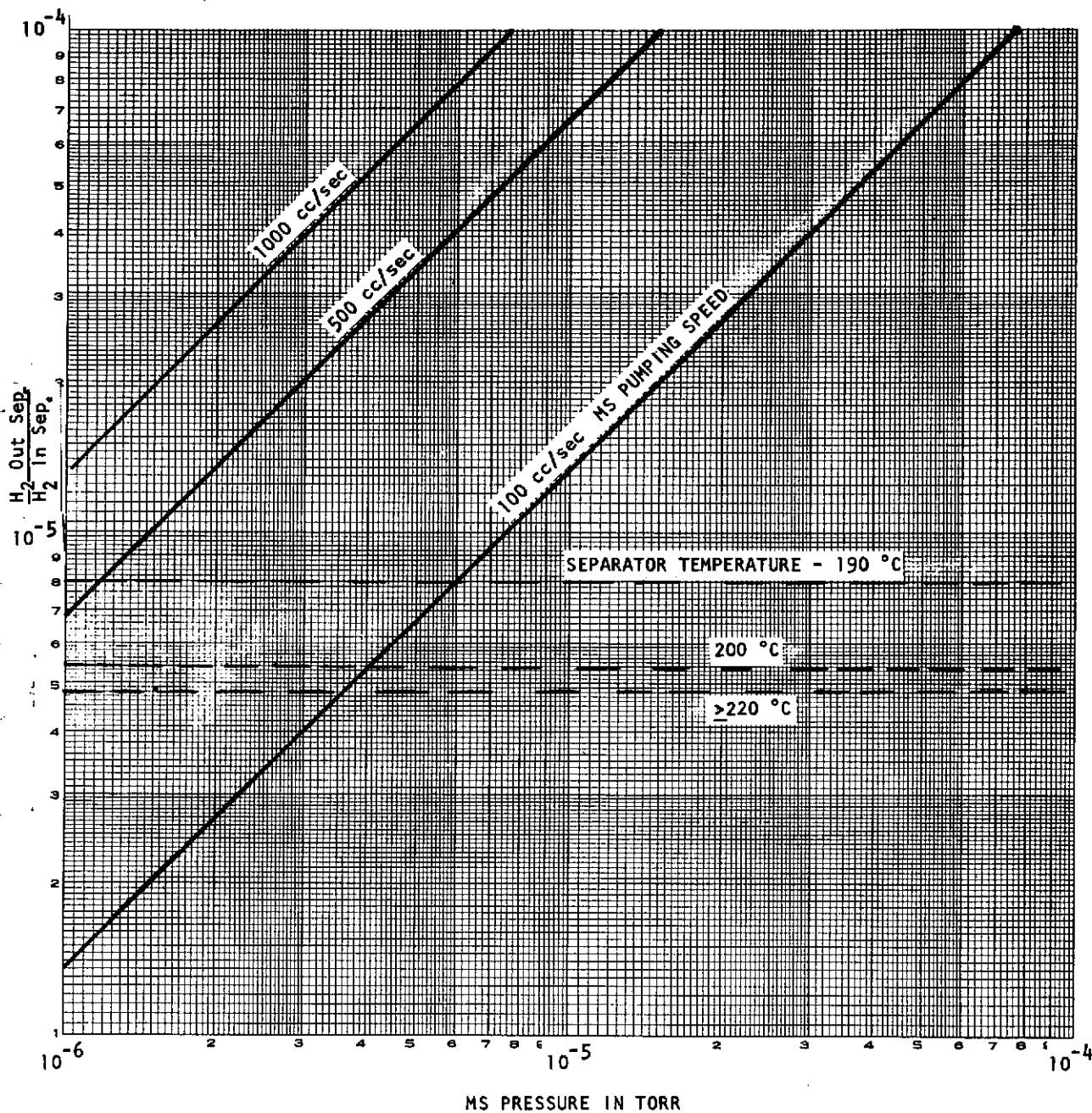
*If a 10:1 divider is used divide required pumping speed by 10.

ure 6-9. MS Pressure Relative to Separator Hydrogen Rejection
Ratio, Pumping Speed* and Separator Temperature

An example of how the total pressure in the ion source can be deduced from the various component partial pressures that were obtained above is shown in Table 6-4. The carrier gas appears to be the least worry as it is a relatively low partial pressure, and the ion fragments produced by gas ionization are well out of the proposed mass range of 55 to 240 amu. The column bleed also produces a considerable partial pressure; however, the ion fragments produced from the ionization process are likely to be less than an m/e of 150 (see Laboratory Investigation, Section 7). However, the column bleed may be a problem for very low levels of amino acids. The junk and amino acid peaks appear to cause no problem, if the larger peaks are reduced with a flow divider before entering the MS, allowing a maximum throughout of 4.0×10^{-3} torr cc/sec into the ion source.

Another mode of operating the ion source is that currently used on the GCMS which is to allow operation in the nonlinear region and correct for the effect with a computer program. The change from linear to non-linear operation during a wide GC peak, which allows many mass scans, should be relatively easy to determine in practice by the time varying mass spectrum, but it would appear that this method is likely to result in some loss of data. However, for the case of narrow but large peaks, with a width equivalent to the MS scan time, an AA scan will be much more difficult to analyze. Furthermore, if a junk peak or a large amount of column bleed is also present, the analysis would be further complicated. For the Wet Chemistry operation where the high mass range is very important, the majority of the amino acids will be subject to nonlinear effects for GC peaks containing $>10^{-9}$ moles. The loss of data that is likely to result from the necessity to determine if the ion source is operating in a nonlinear region, in addition to identifying an amino acid from the system background, may not be feasible for Wet Chemistry operation. It appears that a tradeoff study between the two methods is needed to clarify the situation.

6.1.5.4 The Analyzer Requirements

The analyzer pumping requirements are simpler than those for the ion source, as in this case pumping is only needed to lower the pressure sufficiently to reduce collisions between ions and residual molecules. In

Figure 6-10 the MS analyzer pressure is displayed as a function of system pumping speed, GC peak width, and molar concentration. Again the figure for molar concentration is the amount entering the ion source. For the desirable analyzer pressure of 10^{-6} torr, with the present pumping speed of ~300 cc/sec, the maximum 5-second GC peak has a magnitude ion of 10^{-10} moles. This figure is increased to 3×10^{-10} moles for a 5-second peak and 10^{-9} moles for the average 15-second peak for a 1 liter/sec pumping speed. The present system is therefore restricted to operating over an input range of 10^{-10} to 10^{-11} moles if a 5-second peak is obtained. An increase in pumping speed is therefore necessary if a wider operating range is required, and if losses due to ion collisions with residual gas molecules are to be minimized.

In terms of the hydrogen background from the GC carrier gas, the additional pressure in the analyzer that is produced as a function of separator and analyzer pumping speed is shown in Figure 6-9. At the proposed operating temperature of $220^{\circ}C$, ~ 300 cc/sec are required to keep the analyzer at 10^{-6} torr.

The partial pressure resulting from the column bleed throughput of 1.7×10^{-5} torr cc/sec should be 3×10^{-8} torr, and is therefore insignificant.

An example of how the four input components effect the total analyzer pressure can also be seen in Table 6-4. If the amino acid and junk peaks are limited in the same manner suggested for controlling the ion source pressure, the present system is just adequate.

6.1.5.5 Conclusion

The present system appears to have a marginal capacity to cope with the expected range of peak widths, concentration, and the hydrogen carrier gas background. In both departments of ion source and analyzer a wide range of operation cannot be obtained with the present pumping capacity. An increase in pumping capacity to the originally specified level of at least 1 liter/sec, will generally improve the system's capability. If an increase in analyzer magnet strength to improve sensitivity is initiated, a further increase in pumping capability can be achieved with very little increase in power or weight.
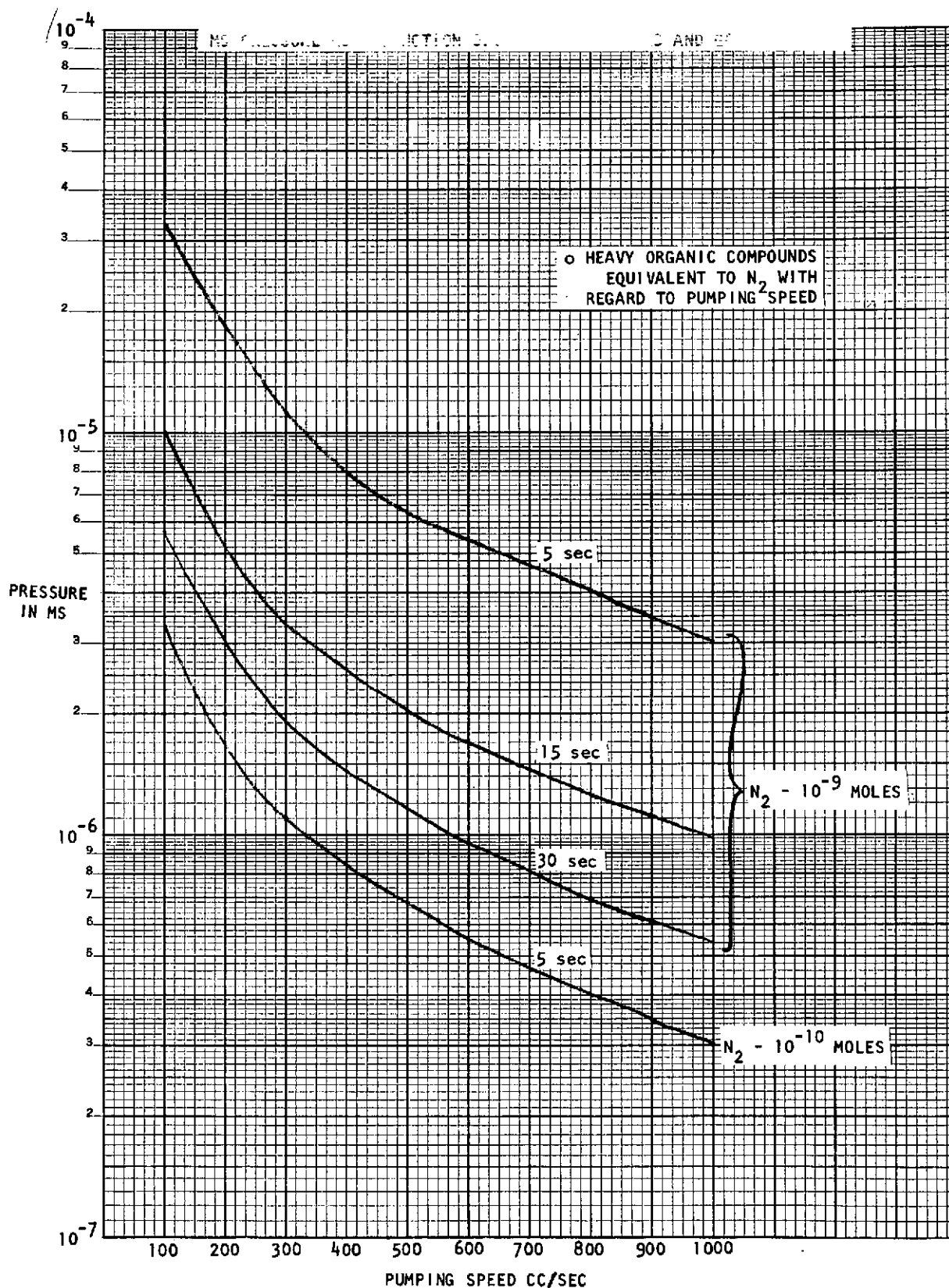
Figure 6-10. MS Pressure as a Function of Pumping Speed and GC Peak Width

A tradeoff study to determine the best method of coping with the ion source high mass non-linearity is required. This study should evaluate the three processes of ion source pressure limitation, increasing the maximum linear operating pressure and the present system of data correction techniques.

It should also be possible with the aid of the figures and tables in this study, to quickly evaluate what effects any proposed change in the system would have on the MS vacuum requirements.

6.2 CONCEPTUAL INSTRUMENT SYSTEM DESIGN

A Wet Chemistry/Mass Spectrometer instrument system schematic is shown in Figure 6-11. It shows the addition of a hydrogen gas supply system to the Wet Chemistry instrument. This is necessary since the GC-carrier gas has to be pure hydrogen to operate with the MS, as discussed in Section 5. On the other hand, for proper operation of the flame ionization detector (FID), the hydrogen has to be diluted by adding helium which is supplied by the He gas supply system. The Wet Chemistry/ Mass Spectrometer interface shows the fixed 1:10 effluent divider, to bring the flow rate into the mass spectrometer down into the region that can be handled by the MS. Additional regulation of the effluent flow rate is provided by the programmable divider, which is controlled by the flame ionization detector signal. A flow restrictor delays the appearance of the gas flow peak in the programmable divider until the FID analysis is completed and fed into the programmable divider control electronics. The hydrogen carrier gas is finally removed in the hydrogen separator, and only the amino acid derivatives enter the mass spectrometer ion source.

Except for the 1:10 divider, which is located at the GC-column outlet, the interface components are contained in a thermally controlled enclosure like in the current Viking GCMS.

Figure 6-12 shows the integrated Wet Chemistry/Mass Spectrometer instrument. Both instruments (and also the Wet Chemistry electronic subsystem) are mounted independently to the lander mountings plate. This assures minimum design changes in the existing Viking MS
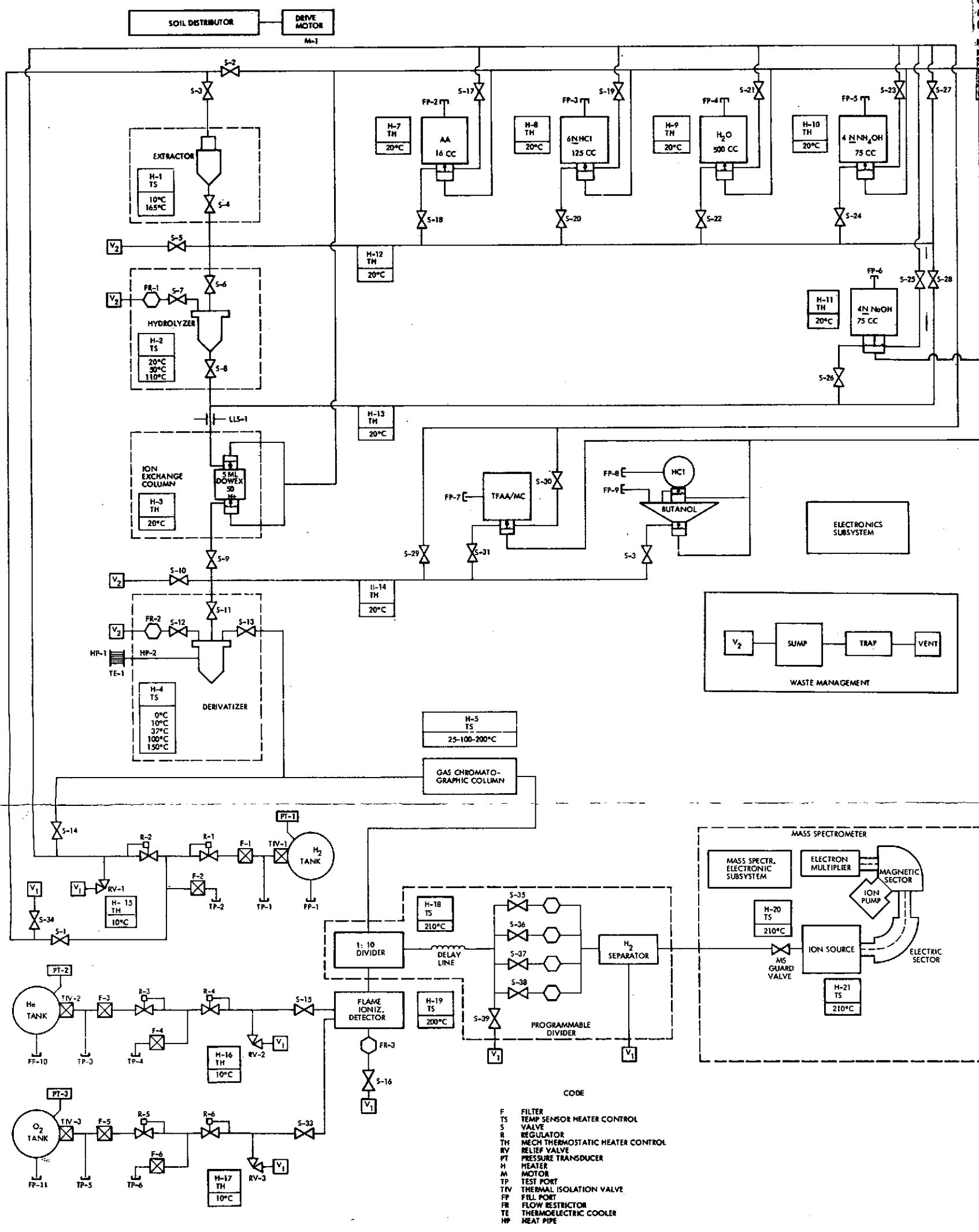
Figure 6-11. Baseline Instrument System Schematic

CODE

F	FILTER
TS	TEMP SENSOR HEATER CONTROL
S	VALVE
R	REGULATOR
TH	MECH THERMOSTATIC HEATER CONTROL
RV	RELIEF VALVE
PT	PRESSURE TRANSDUCER
H	HEATER
M	MOTOR
TP	TEST PORT
TIV	THERMAL ISOLATION VALVE
FP	FILL PORT
FR	FLOW RESTRICTOR
TE	THERMOELECTRIC COOLER
HP	HEAT PIPE

SOIL PROCESSOR

WET CHEMISTRY
ELECTRONICS SUBSYSTEM

EXCESS SOIL DUMP CONTAINER

WET CHEMISTRY
MECHANICAL SUBSYSTEM
(REF)

MASS SPECTROMETER

MOUNTING & INTERFACE PLANE

WET CHEMISTRY
GAS CHROMATOGRAPH
COLUMN

H_2 SEPARATOR
AND EFFLUENT
DIVIDER (REF)

ION SOURCE
(REF)

WET CHEMISTRY
MECHANICAL SUBSYSTEM

MAGNET (REF)

MASS SPECTROMETER
ELECTRONICS SUBSYSTEM

ION SOURCE

ELECTROSTATIC SECTOR

DRIFT TUBE

H_2 SEPARATOR
AND EFFLUENT
DIVIDER

MAGNET

ION PUMP

ELECTRON MULTIPLIER

WET CHEMISTRY
GAS CHROMATOGRAPH
COLUMN (REF)

VALVE (V7)

MASS SPECTROMETER ELECTRONICS SUBSYSTEM OMITTED IN THIS VIEW FOR CLARITY

Figure 6-12. Wet Chemistry/Mass
Spectrometer Instru-
ment Prototype

6-37

support structure and in the current Wet Chemistry design. The MS components are mounted on one side of a mounting plate and the other side contains the MS electronic subsystem which incorporates the ion pump electronics, ion source and bias voltage control electronics, and the scan control and electron multiplier electronics. Additional MS control and data processing electronics are packaged in the Wet Chemistry electronic subsystem.

6.2.1 Weight and Volume

The weight of the integrated instrument is estimated to be 51.4 pounds. This breaks down into 29.4 pounds for the basic Wet Chemistry instrument and 22 pounds due to the addition of the mass spectrometer. A detailed weight breakdown of the basic Wet Chemistry instrument (without the added H_2 gas supply system) is given in Table 6-6. The added 22 pounds are broken down in Table 6-7.

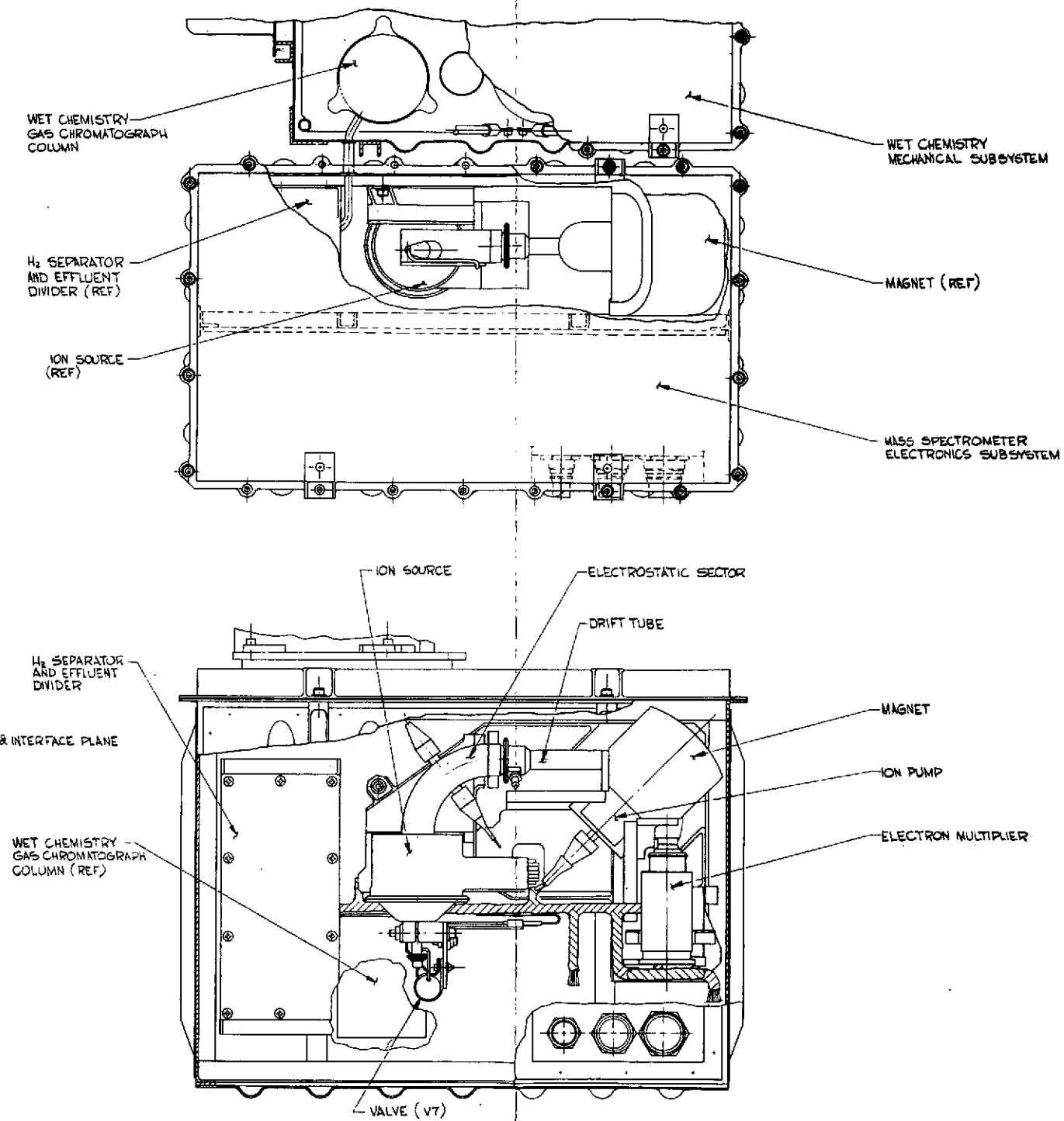The additional volume necessary to allow the integrated instrument is approximately 800 cubic inches.

6.2.2 Electrical Subsystem and Power Consumption

The incorporation of the MS into the Wet Chemistry experiment results in relatively minor changes to the electronic subsystem (ESS). The added control and data processing circuitry required in the ESS will amount to approximately 160 components. These components will bring the total ESS part count to 1320, which can still be packaged within the volume allocated to the ESS. The weight impact of the added electronics is 0.7 pound and thus the total estimated weight of the electronic subsystem is 9.7 pounds.

A block diagram of the new circuitry is shown in Figure 6-13. The control logic provides the necessary digital signals required to enable the mass spectrometer, select the mass spectrometer scan range and enable the other control functions (Items 1 through 11) in Table 6-8. These signals are generated in response to internal sequencer or Lander commands.

The mass spectrometer produces both science and engineering data. The engineering data (Items 15 through 21 of Table 6-8) will be sampled by the existing ESS A/D converter at a rate consistent with scientific data rates. The science data or the Resolved Ion Current (RIC) are provided

Table 6-6. Weight Summary

	Weight (Pounds)
Soil Distributor	0.3
Test Cells	
Extractor	0.4
Hydrolyzer	0.6
Derivatizer	0.4
Ion Exchange Column	0.2
Gas Chromatographic Column	0.5
Flame Ionization Detector	0.2
Reagent Injectors	
Amino Acids	0.3
HCl	0.6
H_2O	0.5
NH_4OH	0.5
NaOH	0.5
HCl/Butanol	0.3
TFAA/MC	0.4
Isolation Valves	0.8
He/H_2 Subsystem	1.3
O_2 Subsystem	1.3
Solenoid Valves and Block	0.8
Gas Operated Valves	1.5
Plumbing	0.5
Waste Management	0.2
Thermoelectric Installation	0.3
Primary Structure	5.9
Electronics Subsystem	8.4
Electrical Installation	0.6
Total Dry Weight	27.3
Consummables	
Gases	0.3
Liquids	1.8
Total Weight	29.4

Table 6-7. Additional Weight Breakdown

	Weight (Pounds)
Mass Spectrometer Analyser	6.0
Mass Spectrometer Electronics	9.5
Mounting Plate	3.5
Enclosure	1.7
H_2 - Gas Supply System	1.3
Total	22.0

in the form of half cosinusoid pulse, nominally 12.93 milliseconds wide at half peak height. The output voltage varies logarithmically from +9.75 to 1.0 volts corresponding to 10^{-13} amps to 10^{-6} of EMT output current with a scale factor of 1.25 volts/decade. The EMT output signal is first processed with an active 3-pole Bessel filter with a 1 kHz cutoff. The purpose of the filter is to reduce the electronic noise generated in the RIC electrometer preamplifier as well as produce the highest signal-to-noise ratio at the peak of the output pulse for an input pulse of known shape. After the EMT output is filtered, it is processed by a Sample and Hold circuit and converted by a 9-bit successive approximation A/D converter. This new A/D converter has been added because of the high data rate requirement (one sample every 2.58 milliseconds of the mass spectrometer). The output of the A/D converter is then sent to the data formatting logic for direct transfer to the DAPU.

The regulated voltage supplies required by the mass spectrometer will be produced by the present ESS power supply. The power delta due to the new ESS electronics is approximately 0.4 watt and thus the total estimated ESS power increases to 5.0 watts continuous. Current mass spectrometer operating power is estimated at 27.5 watts with the ion source at $210^{\circ}C$. The total power consumption of the integrated instrument is thus approximately 32.5 watts.
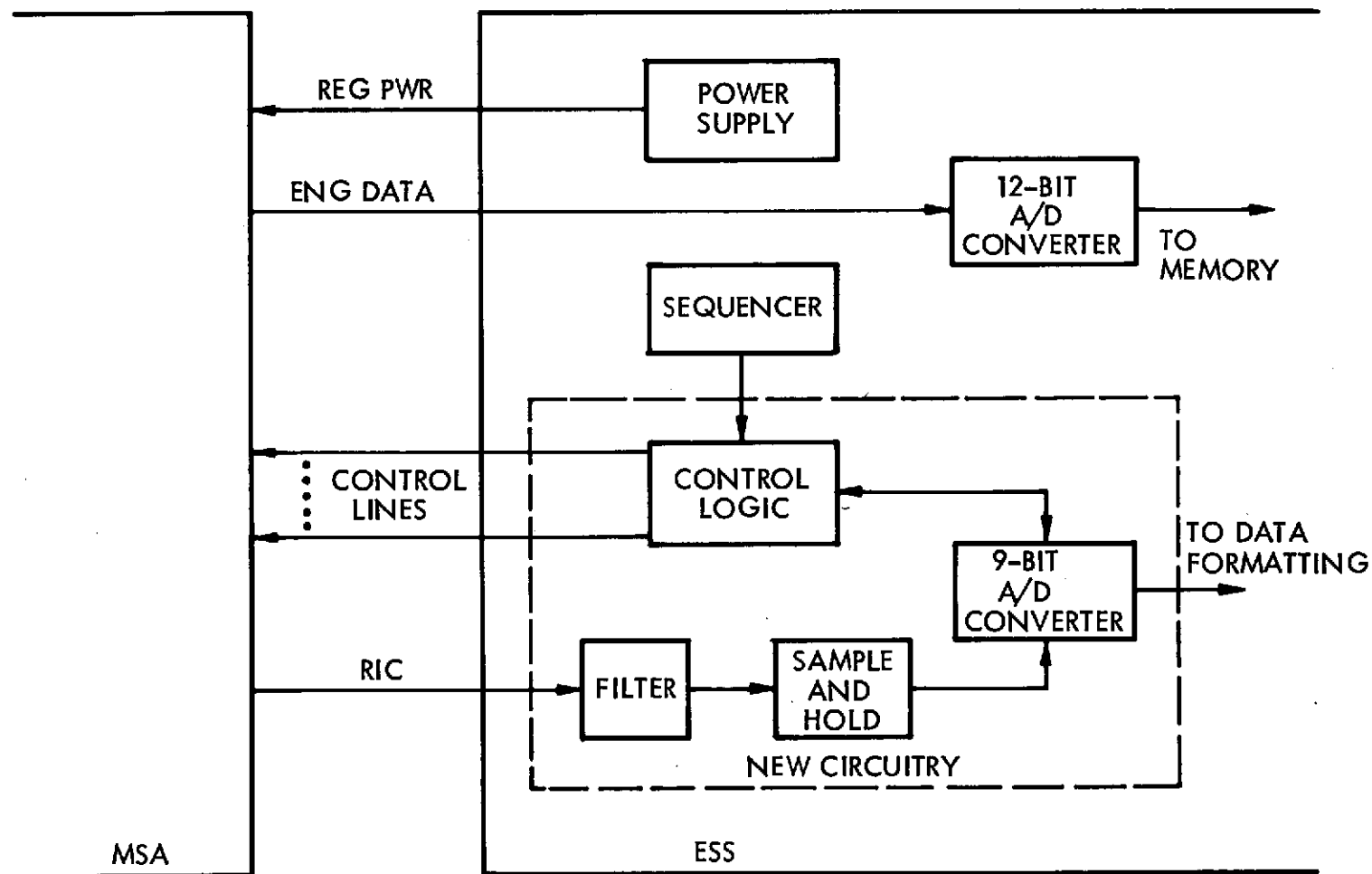
Figure 6-13. Block Diagram, Wet Chemistry ESS and Additional Mass
Spectrometer Control and Data Analysis Electronics

Table 6-8. ESS/MSA Electrical Interface

Item	Name	Parameter	Flow ESS MSA	Type	Range
1	IBSEL	ION BEAM VOLTAGE SELECT	>	DIGITAL	0/1
2	ISFSEL	ION SOURCE FILAMENT	>	DIGITAL	0/1
3	INSHEN	ION SOURCE HEATER ENABLE	>	DIGITAL	0/1
4	EMTSEL1	EMT HV SELECT-1	>	DIGITAL	0 1
5	EMTSEL2	EMT HV SELECT-2	>	DIGITAL	0/1
6	MSENBLE	MSA ENABLE	>	DIGITAL	0/24.8 kHz
7	MSENBLE*	MSA ENABLE*	>	DIGITAL	0/$\overline{24.8 \text{ kHz}}$
8	SCANIT	SCAN INITIATE	>	DIGITAL	0/1
9	RANSEL1	SCAN MONITOR RANGE SELECT 1	>	DIGITAL	0/1
10	RANSEL2	SCAN MONITOR RANGE SELECT 2	>	DIGITAL	0/1
11	RANSEL3	SCAN MONITOR RANGE SELECT 3	<	DIGITAL	0/1
12	EMEROL	EMERGENCY OVERLOAD DISCR. STATUS	<	DIGITAL	0/1
13	UNDRLD	UNDERLOAD DISCR. STATUS	<	DIGITAL	0/1
14	OVRLD	OVERLOAD DISCR. STATUS	<	DIGITAL	0/1
15	IONSORT	ION SOURCE TEMP. MONITOR	<	ANALOG	0-5V
16	IPIMON	ION PUMP CURRENT MONITOR	<	ANALOG	0-5V
17	IPVMON	ION PUMP VOLTAGE MONITOR	<	ANALOG	0-5V
18	TICMON	TOTAL ION CURRENT MONITOR	<	ANALOG	0-5V
19	STRAYT	SENSOR TRAY TEMP. MONITOR	<	ANALOG	0-5V
20	EMTMON	EMT HV MONITOR	<	ANALOG	0-5V

Table 6-8. ESS/MSA Electrical Interface (Continued)

Item	Name	Parameter	Flow ESS MSA	Type	Range
21	SCANVM	SCAN VOLTAGE MONITOR	<	ANALOG	0-5V
22	RICSAH	RESOLVED ION CURRENT SAMPLE	<	ANALOG	0-5V
23	ESS-9V	ESS -9 VOLT REFERENCE	<	BIAS VOLT.	-9.0 ± .0014 volts
24	ESS+5V	ESS +5 VOLT BIAS	<	BIAS VOLT.	+5v ± 5%
25	ESS-5V	ESS -5 VOLT BIAS	<	BIAS VOLT.	-5v ± 10%
26	ESS+12V	ESS +12 VOLT BIAS	<	BIAS VOLT.	+12v ± 7%
27	ESS-12V	ESS -12 VOLT BIAS	<	BIAS VOLT.	-12v ± 7%
28	ESS+24V	ESS +24 VOLT BIAS	<	BIAS VOLT.	+24v ± 7%
29	ESS-24V	ESS -24 VOLT BIAS	<	BIAS VOLT.	-24v ± 7%
30	+5RTN	+5 VOLT RETURN	<>	BIAS RET.	GRD
31	BIAS	BIAS (-5, ±12, ±24) RETURN	<>	BIAS RET.	GRD
32	SIGRTN	SIGNAL RETURN	<>	BIAS RET.	GRD

6.3 COMPARISON OF EXPERIMENT REQUIREMENTS WITH VIKING '75 PERFORMANCE CAPABILITIES

A comparison between the requirements for the WCMS and the present Viking '75 MS is shown in Table 6-9. It can be seen that the Viking '75 MS capability is quite compatible with the WCMS in nearly all of the major areas. The area in which the disagreement could have the most serious potential for difficulties is resolution. However, the quoted figure is quite conservative and may be relaxed considerably when the final components for the Wet Chemistry system have been selected.

6.4 MASS SPECTROMETER UPGRADING

The main areas that may require upgrading are resolution, stability and tuneability, while attempting to maintain the sensitivity of the MS at or above the premodification level. In some cases resolution and stability are interrelated, but for now they will be treated independently.

6.4.1 Resolution

The analyzer resolution limitation is due both the the magnetic sector image magnification and various aberrations among which the relative ion velocity spread ($\Delta v_i / v_i = \beta$) (which is a function of the voltage drop in the ionizing region and the accelerating voltage) is the most significant. Modifications in these two areas shall be considered in the following discussions. While modifications will always be related to these areas, the approach may frequently seem oblique, as parametrically these areas are very complex.

With regard to relative ion velocity spread, a direct approach of reducing this parameter by reducing the ionizing region potential gradient is not ideal since this also causes reduced sensitivity and greater susceptibility to ion space charge effects. Beta, or relative ion velocity spread may be reduced, however, by increasing the magnetic sector magnetic field strength which, for any given mass, requires that the mean ion energy be increased. Since the absolute ion velocity spread (Δv_i) is fixed by the ion source ionizing region gradient, beta ($\Delta v_i / v_i$) is effectively reduced.

Table 6-9. Present MS Performance with Wet Chemistry MS Requirements

Parameter	Viking 1975 Mass Spectrometer	Wet Chemistry/ Mass Spectrometer	Comments
Mass Range m/e	11.5 to 223	55 to 220	Appears adequate.
Scan Time	10.3 secs	5 secs	WCMS requirement appears feasible.
Sensitivity 10n amps/torr (N2)	3×10^{-6}	6×10^{-6}	Present MS figure is really adequate but WCMS system MS only receives 10 percent of the eluted material from the GC.
Resolution M/ΔM	181 with 15% valley	200 with 5% valley	The WCMS figure is nominal as the system components that regulate resolution have not been defined at present.
Pumping Speed cc/sec	500	1000	Present MS pumping is extremely marginal, and this does need improving.
Noise Level (EMT gain 10^3)	2×10^{-12} A	2×10^{-12} A	These figures can only be met with tighter temperature control on the electrometer. This is quite feasible.
Minimum Detectable Signal	3×10^{-12} A	2.5×10^{-12} A	
Ion Source Temperature	210°C	220°C	Compatible.

The first discussion will concern itself with methods for magnetic sector modification; later, in Section 6.4.1.2 magnification and other image aberrations will be considered.

Finally, system resolution is greatly affected by the support electronics. Section 6.4.1.3 will consider these effects and offer some solutions.

6.4.1.1 Magnetic Sector Modification.

Several methods of increasing the magnetic field strength are available. The simplest technique is to increase the magnet energy to its maximum stable value, about 7 percent below the saturation level, to achieve an MV product for the system of 33000. This permits mass 240 ions to focus at an accelerating voltage of 137 volts which is nearly equal to the accelerating voltage for m/e 200 in the existing design. The velocity of m/e 240 will be about 10 percent less than that of the mass 200 ions, and in theory the voltage drop in the ionizing region should be decreased about 10 percent to achieve the same beta. In practice, the resolution could be achieved by tuning the instrument within the range of voltage variation currently available in the source. The resulting resolution should be close to that achieved in the present system. No difficulty is anticipated in operation of the magnet at the higher energy.

While this first method on the surface sounds very desirable since no mechanical alterations are needed, it will be shown later in a discussion of electronics noise that greater improvements are required.

The second solution, and perhaps the most favorable would be to remove the integrated ion pump from the magnetic sector as may be seen in Figure 6-14. This method will remove approximately 1 square inch of pole piece allowing a more concentrated field with fewer fringe losses. It is anticipated that an MV product of 41000 would be attained, yielding a scan voltage of about 170 volts at m/e 240. This is a considerable advantage in terms of beta and ripple.

Removal of the integrated pump would, of course, necessitate the addition of an outboard ion pump, a modification also desirable from the standpoint of increased pumping speed and its many virtues. It is
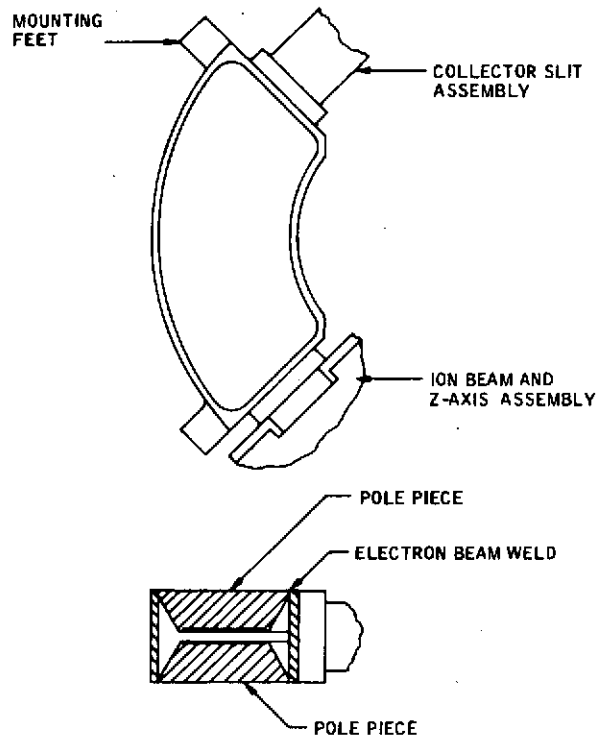
Figure 6-14. Modified Magnetic Sector Assembly Reflecting
Recessed Inner and Outer Radii Boundaries
and Removal of Integrated Ion Pump

recommended that a larger ion pump with a speed of 2 to 4 liters/second
be incorporated near the ion source as shown.

The third method of increasing the magnetic field is to enlarge the
magnet. This change, along with eliminating the integrated sector pole
pieces, is advantageous in two respects. First, greater magnetic field
strength, as previously described, will enhance resolution. Also, the
ability to position the magnet gives greater latitude in tuning and a higher
degree of accuracy in achieving simultaneous (angular) and (energy
spread) focusing at the image slit, thereby yielding improved sensitivity
and resolution.

One disadvantage is the increased magnet weight. A nonintegrated
ion pump (external to the magnetic sector) would also be required.

6.4.1.2 Object Slit, Adjustment, and Z-Axis Focusing

To increase the mass spectrometer resolution to better than a 5 percent valley as mass 240, the slit dimensions and the beam aberrations could be reduced. The calculated beam width in the present system is derived from the magnified object slit width, the image defect aberrations (uncorrected second order effects), the Berry curvature, and defects due to mechanical misalignments.

In the existing instrument

$$S_o = S_i = 0.002 \text{ inch} \qquad \text{The object and image slit width}$$

$$y_i = 0.0005 \text{ inch} \qquad \text{The second order terms}$$

$$B = 0.0015 \text{ inch} \qquad \text{Berry curvature aberration}$$

$$a = 0.002 \text{ inch} \qquad \text{Mechanical misalignments}$$

The resolving power is given by

$$RP = \frac{rm/2 \ (1 - M_m)}{S_o + (S_i \ M_m + y_i + B + a) \ (1 - V/100)}$$

$$M_m = \text{magnification of the magnetic sector} = -0.678$$

$$V = \text{percent valley between adjacent peaks}$$

Mechanical misalignments could be reduced 50 percent, and the desired resolution could be achieved by narrowing the slits to 0.0015 inch, and accepting a 25 percent reduction in sensitivity. In order to improve the mechanical alignment capability for obtaining simultaneous and focusing at the image slit, it is suggested a bellows be included in the drift tube region. This is a relatively minor modification to the analyzer which could result in considerable improvement in performance. Of course the mounting plate would require modification and positioning tooling would be needed for test. Some additional discussion of this is presented in a later section. Without this flexibility for tuning, the slit dimensions must be reduced to 0.0009 inch and a 55 percent decrease in sensitivity sustained.

The sensitivity losses incurred due to reduced object slit area can largely be offset by including a Z-axis focusing lens in the drift tube. Theoretical analysis of the effect of Z-axis focusing shows that transmission of all ions can be increased by at least a factor of two, and that mass discrimination can be reduced by about 50 percent. Transmission of high mass ions is increased by more than a factor of two. Some experiments have been performed in the existing system in which a negative potential was applied to the beam alignment slit; transmission of all ions was increased by a factor of 2.5 to 3 at the optimum voltage. Mass discrimination was not significantly changed. This is not in any sense an idealized situation. There were no ground plane electrodes which would normally be employed, and the positioning of the lens was fixed. As an approach to minimal design changes, the beam alignment slit could be used as a sort of Z-axis focusing lens. The only redesign effort would be in the scan supply to provide the necessary negative voltage. This might be typically 50 to 60 percent of the scan voltage. Since the scan supply should be redesigned to reflect the change in mass range and reduced ripple, the additional effort would not be extensive.

Another approach would be to implement a separate Z-focus assembly within the drift tube area at an optimum position. This would be a three-electrode system requiring a larger diameter for the drift tube in order to assure field uniformity. Several desirable effects are gained with the implementation of this lens system. Included in these are:

a) A factor of two to three increase in sensitivity.

b) Less high mass sensitivity losses due to the spreading of Z-axis beams which is more acute at low scan voltages.

c) Greater stability from fewer ion collisions on the magnetic sector pole pieces. This is discussed further in the section on stability

The design effort for this modification has already been performed, and it was found that the resulting system would fit within the existing instrument configuration. If this level of modification is undertaken, it should include the bellows to permit better alignment of the ion optical path. It should also be noted that the Berry curvature may be somewhat altered by the Z-axis focusing. Additional comments on this are in the section covering stability.

6-49

6.4.1.3 Magnetic Sector Design and Fringe Field Considerations

The design of a magnetic sector mass spectrometer is accomplished by finding a set of geometrical and field parameters for which certain aberrations are minimized or made equal to zero. For a second order double focusing instrument first and second order angle and velocity aberrations are made equal to zero. Expressed analytically the equation for an ion trajectory with an initial angle and velocity with respect to the "central ray" is:

$$y_m = B_1 \alpha + B_2 \beta + B_{11} \alpha^2 + B_{12} \alpha\beta + B_{22} \beta^2$$

Where y_m is the displacement of the aberrant ray from the central ray at a point in image space. The coefficients B_{ij} are functions of the geometrical parameters of the system, including the distance along the central ray in the image space, x_m. In a fully second order double focusing instrument the geometrical parameters are adjusted so that all of the B_{ij} are made equal to zero for the same conditions including the same value of x_m. Thus if the ion current collector is placed at x_m a narrow ion beam width and high resolution will result. Many geometries have been solved for which these conditions are met. Since there are ten geometrical factors in the general case there is a great deal of flexibility possible in achieving complete second order double focusing. These parameters are:

$(\ell_o)_e$ = object distance to electric sector

ϕ_e = electric sector angle

r_e = electric sector radius

d = electric sector to magnetic sector spacing

ϵ' = angle of central ray with respect to the normal at the magnetic sector entrance boundary

ϕ_m = magnetic sector angle

ϵ'' = angle of the central ray with respect to the normal at the magnetic sector exit boundary

x_m = image distance

R' = radius of curvature of the magnetic sector entrance boundary

r'' = radius of curvature of the magnetic sector exit boundary.

The magnetic sector radius, r_m, is a scaling factor for all of the other distances and therefore does not appear as a separate parameter. In the Viking '75 design, six parameters were arbitrarily chosen: ϕ_e, ϵ', ϕ_m, ϵ'', R', and R''. The remaining parameters should be sufficient to make four of the B_{ij} equal to zero. There was, however, an additional constraint applied to the design. That was that the electric and magnetic sectors should be independently first order alpha focusing. This gives a first order focal point between the sectors where the beta stop is located. The purpose of the beta stop is primarily intended to be a tuning aid for aligning the ion beam in the electric sector. In theory the extent of the allowed beta variation can also be limited by restricting the transmission at this point but this is not practical in a flight instrument where long term stability is essential. Nonetheless, this added constraint reduced the number of aberration coefficients that can be made equal to zero, to three. The ones selected were B_1, B_2 and B_{11} corresponding to α, β and α^2. The values of B_{12} and B_{22} are nonzero. Computation of the theoretical values for B_{12} and B_{22} as well as the limitations on α and β indicate that the contribution of the $\alpha\beta$ and β^2 aberrations is relatively small; thus, in spite of the nonoptimum geometry, the resulting second order aberrations are not the primary factors limiting resolution. At the same time, an improved instrument could take advantage of slightly modified geometries making B_{12} and B_{22} equal to zero.

A potentially more serious difficulty results from the fringe field of the analyzer magnet. Typically, magnetic sector design assumes initially an ideal magnet with no such field; then some type of correction is made for the effects of the fringe field. Various designers have developed different techniques for correcting this problem. They usually involve compensating for the bending and offset of the central ray in the fringe field. These methods vary in their accuracy but more properly account for focusing. Later workers have improved the methods used to account for the prebending, but more have adequately accounted for the focusing. Some maintain that the focusing action of the fringe field is comparable to

an equivalent uniform field so long as the integral along the trajectory is the same in both cases. This unfortunately is not true. In those instances where the fringe field is short, for example, due to the use of Herzog shunts, it may be approximately true. This is not the case in the Viking '75 analyzer. There are not Herzog shunts, and the fringe field is relatively extensive.

As a result, even if one of the approximate compensation techniques had been properly used, the design would not necessarily assure that the B_1, B_{11} and B_2 focal points coincided.

At the same time, there is an additional difficulty arising from the fact that even the approximate compensation techniques were not properly applied in the design of the Viking '75 analyzer. The only fringe field compensation employed was the standard one gap correction to the positions of the entry and exit pole faces. It is often found that the integral of the fringe field from the object point to a point inside the magnet gap (where the magnetic field is constant) is approximately the value that would be obtained if the magnet were ideal, with an effective sharp cutoff boundary one gap width outside the real boundary. This was the assumption upon which the Viking '75 analyzer design was based. It turns out that the actual integral is very nearly equal to this assumed value, and, therefore, the one gap correction does properly correct for the deflection of the central ray in the fringe field. However, no allowance was made for the associated offset as illustrated in Figure 6-15. Thus, the central ray enters the fringe field at a point δ below the assumed point. This changes the angle ϕ_m that the ray turns through in the magnetic sector. The resulting change in the distance parameters (all of which are normalized with respect to r_m) in relation to the angular parameters changes the aberration coefficients B_{ij}. Experimental data show that the α focus (here assumed to be first order) is approximately 0.110 to 0.120 inch out beyond the theoretically expected point. It is more difficult to measure the β focus, but due to their differing forms there is no reason to expect that the first order α and β foci will be coincident in the face of the change in the normalized distance parameters.
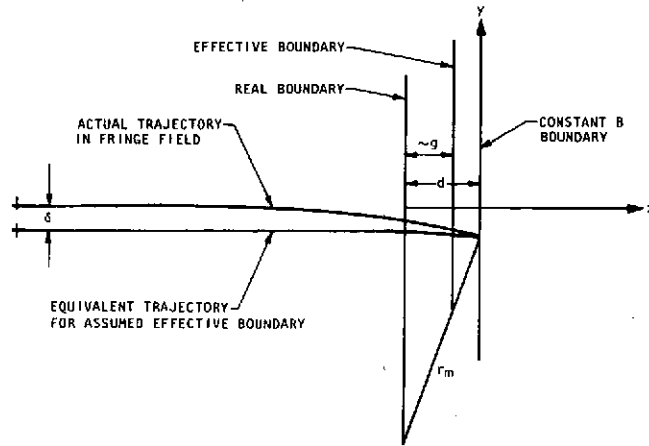
Figure 6-15. Fringe Field Considerations

In addition, as previously stated, the focusing effects of the fring field were not properly accounted for. Perkin-Elmer, in an independent effort, is currently establishing design techniques which properly account for fringe field. They involve the derivation of B_{ij} coefficients for the fringe field itself and their combination with the Hintenberger-Konig equations for the uniform field portion of the magnetic sector. The basic concept is shown in the equations in Figure 6-15. The slope of the central ray at x = 0 is a function of the integral of the flux from the object point to the constant field boundary, which is not a function of the fringe field distribution. The offset at x = 0 is the integral field which do depend upon the fringe field distribution. The expression for yz = 0 is also a function of α and β when the trajectory being calculated is not the central ray. By taking partial derivatives as indicated and keeping only first and second order terms in α and β the B_{ij} for the fringe field can be found. These B_{ij} also depend upon the details of the fringe field distribution. Once expressions for the B_{ij} are derived, it is a straighforward but grinding process to combine them with transfer expressions through the constant field region and then on through the exit fringe field to obtain overall focal properties. This allows geometrical parameters to be computed to give various $B_{ij} = 0$ resulting in the proper elimination of selected aberrations.

This work has not been completed, but it is expected that the design equations will be completed and computerized in the not too distant future. This will allow more detailed investigation of the effects of the fringe field with possible application to the Viking '79 instrument. At the same time, it may be found that a more detailed understanding of fringe field effects will indicate that Herzog shunts would be useful in improving resolution without requiring substantial additional changes.

6.4.1.4 Electronics Considerations

Modifications to the analyzer, by itself, to achieve the desired resolution will not be wholly adequate. A higher degree of electronics stability will be necessary to realize the increased overall system performance. Paramount in this respect is that of minimizing the electric sector ripple without causing any loss of sector scan tracking.

To evaluate the impact of electric sector voltage ripple on resolution it would be well to begin with the premise that the basic analyzer magnetics are as in the Viking '75 analyzer, but, by other means, the resolution is raised to obtain a zero percent valley between equal sized adjacent peaks at m/e 240. As in Figure 6-16a, the peaks are idealized, triangular shaped and without peak tails. Ripple on an electronic sector will modulate the ion beam position sufficiently to cause beam spreading at the image slit, resulting in reduced resolution and peak crosstalk as may be seen in Figure 6-16b.

The following equations, variations on those by Johnson-Nier[*], describe the first order deviations of a trajectory from the central ray as caused by electric sector voltage ripple.

$$y_e = \beta \ r_e [1 - \cos\sqrt{2} \ \phi_e + (\sqrt{2} \ (\ell_i)_e / r_e) \sin\sqrt{2} \ \phi_e] \quad (6-2)$$
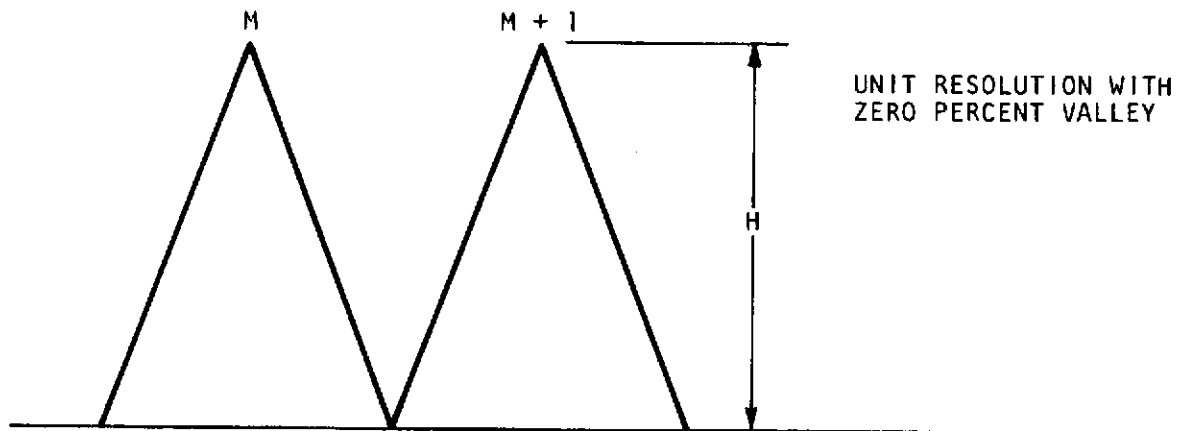
$$= 3.7 \beta$$

and

$$\beta = 1/2 \frac{dV}{V} \qquad \text{where } \frac{dV}{V} \text{ is the fractional variation in} \\ \text{each sector voltage (zero to peak)}$$

[*]E. G. Johnson and A. O. Nier, Physical Review, Vol. 91, No. 1, July 1953.

M   M + 1

UNIT RESOLUTION WITH
ZERO PERCENT VALLEY

H

(a) Basic Analyzer (No Ripple on Electric Sectors)

M   M + 1

RESOLUTION DEGRADATION
DUE TO ELECTRIC
SECTOR RIPPLE

H

KH

b   ε
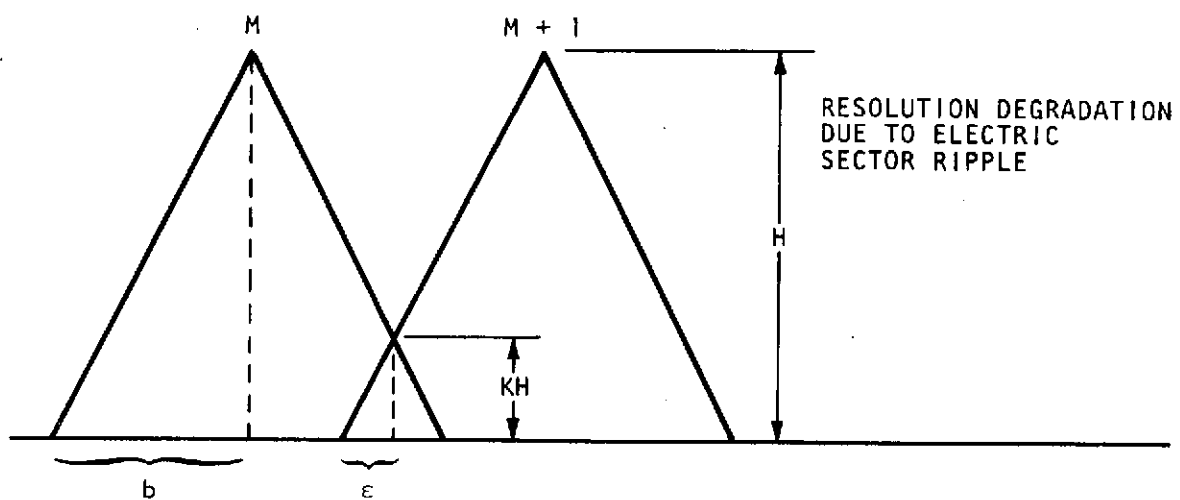
$b = 1/2$ PEAK BASE WIDTH $= 1/2 (y_m + y_c)$

$\varepsilon = 1/2$ PEAK BASE WIDTH EXAGGERATION DUE
TO RIPPLE ON AN ELECTRIC SECTOR

(b) Basic Twin Peaks as in (a) but With Ripple
on an Electric Sector Causing Losses in
Resolution

Figure 6-16.

then

$$y_m = y_e \left[\cos \phi_m - ((\ell_i)_m / r_m \sin \phi_m)\right] \qquad (6-3)$$

$$= 0.677 \, y_e$$

$$= 2.52 \, \beta \text{ inches} \qquad (6-4)$$

$$= 1.26 \frac{dV}{V} \text{ inches}$$

From Figure 6-16 one can see that for a peak to valley ratio (K),

$$\frac{KH}{\epsilon} = \frac{H}{b + \epsilon}$$

and

$$\epsilon = \frac{bK}{1-K} , \qquad (6-5)$$

for peak separation with zero percent valley

$$b \equiv y_c = 1/2 \text{ the image slit width.}$$

Combining Equations (6-4) and (6-5)

$$1.26 \frac{dV}{V} = \frac{y_c K}{1-K}$$

$$dV = \frac{y_c KV}{1.26 \, (1-K)} \qquad (6-6)$$

If $y_c = 0.001$ inch

$V = 7.8$ volts (electric sector potential)

$K = 0.05$

$$dV = 3.26 \times 10^{-4} \text{ volts (zero to peak sector ripple)}$$

Thus, the maximum zero to peak ripple which can be tolerated on an electric sector and yet maintain a 5 percent valley is 326 microvolts. The ripple tolerance is, in fact, significantly less than this when peak tails are taken into account. It would probably be reasonable to require that the sector ripple be no greater than 250 microvolts to insure the desired valley resolution.
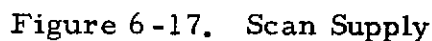
High frequency, low duty cycle, sector ripple as is usually manifest with converter spikes, is not only easily filtered, but also exhibits minimal effects upon the analyzer performance. The greatest difficulty arises from ripple of long duty cycle at frequencies relatively near the mass peak scan rate. These frequencies, of course, cannot be filtered since electric sector tracking would be seriously affected.

To help alleviate this problem it would be highly desirable, both from the standpoint of analyzer basic resolution and electronics ripple and stability, to increase the magnetic field strength in the magnetic sector.

Pursuing ripple further let us assume that, as previously discussed, the integrated ion pump is removed. The increased magnetic sector filed strength would net an MV product of 41000 thereby increasing the m/e 240 sector voltage from 7.8 to 11.5 volts. Using the same methodology as before and neglecting peak tails, zero to peak sector ripple of 0.00048 volt can be tolerated. Allowing margin to account for peak tails approximately 400 microvolts would be reasonable.

Since the mass range in Viking '79 is 50 to 240, the scan voltage range, considering mV = 41000, is approximately 820 volts down to 170 volts. This voltage range, somewhat reduced from Viking '75, is much more conducive to reduced ripple levels and tighter tracking if for no other reason than lowered source impedance.

A functional diagram of a low sector noise type scan supply may be seen in Figure 6-17. Here, sector to sector, and sector to ground ripple was considered the single most critical factor, and the circuit was designed with this as the overriding criterion. The circuit allows that a minimal sector source impedance is available with common mode

Figure 6-17. Scan Supply

influences a secondary issue. Also, it is most important that sector to sector and sector to ground tracking be precise; the circuit inherently accounts for this. The high voltage scan circuit derives its control signal from the sector potential instead of the more widely used conversely configured system.

Ripple on the scan high voltage is interpreted by the electric sectors, if they have no ripple, as increased ion energy spread. This is not acute since the purpose of the electric sectors is to compensate for ion velocity spread. Ripple on the scan high voltage must not,

however, be great enough to cause the ions, divergent in the electric sector, to collide with the sectors. As a side note, it is clear that a modification to the instrument to enlarge the electric sectors will result, secondarily, in greater source voltage ripple tolerance.

Ripple on the other analyzer electrodes is much less a factor in resolution. Tens of millivolts of ripple are tolerable elsewhere.

Another area where electronics have resolution alterning effects is in the logarithmic electrometer amplifier. At very low input currents the amplifier response is such that some peak valley realizations are lost. At the higher input currents ($>10^{-11}$ amps) the response is sufficient to have minimal effects.

Utilizing most of the previously described modifications, it appears that the resolution can be increased to $M/\Delta M = 240$ with a 5 percent valley while maintaining the sensitivity at the Viking '75 level.

6.4.2 Stability

Apart from the design changes for improving performance specifications, there are other considerations that should be noted regarding the ability of the current design to reliably perform to specifications. While there is emphasis on maintaining the existing design intact to the greatest possible degree, certain practical considerations dictate more substantial changes. There are two broad areas that have accounted for a great deal of time-consuming test and retest, and ultimately have resulted in serious compromises in performance. These are poor stability and insufficient flexibility in tuning. These areas are discussed in this and the following sections with recommended modifications.

The history of the Viking analyzer provides ample evidence of instability. It is usually manifested as a decrease in resolution at the high mass end of the spectrum. The basic instrument is capable of a resolution typified by less than 10 percent valley between m/e 181 and m/e 182. When performance deteriorates, the valley may increase to 30 or 40 percent. In nearly every instance the cause of deterioration

has been traced to charge-up of surfaces within the analyzer, usually within the magnetic sector. Specific and careful stability tests have not been very successful in isolating, clarifying or quantifying this effect and it continues to plague instrument test. The single most successful method of dealing with this problem has been to coat the magnetic sector surfaces with Aquadag (a colloidal suspension of graphite). In some instances multiple coatings have been required, and even then deterioration has recurred. These is a serious question regarding the durability of the Aquadag coat and the reliability of flight instrumentation utilizing this surface coating.

Typically in high resolution instruments two approaches are used to minimize surface charging effects: (1) the number of ions striking surfaces in the analyzer region is reduced to an absolute minimum; and (2) the criticality of ions striking a particular surface is minimized. Several design factors are important in minimizing ion current striking the analyzer surfaces.

6.4.2.1 Magnetic Sector Gap

The gap in the existing design is 0.100 inch; it is the narrowest point along the analyzer path length. Many ions strike the magnetic sector pole pieces. Increasing the gap would reduce this number and increase sensitivity at the same time. The disadvantage is that the increased gap would demand a larger analyzer magnet.

6.4.2.2 Magnetic Sector Baffle

A baffle should be added in front of the magnetic sector to intercept those ions that would otherwise strike the pole pieces. This would also cut off some ions that would otherwise be transmitted. The advantage, however, is that this surface is less critical because the transmitted ions pass by it more rapidly and are less affected by surface charges.

6.4.2.3 Object Slit Height

Reduction of the object slit height will limit the range of Z-axis initial conditions and eliminate many ions that would otherwise strike analyzer surfaces. While there is some attendant loss in sensitivity, this is not too severe.

6.4.2.4 Z-Axis Focus

Addition of a Z-axis focus lens at the alpha focus, between the electric and megnetic sectors, will improve Z-direction transmission of ions as discussed earlier. Figure 6-18 illustrates an existing design of a Z-axis focusing lens for this instrument.

By properly implementing all of these steps, it is possible to devise a design in which a fairly small fraction of ions entering the analyzer are not transmitted, and these will all strike the vertical baffle in front of the magnetic sector. Even with these improvements some ions will strike analyzer surfaces, and the potential for surface charging still exists. The following changes could further reduce the possibility of deleterious effects.

6.4.2.5 Heated Surfaces

Those surfaces receiving the preponderance of ions should be heated. The vertical baffle and the image slit fall in this category. By keeping them hot, adsorption of compounds which may form
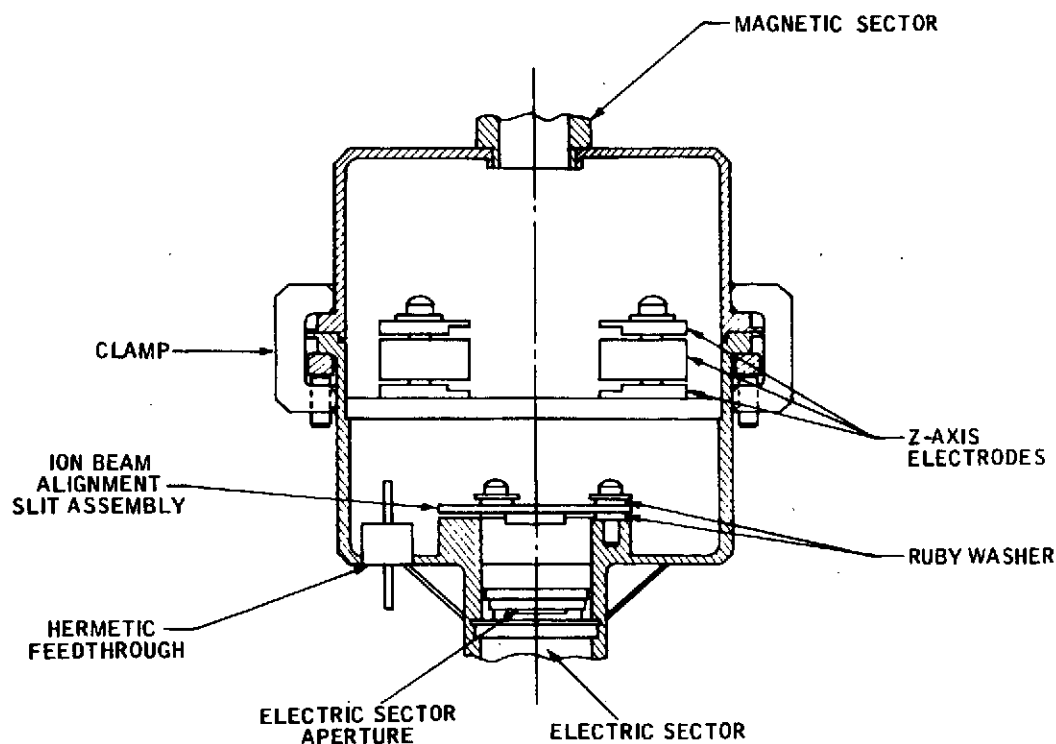

Figure 6-18. Beam Alignment and Z-Axis Assembly

insulating surfaces is reduced. Of course, power demands for heating would probably be a few watts.

6.4.2.6 Pumping Speed

The present Viking ion pump has a speed of only a few hundred cc/sec and is extremely small by conventional mass spectrometer standards. It would be feasible to increase the ion pump speed to a few liters per second. Any increase above this would be too costly in weight and ineffective because of the conductance limitations in the analyzer. There is an existing design for a 4-liter per second ion pump which has flown on Skylab I. It weighs approximately 4 pounds. A design has already been made, as may be seen in Figures 6-19, 6-20, and 6-21 which is a union of the Skylab type ion pump and the Viking analyzer.

6.4.2.7 Remote Surfaces

The discussion thus far has referred to ions striking surfaces that are out of the central plane. Ions also strike the outer and inner radial boundaries of the magnetic sector, and the end of the sector around the image slit. While these surfaces may charge up, the effect can be minimized by displacing them as far as is reasonable from the optical axis. This would lead to some enlargement of the analyzer housing but the weight penalty would not be serious. A completed design may be seen in Figure 6-14.

6.4.2.8 Ion Energy

One of the factors affecting the degree surface charging deteriorates performance is the velocity of the ions as they pass the charged surface. This is confirmed by the data that show a more rapid fall off in resolution with increasing mass than can be accounted for by beta effects alone. Therefore, in theory, the effects of charging can be reduced by increasing the ion energy. This necessitates a larger analyzer magnet since either the radius of the magnet or the field strength must be increased in proportion to the square root of the velocity. This is not an appealing approach since energy does not increase very rapidly with weight for a magnet. At the same time other considerations previously mentioned also point in this direction.
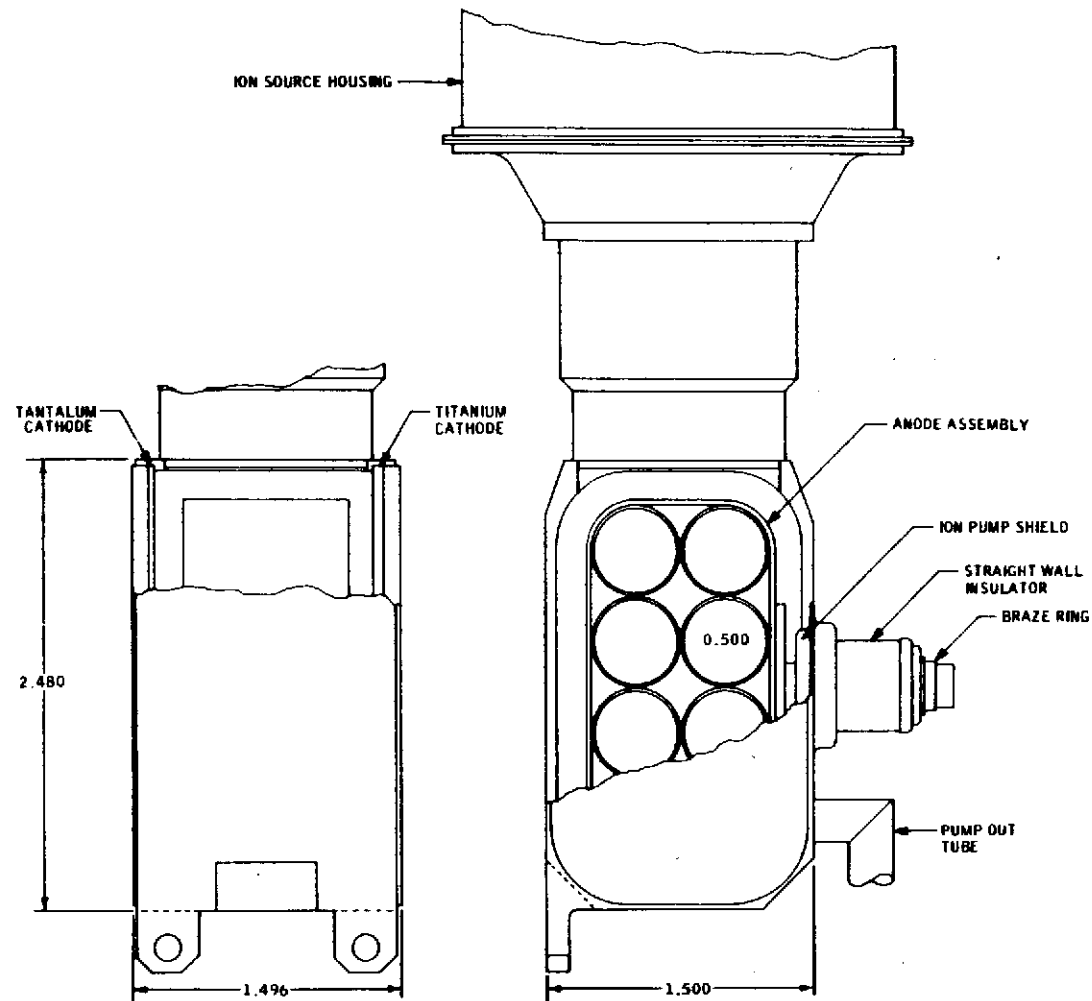
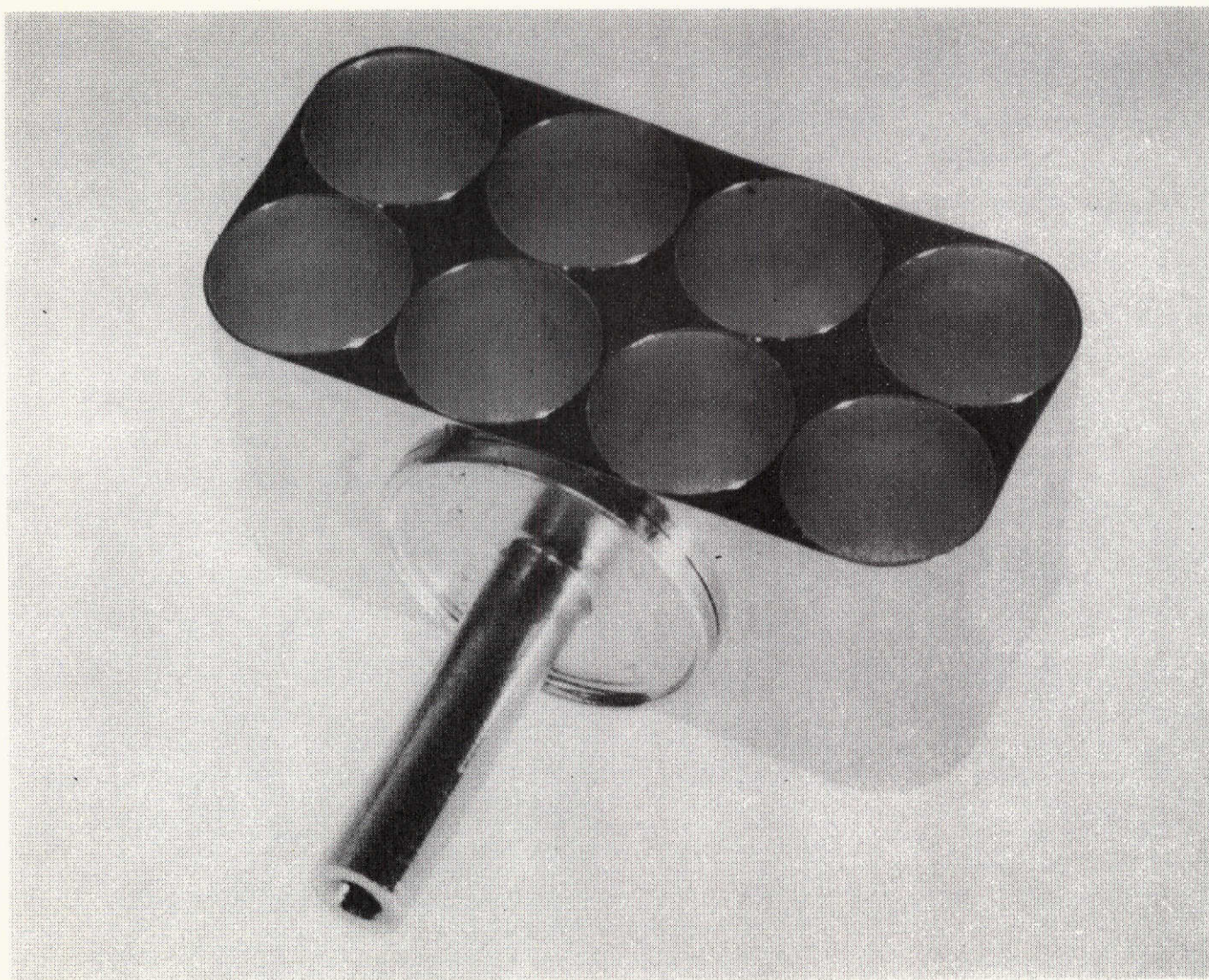Figure 6-19. Ion Pump Assembly and Mounting
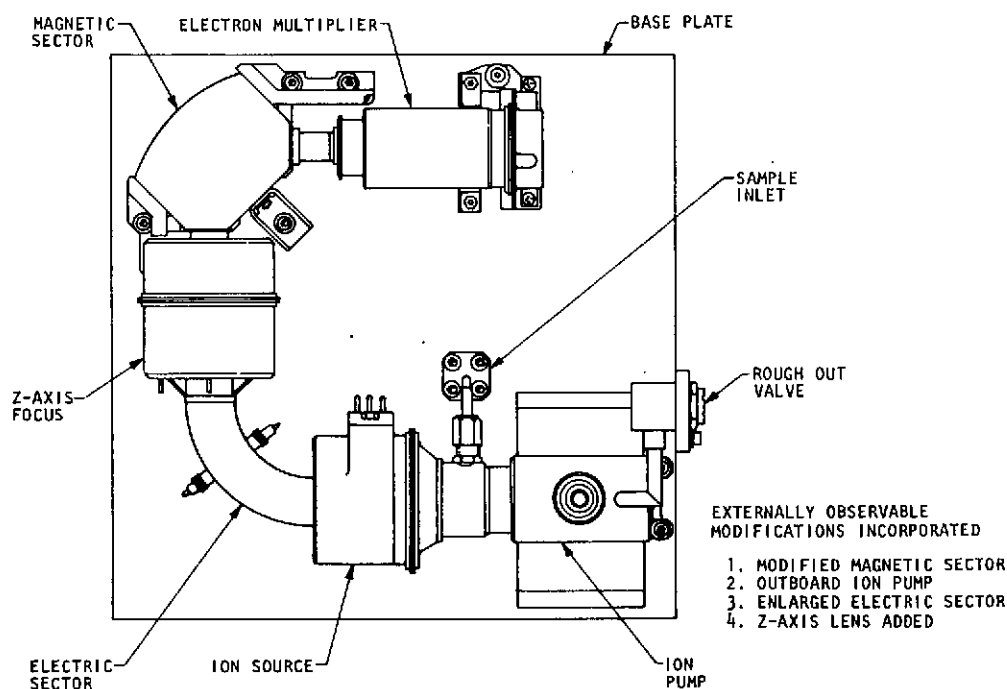
Figure 6-20. Ion Pump Anode Assembly

Figure 6-21. Wet Chemistry GCMS Assembly Analyzer Outline Prototype

In summary, there are several possible improvements that can potentially be made in the existing Viking analyzer to improve stability. Taken in aggregate they represent fairly significant design changes with associated power and weight penalties. While this is not particularly desirable, neither is the alternative, and therefore they should be considered.

6.4.3 Tuning

The capability for tuning the existing design is severely limited. This causes less then optimum performance in many respects. In the ion source, for example, there is considerable difference in sensitivity between the two filaments because potentials are not changed when the filaments are switched. The advantages of greater flexibility in mechanical alignment have already been described. These and certain other modifications which would substantially improve performance are discussed below.

6.4.3.1 Flexible Tuning Between Filaments

As a minimum, it is suggested the electron focus and repeller voltages be switched when switching between the two filaments. This would permit optimum alignment of both electron beams with respect to the repeller and would result in improved resolution and sensitivity with either filament. In the present system, compromise settings to achieve acceptable performance from both filaments result in considerably less than optimum sensitivity and/or resolution with either filament. Modifications are primarily in the operation control logic and analyzer power supply and are not difficult.

6.4.3.2 Wider Electric Sector

The sector in the existing instrument is relatively narrow, primarily to achieve a good aspect ratio (height to width) in the sector with a minimum size assembly. A number of experiments have indicated that improved resolution might be obtained if the beam were somewhat off center in the sector. In the narrow gap of the present design, the beam cannot be moved very far without striking the sector plates; this considerably restricts the degree to which the system can be tuned. Charging problems to date have not been identified in this part of the instrument, but increasing the spacing between the sector plates would reduce any effects which might exist. The overall conductance of the system would be slightly increased. The main benefit would be the increase in resolution and sensitivity which would result from the improved tuning capability. The modifications required would involve increasing the height as well as the width of the sector in order to maintain the aspect ratio, so that the overall sector dimensions would increase. The weight penalty would not be severe. The deflection voltages would be increased for the wider gap, and this would involve relatively minor electronics redesign. The electric sector field terminations, Herzog shunts, would also require redesign for the scaled up sector configuration.

6.4.3.3 Bellows Drift Tube

This subject has been referred to earlier. It might be pointed out by way of amplification that this additional flexibility would give some control over the entrance of the beam into the magnetic sector.

It would permit some lateral or Y-axis tuning of the image slit plate. This involves a modest amount of redesign in the drift tube area and a means of tying down the final instrument configuration.

6.4.3.4 Berry Curvature Compensation

The existing design provides a certain amount of correction for Berry curvature in that the slits are curved in the image slit plane. The radius of curvature was determined experimentally at JPL using the Bell Jar system. However, no two magnets are completely identical, and the fringe fields may vary slightly from unit to unit. For these reasons it would be desirable to have some capability for correcting this aberration within the system tuning procedure. Furthermore, if a Z-axis lens is built into the drift tube to improve transmission or if Herzog shunts are used, there may be significant change in the image plane which would necessitate correction at the resolving slit.

6.4.4 Sensitivity

Although most of the previously described modifications at least indirectly affect sensitivity, there are a few more considerations, e.g., the electron multiplier may be set at a gain of 10^4. In Viking '75 the gain was changed from 10^3 to 10^4 in late 1973. It was found that this could be done with relative impunity, and even a small gain in signal to noise is realized. Therefore, if after all the other modifications are completed, the basic analyzer sensitivity less electron multiplier remains the same, additional output may easily be obtained by multiplier gain adjustment.

Finally, it may be advisable to provide scanning voltages to the ionizing region. It might then be possible to realize somewhat higher sensitivity for low masses with lesser pressure effects.

6.4.5 Analyzer Linearity

6.4.5.1 Space Charge Effects

As previously alluded to, there may be an advantage to scanning the potential gradient in the ionizing region. It is not clear cut at this time, and additional analysis of the situation is necessary. It is clear, however, that space charge effects in the ion source prevail at moderate

ionizing region pressures. In this report a method has been described for approximately calculating degrees of nonlinearity due to pressure which might be expected for specified ion source ionizing region geometries. For instance, by calculating $\Delta\alpha_2/\alpha_2$ with a known, well characterized source geometry, projections can be made for other similar geometries.

On one type of mass spectrometer having a source geometry somewhat similar to Viking, a 10 percent nonlinearity occurred when $\Delta\alpha_2/\alpha_2 = 3.08 \times 10^{-4}$ for Xenon, m/e 129. On the Viking instrument nonlinearity data for the source alone were not available. However, it seems reasonable to use the $\Delta\alpha_2/\alpha_2$ determined above and calculate a projected pressure at which a 10 percent nonlinearity in the Viking source would occur. Utilizing the Viking source parameters and performing the necessary calculations, the pressure at 10 percent nonlinearity was found to be about 2×10^{-5} torr at m/e 129.

6.5 ALTERNATE GAS CHROMATOGRAPH DETECTOR

The baseline wet chemistry instrument design uses a hydrogen flame ionization detector (FID) to measure the amount of amino acid derivatives in the GC column effluent. Retaining the FID in the integrated wet chemistry/mass spectrometer instrument requires the addition of a third gas supply system to operate the FID, and a 1:10 effluent divider to split the GC effluent into two components: one flowing into the FID and another one flowing into the MS ion source.

It seems advisable to investigate the possibility of using an alternate GC detection to reduce the added complexity and also the weight of the integrated instrument. Two attractive alternatives to the FID that warrant closer investigation during future studies exist:

      1)   The use of an electron capture detector

      2)   The use of the MS ion source current monitor.

6.5.1 Electron Capture Detector

The use of a state-of-the-art electron capture detector for the wet chemistry instrument was considered during a previous study (TRW Final Report No. 23197-6001-RU-00). This study stated several reasons for evaluating an electron capture detector. One important reason is that

the electron capture detector appears generally to be more sensitive than the FID, and, in addition, some of the interfering material observed by flame ionization detection may be less sensitive to electron capture detection. Hence, an improved signal to background ratio might be obtained. Electron capture detection also offers some design simplifications for the wet chemistry/mass spectrometer instrument.

The use of an electron capture detector would require certain modifications to the instrument system in the following areas: the electronic subsystem needs to be modified in the front end of the analog data system to adapt to the particular detector finally chosen. The helium admixture in the carrier gas would not be required and pure H_2 could be used. The oxygen for the flame ionization detector would be replaced by the electron capture gas which would be nitrogen or an argon/methane mixture. The need for a third gas system would be eliminated. Finally, the methylene chloride would have to be replaced by ether as a solvent for the trifluoro- acetic anhydride used in the derivatizer of the wet chemistry instrument. The need to split the GC effluent (1:10 divider) would still exist, since the electron capture detector would probably not operate with hydrogen alone. The possible weight saving due to elimination of the third gas system is about 2 pounds. The system weight would then be 49.4 pounds.

6.5.2 <u>MS Ion Source Current Monitor</u>

Possibly the most attractive alternate GC detector is to use an MS ion source current monitor, which is the method used on the Viking '75 GCMS instrument. This would result in considerable weight savings and less complexity of the wet chemistry/mass spectrometer instrument.

Figure 6-22 shows the system schematic using the ion source current monitor. The GC effluent flows through a programmable divider directly into the MS ion source. The divider is controlled by the ion source current monitor. The system needs only one gas supply for the GC carrier gas.

The elimination of the FID, the He and O_2 gas systems and the 1:10 divider considerably reduces the hardware complexity and results in an estimated weight saving of 3.5 pounds. The system weight would thus be 47.9 pounds.
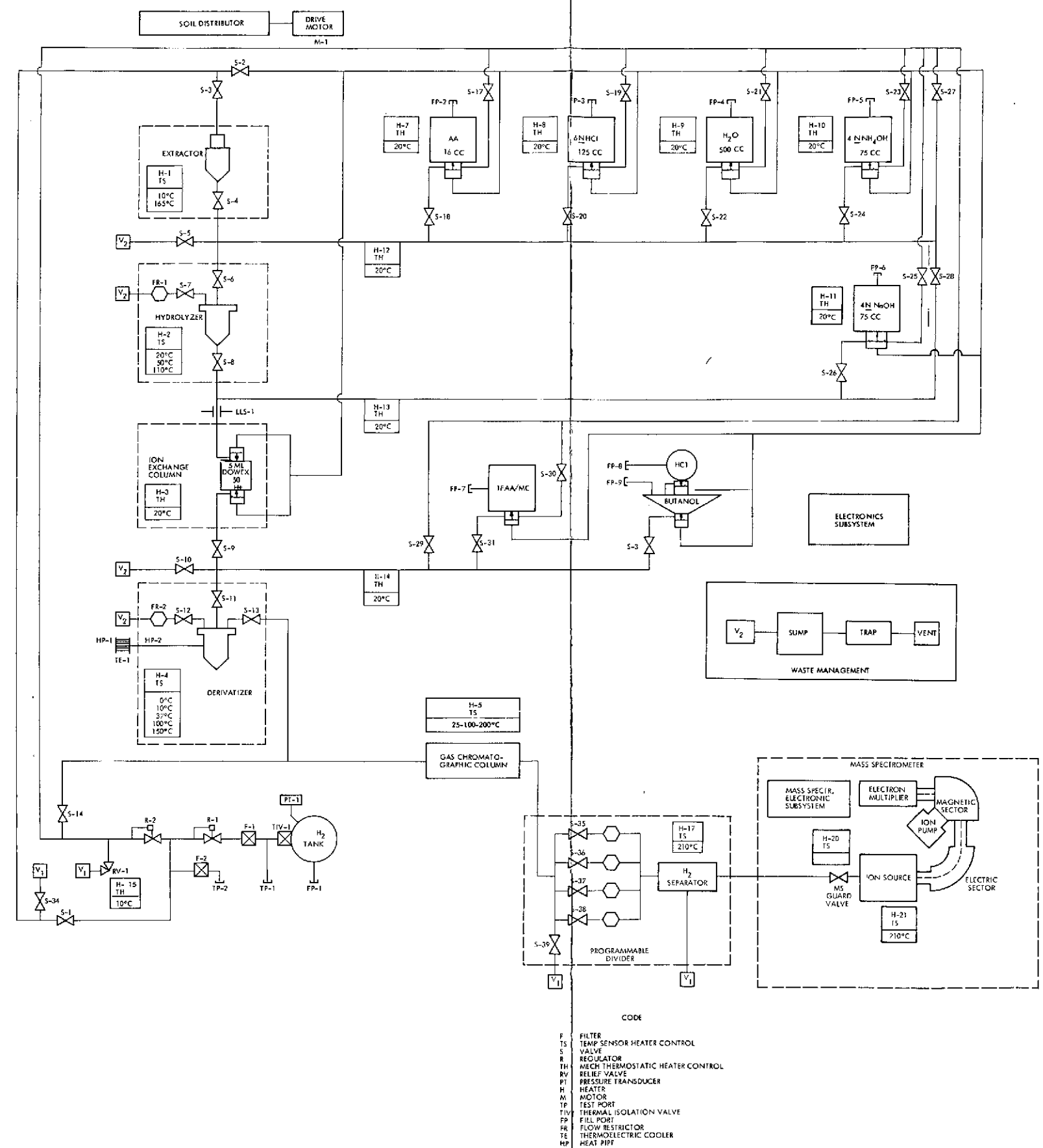
Figure 6-22. Alternate System Schematic

The impact on the instrument electronics would be relatively small since the FID front-end electronics (e.g., the electrometer) is replaced by similar front-end electronics for the ion source current monitor. Some power saving can probably be realized because of the elimination of three heaters for the FID and the He and O_2 gas supply system.

7. LABORATORY INVESTIGATION

A laboratory investigation into the bleed characteristics of two liquid phase gas chromatograph columns has been carried out. The two columns selected were Dexsil 400 and Carbowax 20M. The two columns (Dexsil 400 and Carbowax 20M) were conditioned and were evaluated for column bleed, using a GC hydrogen flame detector. After the initial evaluation of these two columns was completed, they were incorporated in a laboratory GCMS to obtain mass spectra of the bleed component, over the mass range of 50 to 240 amu.

In order to obtain the maximum sensitivity during the MS testing, a known sample of the effluent from the column needed to be directed into the MS ion source. In the case of the present Viking 75 MS, the ion source is not directly pumped and would normally be overloaded by the hydrogen carrier gas. To overcome this problem a palladium separator is used to remove this component prior to injection into the MS. However, it was thought that the palladium separator itself might interact with the amino acids and the bleed component. Therefore, an investigation into any interaction between the palladium separator and the column effluent was carried out prior to the MS investigation.

The carrier gas used for the initial investigation into the column bleed, using the hydrogen flame detector, was a mixture of 40 percent H_2 in He. After the bleed tests were completed the palladium separator was incorporated between the column and the hydrogen flame detector of the present instrumentation. The helium component of carrier flow was found to be adequate to assure normal passage of the amino acids into the flame detector, after the hydrogen has been removed by the palladium separator. The data from the experiments, with and without the palladium separator in the system, were examined for possible interaction between the column. effluent and the palladium separator.

The Carbowax 20M column was then installed in a Perkin Elmer GC system using an FID. The output from the column was split between the FID and a Hitachi RHU-16 MS. The flow into the MS line was made 20 percent of the GC exit flow, and this was passed through a palladium leak to

remove the hydrogen carrier gas before entry into the MS. This GDMS system was used to identify a standard mixture of their amino acid derivatives.

7.1 COLUMN BLEED MEASUREMENTS

The two columns were prepared and conditioned as described in Table 7-1. They were then evaluated for bleed in the following manner. A no-injection column temperature program was performed with the detector at high sensitivity. Changes in baseline were measured at selected temperatures and converted to equivalent nanograms of amino acids by comparison with the response from the standard amino acid injection. The results and experimental details are given in Table 7-2.

The columns tested were both 200-feet long by 0.030-inch ID, with column loading of Carbowax 125 milligrams and Dexsil 109 milligrams. Subnanomole bleeds are observed for both the Dexsil 400 and the Carbowax 20M columns. The results indicate that the bleeds are at least a factor of two less than the figure used in previous calculations (10^{-8} grams). These earlier estimates were based on extrapolation of GCMS column behavior.

7.2 SEPARATOR TESTS

In future tests it is proposed to conduct mass spectrometer analysis of the column bleed and to obtain data from a simulated flight GCMS utilizing laboratory hardware. In order to conduct these tests a hydrogen separator needs to be installed between the column and MS for reasons discussed in earlier reports. It was therefore decided to test the effect of the separator on the amino acid chromatograms utilizing the FID before the major incorporation with the MS. The apparatus used in these tests is shown in diagramatic form in Figure 7-1.

7.2.1 Carbowax

The carbowax column used for the previous measurements of bleed was connected to the GC system in the normal manner. Chromatograms were produced using the previously mentioned amino acid mixture to obtain baseline measurements. Then the separator was installed in the system between the column and the detector. Amino acid injections were

Table 7-1. Column Cleaning Packing and Conditioning Procedure

- Tubing - 200 feet of 0.030-inch diameter stainless steel tubing

- Cleaning of the tubing at 18 psi

50 ml	1:1 toluene/isopropanol
~10 ml	CH_3OH
10 ml	H_2O
25 ml	conc HNO_3
10 ml	H_2O
25 ml	conc NH_4OH
10 ml	H_2O
10 ml	CH_3OH
15 ml	Coating solvent

Dry with nitrogen gas at a pressure of 18 psi for 1 to 1-1/2 hours.

- Coat with appropriate column packing solution and dry with nitrogen gas at a pressure of ~15 psi overnight.

- Condition after attaching to GC and adjusting carrier gas flow to 6 cc/min.

The column is slowly heated to its maximum operating temperature while recording the detector baseline level. If the baseline drift appears excessive (current $>10^{-9}$ A on the laboratory setup), hold this temperature until the expected level is reached. Continue this procedure until the maximum temperature has been reached. Then raise the temperature to 20°C above the maximum value and hold at this temperature for an additional 3 hours; then cool the column. In order to check the column behavior make a test injection of a laboratory standard solution of 2.5 nanomoles each of 10 amino acids, using a program appropriate to the column. If the resolution is acceptable, complete the conditioning of the column by heating the column to 25° to 50°C less than T maximum for 12 hours. The column should be ready for use after cooling. The mixture of the ten amino acids used for the injection contains:

Valine	Proline	Phenyl Alaine
Alanine	Glycine	Glutamic
Isoleucine	B-Alanine	
Leucine	Aspartic	

Table 7-2. Bleed Data

Carbowax 20M Column 9611-002*

Time, Min.	Temperature, $^{\circ}C$	Bleed, coulombs/Sec	Bleed Nanograms/Sec
0	100	-	-
25	125	0.25×10^{-12}	0.25
50	150	1.3×10^{-12}	1.3
75	175	2.9×10^{-12}	2.9
90	175	4.4×10^{-12}	4.4
100	175	5.9×10^{-12}	5.9

*Column found later to be damaged.

Dexsil Column 9611-003 Series I tests.

Time, Min.	Temperature, $^{\circ}C$	Bleed, coulombs/Sec	Bleed Nanograms/Sec
0	100	-	-
25	125	0.35×10^{-12}	0.38
50	150	0.9×10^{-12}	0.9
75	175	2.2×10^{-12}	2.2
90	175	4.1×10^{-12}	4.1
100	175	4.2×10^{-12}	4.2

Dexsil column 9611-003 Series II tests**

Time, Min.	Temperature, $^{\circ}C$	Bleed, coulombs/Sec	Bleed Nanograms/Sec
0	100	-	-
25	125	-	-
50	150	0.30×10^{-12}	0.3
75	175	1.7×10^{-12}	1.7
90	175	3.8×10^{-12}	3.8
100	175	3.8×10^{-12}	3.8

*Detector has been cleaned and reinstalled with some sensitivity change.
**Calibration factor for average amino acid derivative $= 1 \times 10^{-12}$ coulomb/nanogram.
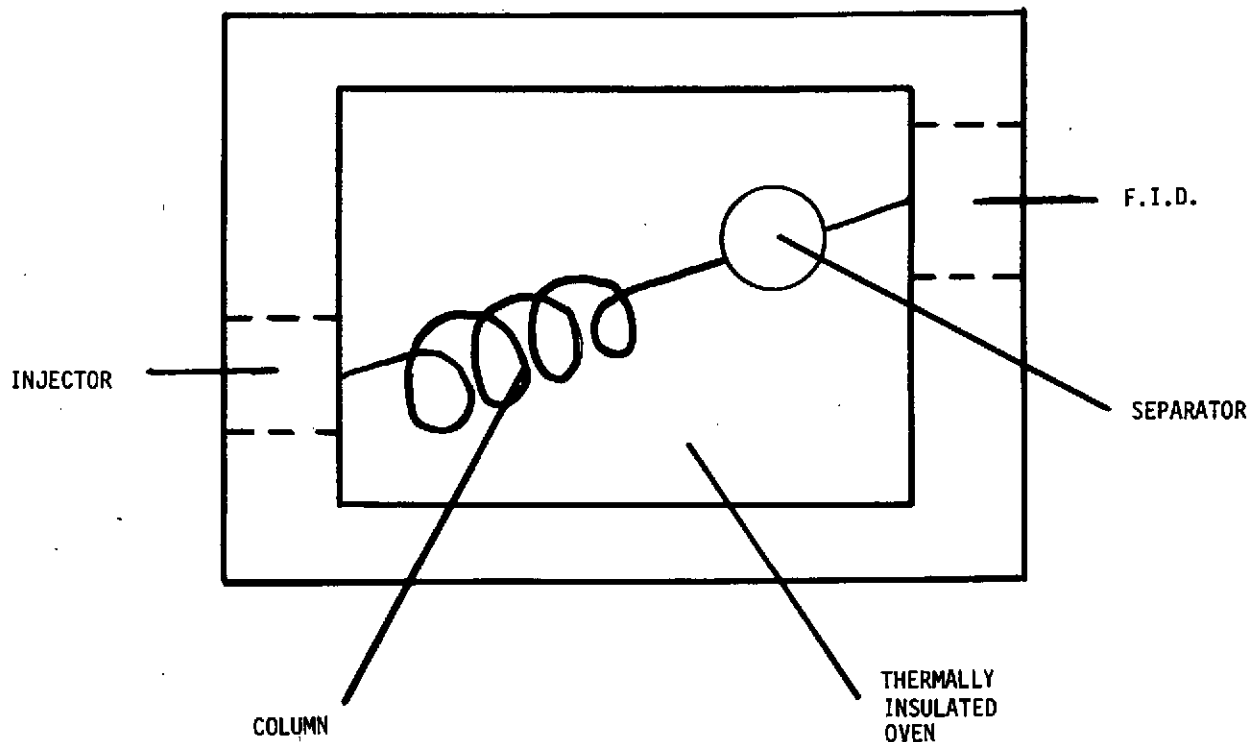
Figure 7-1. Gas Chromatograph-Separator System

made with the separator installed, in an identical manner to the baseline
runs. The separator run was duplicated, and then the baseline condition
without the separator was rerun. In this manner errors due to system
change were minimized.

It appeared from the data that peak retention times increased linear-
ly and that the peak integrals were smaller when the separator was included
in the system. Various alternatives were checked as possible causes of
these changes:

a) Plumbing was improved so that temperature gradients would
    not exist with the separator in line.

b) Flow rates were measured, to verify that the carrier gas
    flow controller was functioning properly.

Multiple runs showed progressively smaller peaks and progressively
longer retention times. No leaks were found at individual fittings, but
when the column was bubble tested it was discovered there was a leak with-
in the column windings. Work with this column was discontinued.

7.2.2 Dexsil Column

The Dexsil 400 column was pressure checked to determine that no leaks existed within the column itself. The tests outlined for the first column were then performed on the Dexsil unit. All of the runs in Series I tests used a mixed carrier gas of He/H$_2$ (60/40). At the end of the Series I test the FID was disassembled and a new test series (II) was started. During Series II tests pure He was also used as carrier gas, with and without the separator in the system, to check the FID performance with a constant flow rate. Leak checks were run at appropriate times to verify that there were no significant leaks present in the system. In addition, flow checks on the carrier gas exiting the column prior to the separator and flow tests of carrier gas exiting the separator were also conducted. This was performed both with the separator heater off and with the separator heater on and temperature equilibrated. A detailed description of the above tests and results are given in Tables 7-3 (Series I) and 7-4 (Series II).

The Series I data are shown in graphical form in Figure 7-2. In each run the sample was a 5 microliter injection of a standard mixture containing 2.5 nanomoles each of ten amino acid derivatives. In this figure the integral for each amino acid peak is compared as a ratio to the integral of the equivalent peak in Standard run 1, which is without the separator in the system. Standard runs 1 through 4 demonstrate reproducibility of about ±5 percent with the average of all runs falling at about 0.92 on this scale. The two separator runs show similar scatter with the average falling at about 0.70 on this scale. This indicates 12 ±5 percent of the sample is lost when the separator is installed into the system.

To verify the separator results in the Series I tests and to demonstrate that observed changes in flow rate were a result of hydrogen loss via the separator (from 5.8 cc/min exiting the column to 3.7 cc/min exiting the separator), He was substituted for the mixed carrier gas in Series II tests. Make up gas was still added after the separator to cut dead volume, and detector fuel gas was also used, both in the same proportions and flow rates as for the H$_2$/He case. These data show more scatter than Series I, nearly ±10 percent, which is still a reasonable reproducibility value for the sample size injected. A comparison of peak heights for runs 1, 2 and 6 also shows data scatter of at least 10 percent.

Table 7-3. Dexsil Column 9611-003 (Series I Tests)

Experimental Parameters

Dexsil 400 column - 200 feet by 0.030 inch - 109 mg loading.
Temperature programmed 100° to 175°C at 1°C/min.
Varian 1800 GC, commercial FID detector
Carrier gas: He/H$_2$ (60/40) - flow rate 6.0 cc/min nominal
Column make-up gas 20 cc/min
Detector fuel gas 20 cc/min, Air 250-300 cc/min
Separator: Trienco Inc. Protran Concentrator 910-PC
Sample: 5μl injection - 2.5 nM each of 10 amino acid derivatives.

Conditioned Column with He/H$_2$ - 6.0 cc/min

Gas Flow cc/min	Separator	Sep. Flow cc/min	Alanine RT	Integral	Notes
6.0	NO	-	1608	20590	Conditioning incomplete
Nominal	NO	-	1654	23920	
			1627	19210	
			1674	16420	
6.0	NO	-	1625	20700	
			1672	18510	

NO INJ. COL. BLEED TEST

Gas Flow cc/min	Separator	Sep. Flow cc/min	Alanine RT	Integral	Notes
Nominal	YES	Cool - 5.8	1639	-	RT slightly longer
		Hot - 3.7	1686	14290	
Nominal	YES	nominal	1661	13730	
		Cool - 5.7	1710	12090	
5.8	NO	-	1603	18840	
			1652	16420	
Nominal	NO	-	1579	20060	
			1625	17770	

The flame ionization detector was removed, dismantled, cleaned, and re-installed at the conclusion of Series I tests.

Table 7-4. Dexsil Column 9611-003 (Series II Separator Evaluations)

Experimental Parameters:

Dexsil 400 Column 200 feet by 0.030 inch - 109 mg loading (9611-003)
Temp. programmed 100° to 175°C (at 1°C/min)
Varian 1800 GC, commercial FID detector
Carrier gas flow nominal 6.0 cc/min
He/H$_2$ (60/40) or H$_2$
He/H$_2$ |Column make-up gas 20 cc/min
mix |Detector fuel gas 20 cc/min; air 250-300 cc/min
Separator: Protran Concentrator 910 PC by Trienco
Sample: 5 µl injection - 2.5 nM each of 10 amino acid derivatives.

Experiment Order	Carrier Gas	Flow Rate Out. Col.	Separator	Flow Rate Out Sep.
1.	He/H$_2$	Nominal	NO	-
2.	He	Nominal	NO	-
3.	He	5.8	YES	Cool - 5.8
4.	He	Nominal	NO	Hot - 5.75 Nominal
5.	He	Nominal	NO	-
6.	He/H$_2$	Nominal	NO	-
7.	He/H$_2$	5.9	YES	Hot - 3.5

The separator results with He carrier were again decidedly lower than the He standard runs, this time about 19 ±10 percent. A comparison of peak shapes using proline (Figure 7-3) from runs 6 and 7, indicates that the addition of the separator into the system does not alter the peak shape.

Table 7-5 presents retention time reproducibility. Runs 1 and 6, duplicate runs using He/H$_2$ carrier gas without the separator, are within a retention time reproducibility of 1 percent.

A comparison between runs 6 and 7 (He/H$_2$ carrier with and without separator) shows an increase in retention time of 3 percent when the separator is in the line. This slowing is attributed to the time to flow through the separator. A similar comparison of runs 1 and 2 also indicates a 3 percent retention time increase when He rather than He/H$_2$ is the carrier gas.
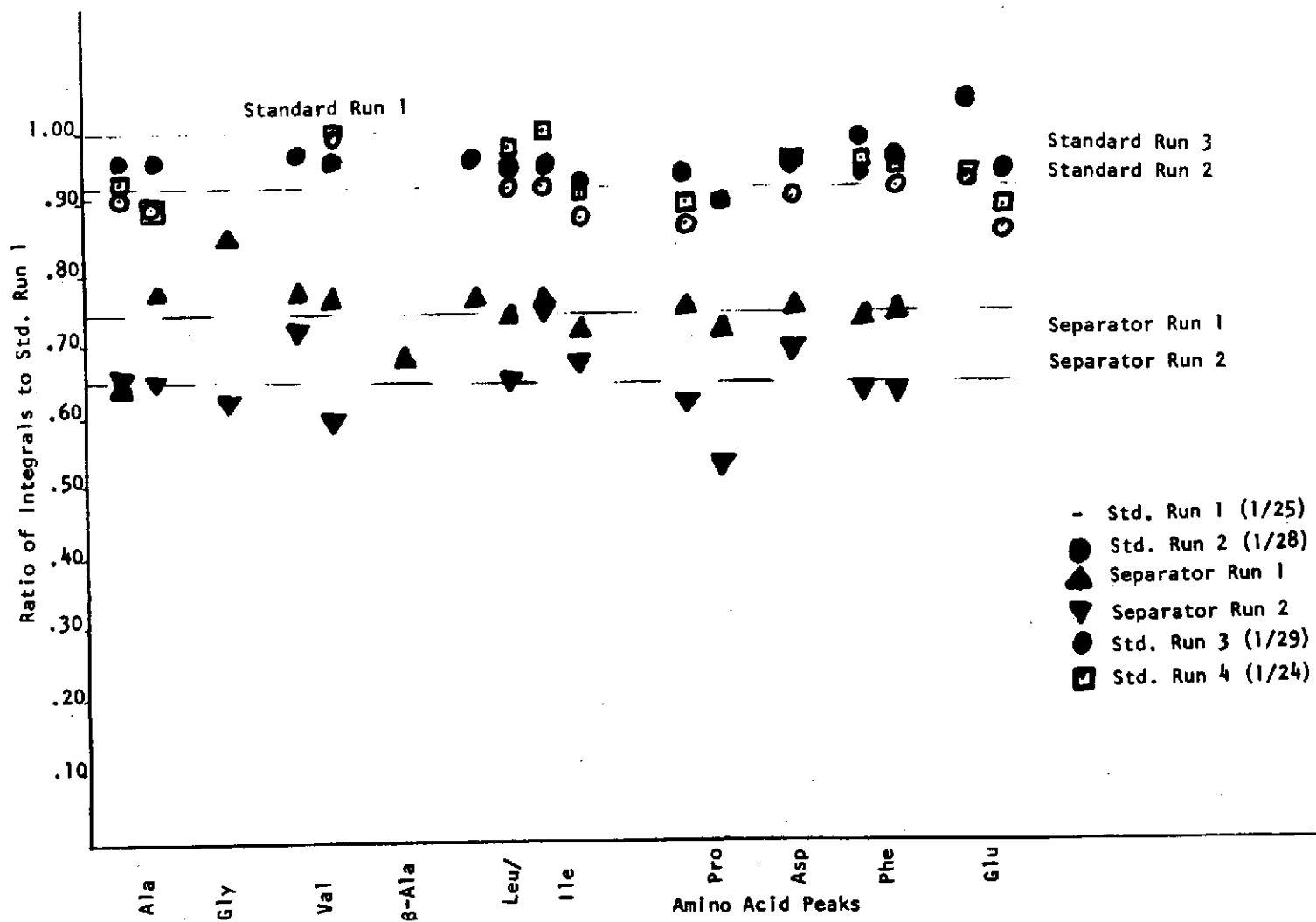
Figure 7-2. Series I Separator Tests on Dexsil 400 Column 9611-003.
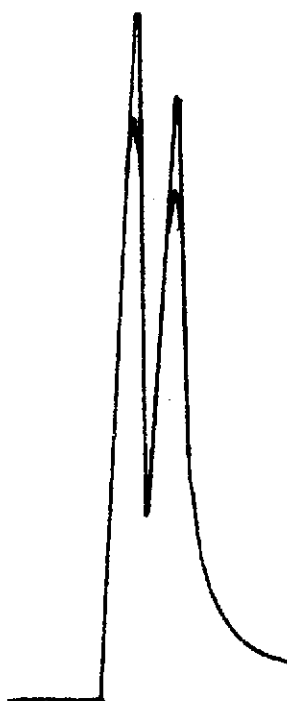(All tests using He/H$_2$ - 60/40 as carrier gas.)

Figure 7-3. 2.5 nM Proline Peaks on Dexsil 400 Column.
Larger peaks are standard run with He/H$_2$
(60/40) carrier gas at 6 cc/minute. The
smaller peaks are under identical conditions
except Trienco H$_2$ Separator in system between
column and detector.

This increase in retention time is a function of molecular weight of carrier gas and of the partition coefficient (sample solubility) of the carrier gas.

The conclusion from the separator experiments was that a measurable amount of sample loss and a slight retention time increase do occur when the separator is incorporated into the system. This loss of amino acids is not surprising since it was later determined that the purchased separator was delivered with a temperature setting of 400°C, instead of the specified 200°C which was originally quoted by the manufacturer for this unit. As the basic chromatogram was only slightly altered by the separator addition, it was decided to start the MS test program with the present separator parameters.

Table 7-5. Retention Time Comparisons (Series II Runs - Dexsil Column)

Run No.	1	6	7	2			
Carrier Gas	He/H$_2$	He/H$_2$	He/H$_2$	He			
Separator	No	No	Yes	No	Retention Time Ratios		
Amino Acids	Retention Time, in Seconds				$\dfrac{\text{Run 1}}{\text{Run 6}}$	$\dfrac{\text{Run 7}}{\text{Run 6}}$	$\dfrac{\text{Run 2}}{\text{Run 1}}$
Alanine	1543	1532	1563	1582	1.01	1.03	1.03
	1590	1577	1611	1628	1.01	1.02	1.02
Glycine	1758	-	1744	1753	-	-	1.00
Valine	2014	2005	2059	2074	1.00	1.03	1.03
	2058	2049	2105	2119	1.00	1.03	1.03
β-Alanine	-	2105	-	2162	-	-	-
Leucine/	2362	2356	2422	2436	1.00	1.03	1.03
Isoleucine	2410	2404	2472	2486	1.00	1.03	1.03
	2436	2431	2500	2513	1.00	1.03	1.03
	2489	2484	2555	2568	1.00	1.03	1.03
Proline	3425	3426	3523	3536	1.00	1.03	1.03
	3469	3468	3566	3577	1.00	1.03	1.03
Aspartic	4219	4222	4332	4354	1.00	1.03	1.03
Phenylalanine	4718	4722	4837	4861	1.00	1.02	1.03
	4751	4754	4870	4894	1.00	1.02	1.03
Glutamic	5163	5165	5287	5313	1.00	1.02	1.03
	5210	5211	5338	5360	1.00	1.02	1.03

7.3 SIMULATED FLIGHT GCMS INVESTIGATION

The basic design of the Wet Chemistry/MS system was checked out by setting up a commercial GCMS system with an interface between the GC and MS that was a flight simulation, as shown in Figure 7-4. There were several goals to the experiment. The main goal was to test the conceptual design by injecting a known standard of amino acid derivatives and analyzing them using the GC detector and the MS in parallel. The second goal was to measure the column bleed cracking pattern to ascertain if it would complicate the amino acid identification.

The tests carried out on the palladium separator in Section 7.1 appeared to demonstrate that the amino acid peaks eluted from the GC passed through the separator without major changes. However, the apparent amino acid peaks that were measured by the FID could in practice be any compound to which the FID was sensitive.

The final goal therefore was to confirm that the amino acids were unchanged in their passage through the palladium leak prior to entering the MS.

The interface between the MS and the GC was made to conform with the proposed flight design. Directly after the GC column the outlet line was split into two with a direct line to the GC and a restricted line to the separator and MS. The restrictor allowed only 20 percent of the GC output to pass into the separator, where the hydrogen carrier gas was received prior to the residue entering the MS. The remaining 80 percent of the flow from the GC passed into the flame ionization detector (FID) for analysis.

Prior to joining the MS to GC, each of these instruments was checked out separately to ensure adequate performance. The system was then integrated and system background measurements were carried out. Then a 5-microliter sample of 2 to 5 nanomoles each of ten amino acid derivatives in methylene chloride was injected in the normal manner into the GC. MS scans were initiated by hand at the appropriate times during the GC temperature programming. The time at which an MS scan was conducted is shown on the GC chromatogram in Figure 7-5, and each scan was 7 seconds in duration.
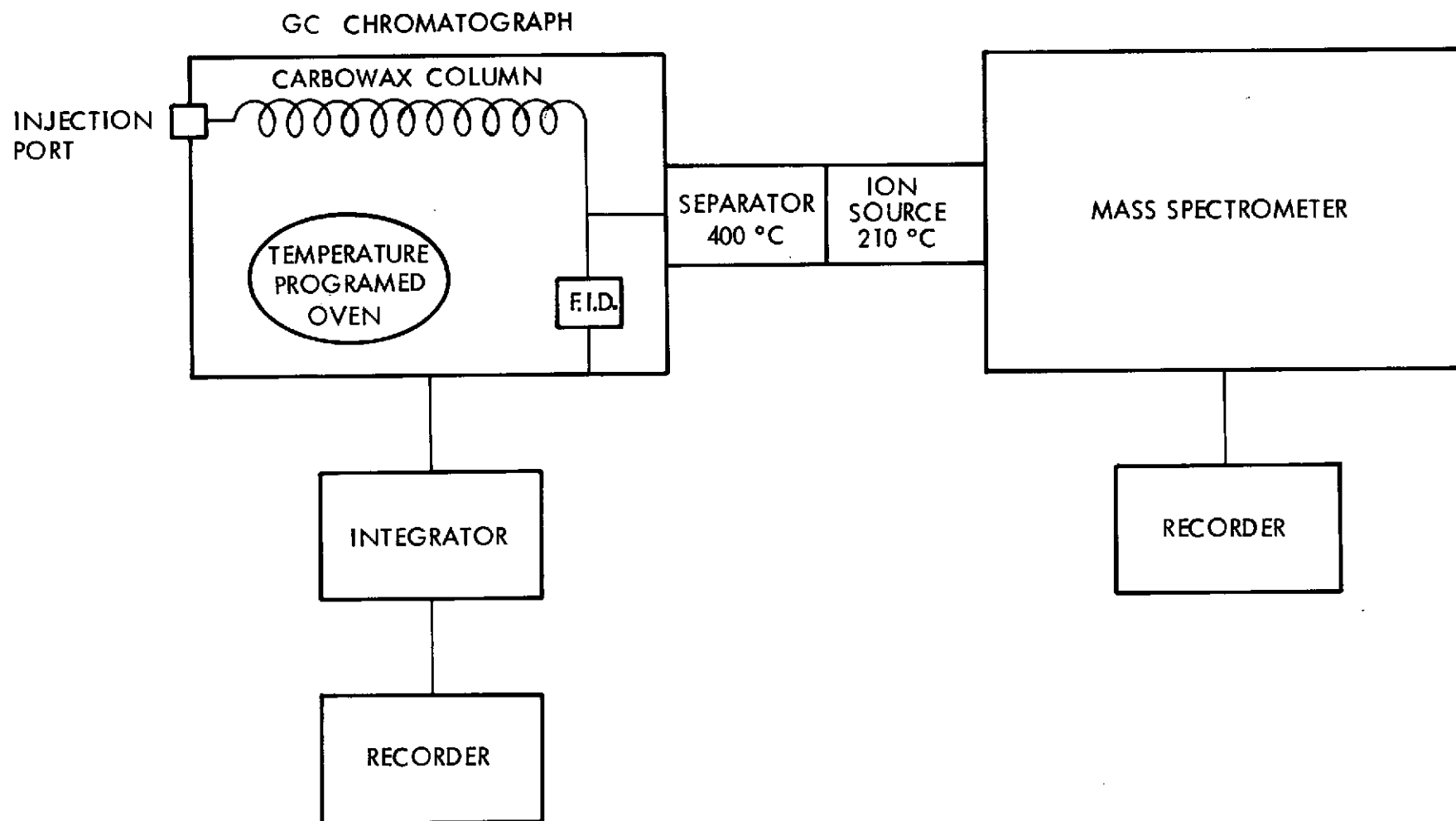
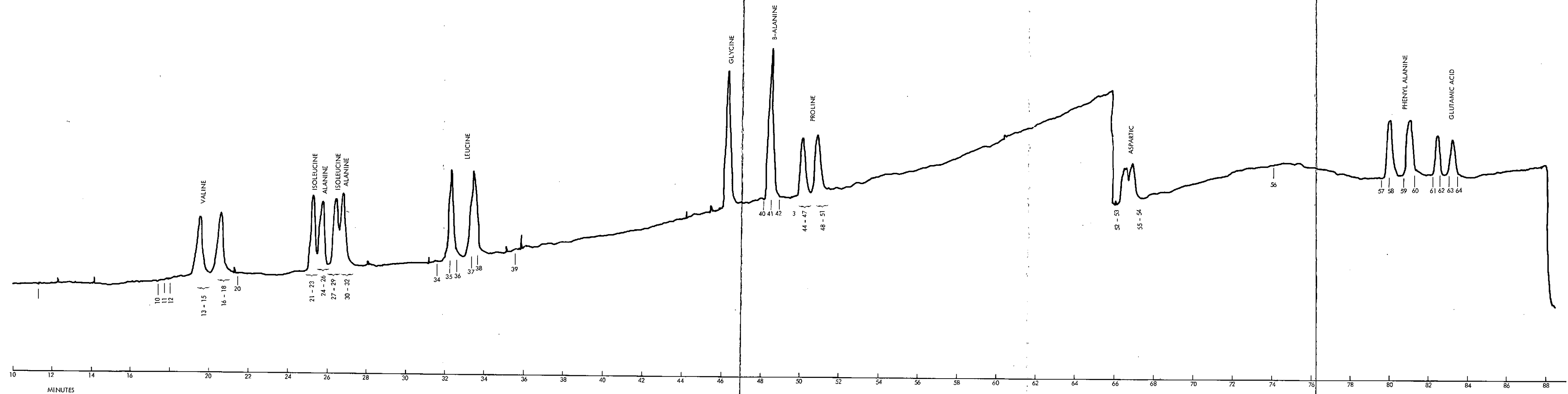Figure 7-4. GCMS Test Setup With Flight-Type Interface

Figure 7-5. Chromatogram of Test Amino Acid Derivatives

The cracking patterns obtained during each of the MS scans are shown in Figure 7-6. It can be observed that they correspond well to published spectra shown in Figures 6-2 and 6-3. The mass spectra have already been corrected for the normal MS background prior to injection. The spectra obtained during periods when no amino acids are present are shown in the last cracking pattern in Figure 7-6. No significant peaks were observed over mass 100 that can be attributed to column bleed. Below mass 100 the situation due to the number of peaks makes detailed analysis extremely difficult. No significant changes in the mass spectra occurred in lower mass number peaks throughout the temperature programmed run. The majority of these low mass peaks are due to normal mass spectrometer instrument background, with the exception of peaks at mass numbers 36 and 38 ($H^{35}Cl$ and $H^{37}Cl$) which are caused by the methylene chloride solvent.

7.4 CONCLUSION

The results of the integrated GC/MS work show that the system can work without apparent degradation of the amino acid derivatives and can provide unequivocal identification of compounds. (A good example of this is the mass spectra obtained during the isoleucine-alanine overlapping peak period. The MS was able to identify the exact order in which the peaks occurred. This was not possible to obtain from the amino acid GC chromatograms obtained in the normal manner.) In addition, these tests demonstrated that the Carbowax 20M column which is used extensively in Wet Chemistry GC work is a suitable column for combination with an MS.
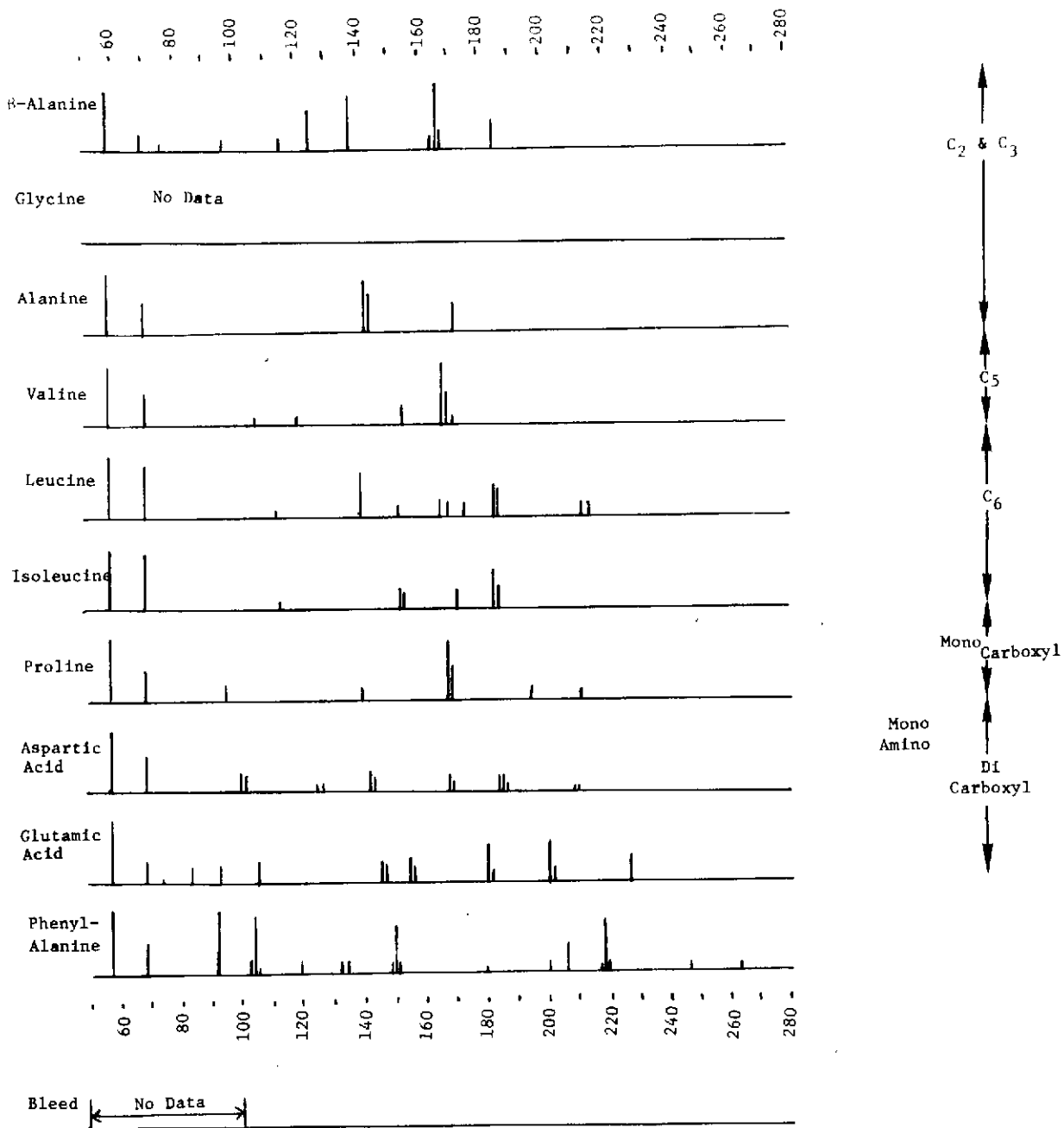
Figure 7-6. Amino Acid Cracking Patterns Obtained From
a Simulation of a Flight GCMS System